Synthesis of Silica Nanoparticles by Control of Mesostructures

メソ構造制御による
シリカナノ粒子の合成

July, 2018

Shigeru SAKAMOTO
阪本　樹

Synthesis of Silica Nanoparticles by Control of Mesostructures

メソ構造制御による
シリカナノ粒子の合成

July, 2018

Waseda University
Graduate School of Advanced Science and Engineering
Department of Applied Chemistry
Research on Inorganic Synthetic Chemistry

Shigeru SAKAMOTO
阪本　樹

Reviewers of This Thesis

Dr. Kazuyuki Kuroda

Professor

Waseda University

Thesis Superviser

Dr. Yoshiyuki Sugahara

Professor

Waseda University

Dr. Toshiyuki Momma

Professor

Waseda University

Dr. Hiroaki Wada

Professor

Waseda University

Dr. Atsushi Shimojima

Professor

Waseda University

Preface

Silica has been widely used in various fields of industries including glass and catalysis by utilizing the advantages, such as thermal and mechanical stabilities, transparency, electric insulation, and biocompatibility. Above all, silica nanoparticles smaller than 100 nm in size are characteristic of the high surface area to volume ratio and the small dimension, therefore they have been widely used as, for example, an additive of composites, a building block of optical thin films, a nanocarieer, and a biomarker.

The versatility of silica nanoparticles derives from the excellent designability of their size, and structure. First, it is possible to afford functionalities and to tailor the hydrophilicity/hydrophobicity by surface modification. The second is the introduction of mesopores in silica nanoparticles, which allows storage of guest species in internal nanospaces. Third, unstable and toxic cores such as metal nanoparticles or quantum dots can be protected by core-shell formation with silica coating. In particular, the tunability of particle sizes is the most important feature to design the functionalities of silica nanoparticles. Bottom-up approaches have often been employed for their synthesis. The synthetic methods have been largely classified into three types; 1) reverse-micelle method based on particle growth in a confined space of surfactant micelles, 2) Stöber method based on particle growth in hydrophilic solution, and 3) flame hydrolysis method based on the reaction of $SiCl_4$ gas with O_2/H_2 gases. However, there have been few reports about synthesizing silica nanoparticles *smaller than 5 nm in size*, due to the difficulty in isolating each nanoparticle without undesirable aggregation. Extra functions are expected to such a small silica nanoparticle, such as specific adsorption of guest species on high-curvature surfaces, strong interparticle interactions of large surfaces, and permeability through biological membranes.

Preface

In this thesis, a novel synthetic route to silica nanoparticles is proposed using reverse-type mesostructures as intermediates. Molecularly designed organoalkoxysilanes can form diverse mesostructures consisting of a silica-organic hybrid composition. It is found in this thesis that a reverse-type mesostructure can be dissociated in organic solvents to form silica-based nanoparticles with smaller size than those prepared by conventional methods. This process has been further extended to form silica nanoparticles using surfactants as a template, and one application of such small silica nanoparticles is also proposed.

This thesis is composed of the following six chapters.

Chapter 1 describes the background of this thesis, and summarizes previous studies referring to silica nanoparticles and silica-based mesostructures. Recent applications and synthetic methods of silica nanoparticles are summarized. Subsequently, various silica-based mesostructures and the formation mechanisms are reviewed. On the basis of these literature survey the significance and purpose of this thesis are presented.

Chapter 2 describes the synthesis of a spherical micelle-type mesostructure using self-organization of organoalkoxysilanes. In order to construct a high-curvature mesostructure, a starting molecule with a bulky hydrophilic head consisting of three disiloxane chains are prepared. After hydrolysis in acidic condition and subsequent evaporation-induced self-assembly (EISA) of the starting molecules, the hybrid mesostructure is readily prepared, which is confirmed by X-ray diffraction (XRD) and transmission electron microscope. Tetragonal phase ($P4_2/mnm$) is predominant in the formed spherical micelle-type mesostructures. Also, rod-type mesostructure is formed instead if the mesostructure is prepared with low water concentration during the EISA process. When rod-type mesostructures are prepared with three starting molecules

bearing different siloxane head (siloxane tetramer, pentamer, and heptamer), thicker silica wall and smaller organic domains is formed when using the larger siloxane head. Thus, it is revealed that molecular design of organoalkoxysilanes is important for controlling the mesostructure and the architecture of resulting silica-organic hybrids.

Chapter 3 describes synthesis of a reverse-type mesostructure using self-organization of organoalkoxysilanes, and dissociation of the mesostructure into silica-organic hybrid nanoparticles. A reverse-type mesostrcture is inverse of a spherical micelle-type, therefore the starting molecule consisting of three alkyl chains and one tetrasiloxane chain is designed, referring to Chapter 2. Hydrolyzed starting molecules self-organized to form transparent solid with three-dimensional polysiloxane framework containing many silanol groups, which are subsequently dissociated into individual nanoparticles in hexane. There emerges a diffraction peak assigned to mesoscopic periodicity in the XRD pattern of the solid, and the hexagonally arranged nanoparticles of ca. 3 nm in size are observed by scanning electron microscope (SEM). Accordingly, formation of reverse-type mesostructure is confirmed. Remarkably, diffraction peaks are shifted towards wider angle when mesostructures are prepared using the starting molecules bearing shorter siloxane chains.

Chapter 4 describes synthesis of a reverse-type mesostructure using concerted self-organization of a surfactant and a silica precursor, and dissociation of the mesostructure into silica nanoparticles. A surfactant of tri-*n*-octylmethylammonium chloride is mixed with a preliminarily hydrolyzed silica source, followed by the EISA process to form a mesostructure. The resulting thick film consists of a reverse-type mesostrcutre considering that the film is dissociated in organic solvents even in the presence of three-dimensional polysiloxane networks. The size of nanoparticles are roughly estimated to be 2-3 nm on the basis of the Guinier plot of small-angle X-ray

scattering. Concentration of surfactants in precursor solution is influential on sizes of resulting nanoparticles. Also, this new method is applicable to form titanium oxide nanoparticle. In conventional reverse micelle method, hydrolyzed silica precursor grow up in preliminarily formed surfactant micelles, whereas this new process is based on concerted self-organization of surfactant and silica source during solvent evaporation.

Chapter 5 describes synthesis of a novel silica-organic hybrid nanoparticles (**HNPs**) with adaptive nanospaces that are capable of containing guest species. **HNPs** are prepared by interconnection of vinyldimethylsilylated silica nanoparticles with an organic linker (1,6-hexanedithiol) using thiol-ene reaction. Each primary nanoparticles are densely packed in the solid state of **HNPs**, on the other hand the surface vinyl groups of the primary nanoparticles in the silica-organic hybrid network of **HNPs** are completely reacted with additional dithiol molecules in the 2-propanol dispersion. Accordingly, there exist adaptive nanospaces in **HNPs** to permit the access of guest molecules onto internal surfaces.

Chapter 6 overviews the results of researches in this thesis. The synthetic routes to silica nanoparticles of unprecedented size region smaller than 5 nm are newly demonstrated. The differences in two types of nanoparticles derived from self-organization of organoalkoxysilanes and from concerted self-organization of a surfactant and a silica precursor are discussed. Furthermore, the promising perspectives for these small silica nanoparticles are proposed.

Contents

Chapter 1

General Introduction

1.1 Silica nanoparticles

1.1.1 Silica nanoparticles

Silica species are abundant resources on earth, and they have often been used for fabrication of ceramics and glasses for a long time. Recently, they have been widely used in diverse fields of advanced technology by taking advantage of the physical, chemical, and biological properties. Silica frits have been applied to enhance the mechanical strength of organic polymers and rubbers by simple mixing. Also, optical transparency and electrical insulation of silica composition have been useful in the fields of optoelectronics as a low index layer of antireflection coatings and a capacitance layer of thin film transistors *etc*. Furthermore, porous silica gels have shown an excellent matrix for gas capture and catalysis.

The wide variation in the morphologies containing films, bulks, rods, and nanoparticles is another attractive point of silica materials. The large specific surface area is a main feature of nanoparticle morphology, which has been beneficial in manufacturing industries for tuning of ink rheology and antiblocking of plastic films. Currently, silica nanoparticles have also been expected as a nano-platform of chemical modification, where various functions have been integrated into each nanoparticle. Silica nanoparticles have been developed in widespread fields of catalysts, optelectric devices, sensors, and medicines. Various applications have been discovered depending on chemical designs of silica nanoparticles.

In this section, applications and synthetic routes of silica nanoparticles are summarized with a focus on recent reports, followed by the suggestion of problems in the current status of silica nanoparticle technology.

1.1.2 Applications of silica nanoparticles

In the second half of the twentieth century, many reports of silica nanoparticles focused on fundamental researches about how to synthesize silica nanoparticles and how to control their sizes. In the last several decades, studies of their applications have been dominant instead, which is accompanied with the evolution of the functionalization. The application fields have been widespread, such as optics,[1-5] catalysis,[6-8] sensing,[9-11] antibacteria,[12,13] drug delivery systems,[14-17] MRI,[18-20] and bioimaging.[21-23]

Applications of silica nanoparticles can be categorized into the following two parts. First is the application as an individual functionalized nanoobject. Diverse functions of metals and organic species are decorated into silica-based nanoparticles via surface modification, core-shell formation and incorporation. As well, mesopores are frequently introduced into silica nanoparticles that are valuable for molecular storage. Second is the application as a nanobuilding block of hierarchical structures such as colloidal crystals and nanocomposites. Additional functions are derived from periodicity and interfacial interaction of silica nanoparticles.

1.1.2.1 Applications of functionalized silica nanoparticles

In functionalized silica nanoparticles, various properties such as fluorescent, magnetic, catalytic, and antibacterial activities have been incorporated into each nanoparticle. There are important roles of a silica matrix for controlling the functions. Herein, the roles are summarized with the quotation of recent reports.

The major role of a silica matrix in nanoparticles is to fix dopants into the polysiloxane framework. The typical example is fluorescent silica nanoparticles that are prepared by incorporation of dyes into silica nanoparticles. Interestingly, luminescence

of rhodamine molecules supported in silica nanoparticles were 20 times brighter than that of their water dispersion, which have been reported by Larson *et al.*[24] The rotation of the dye molecules was limited in a covalently bonded silica matrix, thus leading to the enhancement of luminance. Similarly, multiple dopants with different fluorescent colors were separately incorporated in one nanoparticle, and emitted at the same time without the quenching of the energy transfer from one to the other. Malinge *et al.* have fabricated the white fluorescent nanoparticles, in which naphthalimide (blue) and tetrazine (yellow) were separately doped in the core and the outer shell of a nanoparticle (Figure 1.1).[25]

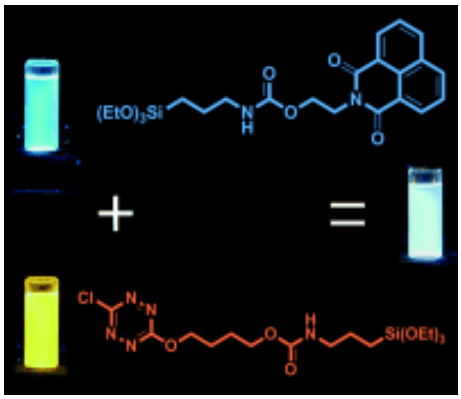

Figure 1.1. Photoluminescence images of silica nanoparticles incorporating only a blue dye, only an yellow dye, and both dyes, which are excited by the ultraviolet light of λ = 330 nm. Reprinted with permission from J. Malinge, C. Allain, A. Brosseau, P. Audebert, "White Fluorescence from Core–Shell Silica Nanoparticles", *Angew. Chem. Int. Ed.* **2012**, 51, 8534. Copyright 2012 Wiley-VCH Verlag GmbH & Co. KGaA.

Outer silica surfaces are meaningful for tuning of dispersibility, functionality, and biocompatibility. First, the hydrophilic silica surfaces of nanoparticles are advantageous for colloidal stability of their dispersion in hydrophilic solvents or polymers. Low compatibility of fullerenes has often been a problem for preparing the

solutions or the composites, which have been overcome by their encapsulation into a silica nanoparticle (Figure 1.2).[26] The fullerene-containing silica nanoparticles with bright photoluminescence and high photostability have been penetrated into live cells to exhibit low cytotoxicity. Similarly, Jane *et al.* have demonstrated the water solubility and buffer-stability of inorganic nanoparticles (Au, Ag, Fe_3O_4, and ZnS−CdSe) that have been coated with a silica shell.[27] Second, surface silanol groups of silica nanoparticles can be functionalized with facile organic modification. Until now, various functional groups, such as methyl, amino, thiol, vinyl, and epoxy groups, have been integrated on the surfaces in order to not only tune the surface properties but also enable further chemical reactions. Chen *et al*. have newly proposed a nanoparticle-type sensor of highly reactive oxygen species (hROS), where Au nanoclusters were decorated on a silica nanoparticle via modified organic linkers.[28] Au nanoclusters did not emit in the presence of hROS such as •OH, ClO^- and $ONOO^-$, hence this nanoparticle has been useful as their sensor. Similarly, Kim *et al.* have fabricated a multifunctional nanoparticle with luminescence and magnetic resonance relativities by the layer-by-layer deposition of Gd complex and poly (styrene sulfonate) on a Ru-doped silica nanoparticle (Figure 1.3).[29] Third, biocompatibility of silica surface has enhanced possibilities of biological applications. Silica is generally low toxic owing to slow dissolution in hydrophilic buffers. Their pharmacokinetic behavior has still been intensely investigated in order to confirm the in-vivo safety.[30,31] Up to date, many harmful nanoparticles have been detoxified with silica coating of their surfaces. Quantum dots that are coated with an outer silica shell have shown the intracellular transportation ability and no toxicity in living cells for long incubation.[32] In another report, only 2 nm of thin silica shell has been effective for suppressing toxicity of Ag nanoparticles on BSA cells, without losing their characteristic ability of plasmonic

sensing or imaging.[33]

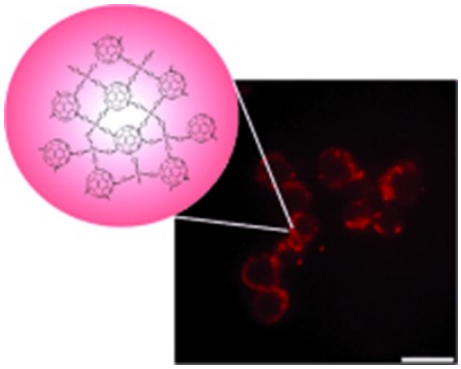

Figure 1.2. Photoluminescence image of fullerene–silica nanoparticles that was excited by the 488 nm Ar^+ laser line. Reprinted with permission from J. Jeong, M. Cho, Y. T. Lim, N. W. Song, and B. H. Chung "Synthesis and Characterization of a Photoluminescent Nanoparticle Based on Fullerene–Silica Hybridization", *Angew. Chem. Int. Ed.* **2009**, 48, 5296. Copyright 2009 Wiley-VCH Verlag GmbH & Co. KGaA.

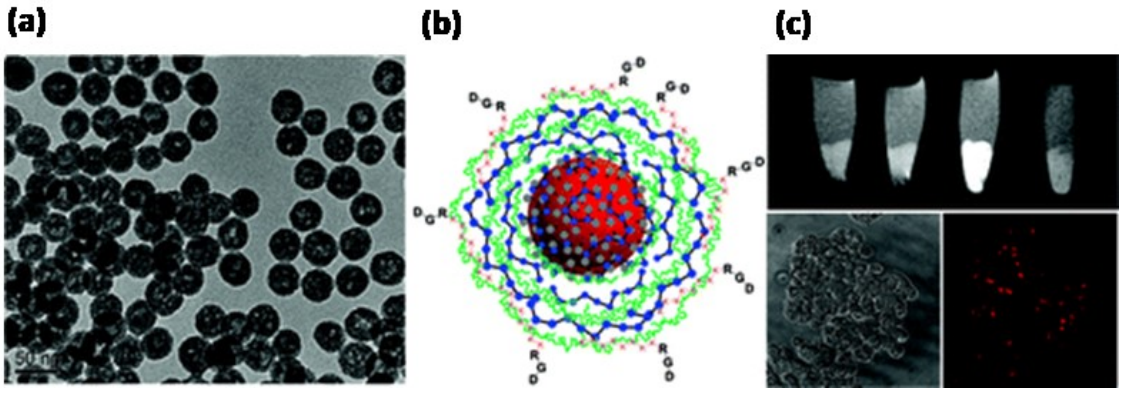

Figure 1.3. (a) TEM image, (b) schematic representation, and (c) photoluminescence images of multifunctional nanoparticles that were prepared by the layer-by-layer deposition of Gd complex and poly (styrene sulfonate) on Ru-doped silica nanoparticles. Reprinted with permission from J. S. Kim, W. J. Rieter, K. M. L. Taylor, H. An, W. Lin, and W. Lin, "Self-Assembled Hybrid Nanoparticles for Cancer-Specific Multimodal Imaging", *J. Am. Chem. Soc.,* **2007**, 129, 8962. Copyright 2007 American Chemical Society.

Another role of silica shell is a spacer to tune the distance between cores and outer surroundings for tuning the interactions. Surface plasmon of the Ag core in Ag@SiO_2 core-shell nanoparticles were coupled with nearby photons of dye molecules dissolved in solution, in which lasing threshold and optical feedback have been tailored by the in-between silica shell thickness (Figure 1.4).[34] Ceylan *et al*. have integrated the magnetic inductive heating and catalytic activity in a core-shell nanoparticle.[35] Magnetic cores have been prevented from coupling thanks to the silica shell separation, resulted in the superparamagnetic behavior, and the good catalytic activity.

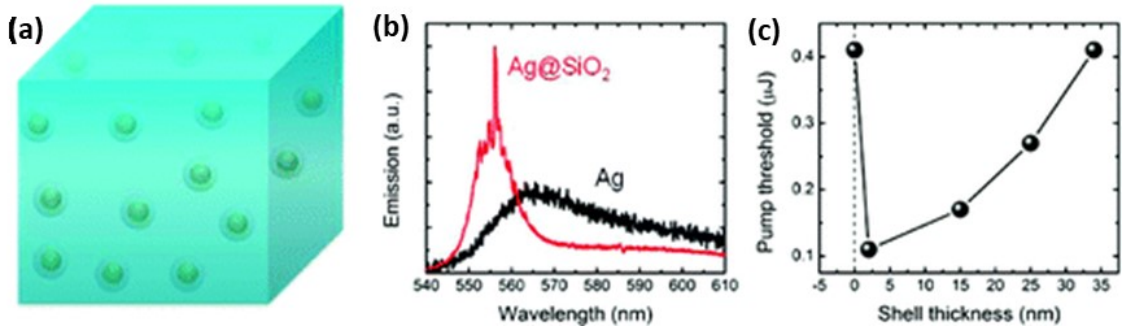

Figure 1.4. (a) Schematic representation of Ag@SiO_2 core-shell nanoparticles in the dye solution. (b) Emission spectra of Ag@SiO_2 (core-shell) and Ag nanoparticles, exhibiting the different optical feedback. (c) Relationship between the pump threshold and silica shell thickness. Reprinted with permission from X. Meng, K. Fujita, S. Murai, T. Matoba, and K. Tanaka, "Plasmonically Controlled Lasing Resonance with Metallic−Dielectric Core−Shell Nanoparticles", *Nano Lett.* **2011**, 11, 1374. Copyright 2011 American Chemical Society.

The role of a silica matrix is further extended through the introduction of meso/micropores. Porous silica works as a nano-carrier or a molecular sieve. The role as a nano-carrier of medicines, proteins, and dyes has been extensively researched for biological applications, along with recent technological advances in the formation of mesoporous silica nanoparticles.[14,36-39] Until now, diverse stimuli such as temperature,

pH, light, and magnetic fields have been applied to release guest species out of mesoporous silica nanoparticles. Also, a mesoporous silica shell is a convenient molecular sieve not only to protect the internal core but also to control accessibility of outer guest species, which have attracted fields of catalysis and antimicrobial. S. H. Joo *et al.* have demonstrated the excellent catalytic activity of platinum@mesoporous silica core-shell nanoparticles for hydrogenations of ethylene or oxidations of carbon oxide, accompanied by the improved thermal stability of the Pt core against unpleasant decomposition or aggregation.[6] Microporous silica hollow nanoparticles that contained Pd clusters inside have shown an interesting size selectivity on the catalytic activity of allyl oxidation (Figure 1.5).[40]

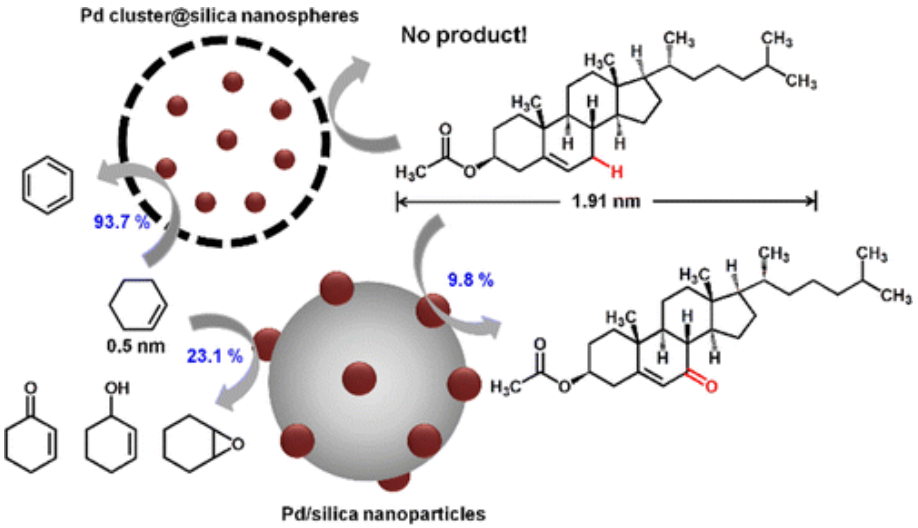

Figure 1.5. Schematic representation of Pd cluster@silica nanospheres and Pd/SiO_2 core-shell nanoparticles, and various reaction yields of catalytic activities. Reprinted with permission from Z. -A. Qiao, P. Zhang, S. -H. Chai, M. Chi, G. M. Veith, N. C. Gallego, M. Kidder, and S. Dai, "Lab-in-a-Shell: Encapsulating Metal Clusters for Size Sieving Catalysis", *J. Am. Chem. Soc.* **2014**, 136, 11260. Copyright 2014 American Chemical Society.

For all the silica nanoparticles, the size is an important parameter to control the

functionality of each nanoparticle because the surface curvature and the specific surface area are dependent on the size. It has been determined that enzymes have been more stably adsorbed on higher curvature surface of smaller silica nanoparticles.[41] Also, the size is a dominant factor to decide the permeability and mobility of silica nanoparticles. A. A. Burns *et al.* have demonstrated the efficient urinary excretion of small-sized fluorescent silica nanoparticles.[42]

1.1.2.2 Applications of hierarchical structures

Hierarchical structures of silica nanoparticles such as colloidal crystals[43, 44] and nanocomposites[45] have induced new functions, which is not observed for each isolated nanoparticle. Herein, remarkable properties of such hierarchical structures are summarized by citing recent researches.

Various properties have been realized on the basis of thin film layers of nanoparticles that are formed by accumulating nanoparticles. Lee *et al.* have revealed that the layer-by-layer stacking of silica and titania nanoparticles exhibited antifogging and self-cleaning properties in addition to the conventional anti-reflection effect.[46] The resulting interparticle nanospaces has played a key role in this coating. Similarly, the formation of an omniphobic film has been demonstrated by layer-by-layer deposition of silica nanoparticles and polyelectrolytes, followed by the fluorination with a silylating agent and a lubricant.[47] Various liquids were clearly repelled by this treatment (Figure 1.6).

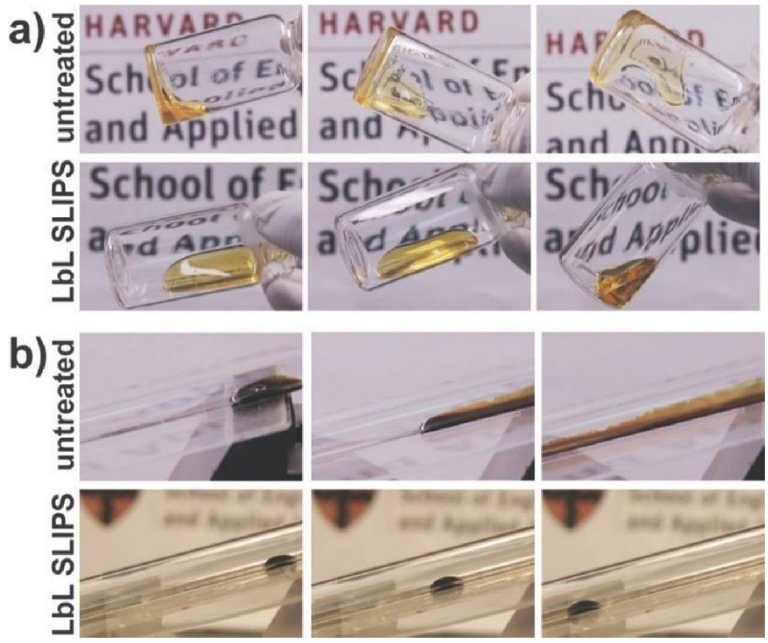

Figure 1.6. Photograph images of (a) honey in vial container and (b) crude oil in glass tube with or without the special layer-by-layer coating. Reprinted with permission from S. Sunny, N. Vogel, C. Howell, T. L. Vu, and J. Aizenberg, "Lubricant-Infused Nanoparticulate Coatings Assembled by Layer-by-Layer Deposition", *Adv. Funct. Mater.* **2014**, 24, 6658. Copyright 2014 Wiley-VCH Verlag GmbH & Co. KGaA.

The affinity between polymer binders and silica nanoparticles is influential on properties at nanocomposites. In recent years, there has been a deeper understanding in correlations between molecular dynamics and resulting physical properties of nanocomposites, using advanced analytic techniques.[48-51] There have been many reports fabricating new functional nanocomposites by choosing polymers and adjusting silica nanoparticle surfaces. Generally, thermal and mechanical stabilities of nanocomposites have increased with nanoparticle concentration, meanwhile shape-memory performance of these nanocomposites has conversely decreased. Agarwal *et al.* have solved this drawback by interparticle connections with polyethylene glycol (PEG) through the surface modification of silica nanoparticles.[52] Ge *et al.* have fabricated a nanocomposite showing a unique color change depending on outer stress.[53] Polydimethylsiloxane has

been immersed into a silica-based colloidal crystal, in which periodic nanopores were generated to express the structural color when the structure was distorted by the outer stress. Furthermore, Zhou *et al.* have improved a washing performance of cloth fibers, such as machine wash durability and antifouling property by the coating of the fibers with a nanocomposite of fluorinated silica nanoparticles and polydimethylsiloxane.[54] In a composite of silica nanoparticles and PEG, the dispersion degree of nanoparticles has influenced the crystallinity and ionic conductivity of PEG, which was confirmed by comparing two nanocomposites prepared by in-situ synthesis of silica nanoparticles in PEG, and by a simple mixture of silica nanoparticles and PEG.[55] Furthermore, silica nanoparticles have adhered hydrogels to each other on the basis of entanglement of swollen polymer network and nanoparticles as shown in Figure 1.7.[56] As a biological application, successful glue of calf's liver pieces has been demonstrated.

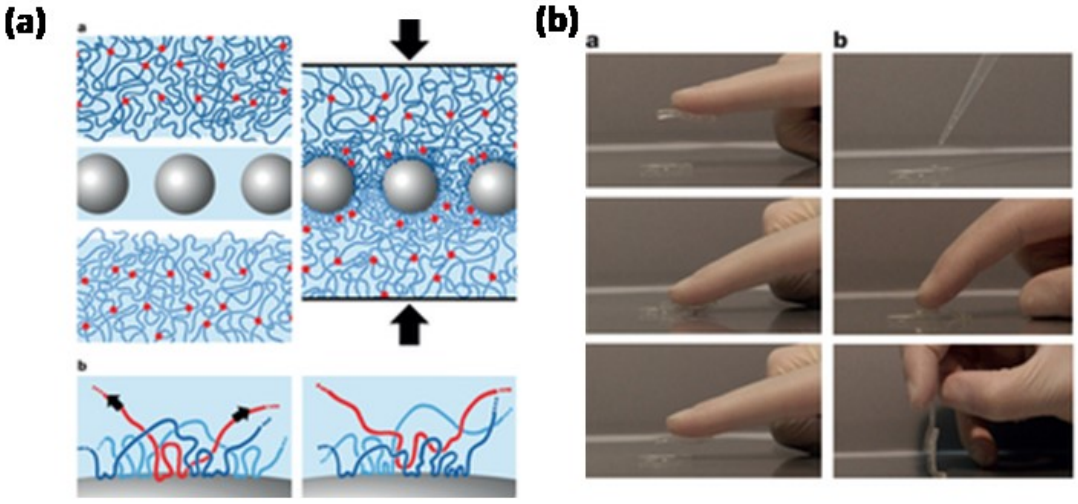

Figure 1.7. (a) Schematic representation of considerable mechanism of the hydrogel-nanoparticle adhesion. (b) Photograph images of hydrogel's gluing without (left) or with (right) silica nanoparticles. Reprinted with permission from S. Rose, A. Prevoteau, P. Elzière, D. Hourdet, A. Marcellan, and L. Leibler, "Nanoparticle solutions as adhesives for gels and biological tissues", *Nature* **2014**, 505, 382. Copyright 2014 Macmillan Publishers Ltd.

The size of silica nanoparticles is an important parameter on the properties of hierarchical structures. N. C. Su *et al.* have confirmed that the permeability deviation from Maxwell's model in silica/PEG nanocomposites increased when silica nanoparticles with smaller sizes were used. [57] Similarly, W. Heni *et al*. have demonstrated that the mechanical stability of a nanoparticle multilayer has increased against cavitation gas bubbling when using smaller nanoparticles.[58]

Small silica nanoparticles are characteristic of high specific surface area and high surface curvature. These features are of great importance for the design of various applications using silica nanoparticles. Unfortunately, however, there are few reports to prepare ultrasmall silica nanoparticles less than 5 nm in size due to the difficulty in isolation of unstable small nanoparticles without undesirable aggregation. Consequently, new synthetic methods of such small silica nanoparticles are needed in order to examine the possibility of such small silica nanoparticles.

1.1.3 Synthetic methods of silica nanoparticles

Synthesis of silica nanoparticles was started by Vail *et.al* in 1925,[59] and comprehensively reviewed by Iler *et.al.*[60,61] Nowadays, silica nanoparticle dispersion in various solvents is commercially available, in which particle sizes range from several micrometer scale down to several tens of nanometer scale. Synthetic methods are largely classified into dry and wet processes.[62,63] Chemical vapor condensation is a typical dry process for the ceramics formation. Tetrachlorosilane gas is hydrolyzed and subsequently polycondensed under H_2/O_2 atmosphere at high temperature, resuling in the formation of well-condensed silica nanoparticles. Spray-drying of melt quartz is another dry process of a synthetic method to silica nanoparticles. These dry processes are advantageous for facile mass production of silica nanoparticle powders, due to the

productivity and solvent-free convenience. Meanwhile, it is difficult to control the particle size and to avoid unfavorable aggregation. Instead, many researchers have favored the following wet process, which is appropriate for small-scale production of monodisperse silica nanoparticles with well-controlled sizes and shape. Nanoparticles grow up from silica precursors such as liquid glasses and alkoxysilanes under the controlled pH and concentrations in solution.[64] In this section, various wet processes in recent reports are summarized, and the issues of conventional methods are discussed. First, the formation mechanism of a polysiloxane network from silica precursors is explained briefly.

1.1.3.1 Formation mechanism of polysiloxane networks

Solution processes of forming polysiloxane networks have permitted the formation of not only ordinary silica nanoparticles but also their derivatives such as hollow nanoparticles and mesoporous nanoparticles. Also, various organic and metal species have been hybridized with polysiloxane networks under moderate reaction temperature.[65,66] Most of the applications in section 1.1.2 depend on the solution processes.

The formation mechanism of polysiloxane networks from alkoxysilanes using solution processes has already been investigated in detail.[67] Alkoxysilanes form polysiloxane networks through two different steps consisting of (i) hydrolysis of alkoxy groups and (ii) subsequent condensation of resulting silanol groups. First, an alkoxy group bonded covalently to silicon atom replaced with a hydroxyl group (Figure 1.8a). Second, a silanol group reacts with each other or with unreacted alkoxy group to form a siloxane bond (Si-O-Si) (Figure 1.8b, c). Both steps are accompanied with the generation of by-products of water or alcohol. Influential factors on hydrolysis and

polycondensation are described as below.

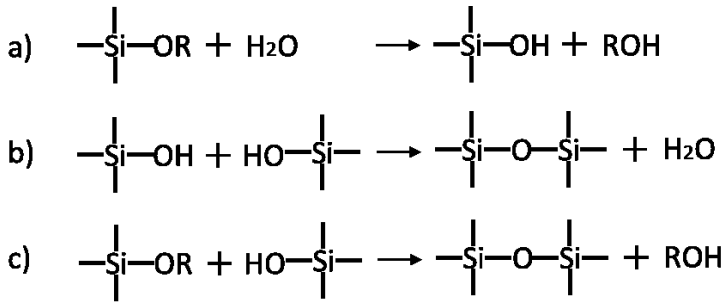

Figure 1.8. Formulae of siloxane bond formation, which consists of (a) hydrolysis of alkoxysilanes, (b) dehydration condensation, and (c) dealkoxylation condensation. R represents an organic functional group, in which small alkanes such as methyl and ethyl groups are usually used.

The process is strongly dependent on pH value of solution. When hydrolysis is catalyzed with hydrochloric acid (HCl) or ammonia (NH_3), there is a definite difference in the structures of resulting nanoparticles that are prepared under the presence of each catalyst.[68] In the case of acidic conditions, the hydrolysis rate is fast in the beginning, and then becomes slower with the decrease in the H_2O concentration. On the contrary, in the case of basic conditions, the hydrolysis rate is lower than the acidic condition. Multiple alkoxy groups in an alkoxysilane molecule is ready to be completely hydrolyzed in basic condition, while monomers with all the unreacted alkoxy groups are present. The reason for this difference is explained by the hydrolytic mechanism and the inductive effect, as follows. In acidic conditions, the protonation of alkoxy groups first occurs, and then H_2O molecules attack silicon atoms by a nucleophilic driving force (Figure 1.9a). Meanwhile, in basic conditions free OH^- ions directly attack silicon atoms under a nucleophilic driving force (Figure 1.9b). The electron-withdrawing effect of adjacent functional groups become larger after partial hydrolysis of an alkoxysilane

bearing multiple alkoxy groups (Figure 1.9c). As a result, the remaining alkoxy group in the alkoxysilane molecule is more likely to be hydrolyzed in basic condition. Inversely, the following hydrolysis is suppressed in the acidic condition. The inductive effect on hydrolysis was investigated using analogous silica precursors that are prepared by replacing methoxy groups of tetramethoxysilane with electron-donating methyl groups ($(CH_3)_nSi(OCH_3)_{4-n}$, $n > 0$).[69] Alkoxysilanes bearing more methyl groups was more rapidly hydrolyzed in acidic conditions, and its reverse tendency was observed in basic conditions.

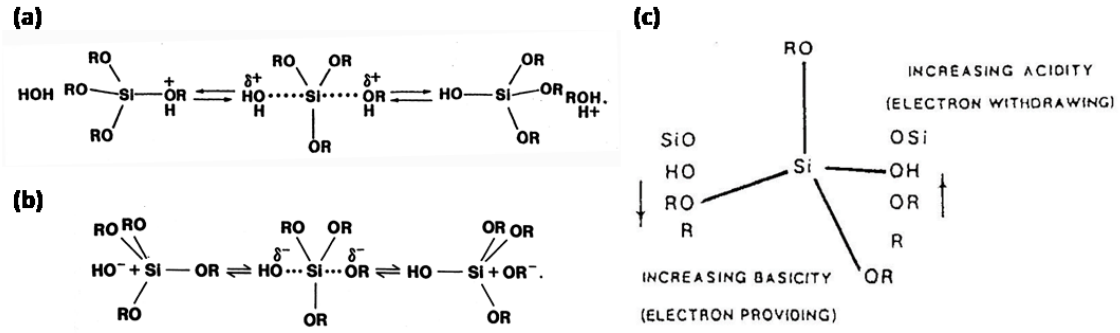

Figure 1.9. Hydrolytic mechanism of alkoxysilanes in (a) acidic condition and (b) basic condition. (c) Inductive effect of different functional groups. Reprinted with permission from C. J. Brinker and G. W.Scherer, "Sol-Gel Science" (Academic Press, Tokyo, 1990). Copyright 1990 Academic Press Inc.

Similarly, the condensation reaction is influenced by pH value of solution. In acidic condition, the H_2O/Si ratio of the precursor solution governs the condensation degree of the resulting polysiloxane networks. In lower H_2O/Si ratios, uncondensed silanol groups are likely to remain because polycondensation of silanols starts before hydrolysis of alkoxy groups are completed. Dealcoholization condensation is dominant for H_2O/Si < 2, and dehydration condensation is dominant for H_2O/Si >2.[70] By contrast, in basic condition the polysiloxane network is well-condensed regardless of the H_2O/Si

ratio, because the network is always constructed after hydrolysis of silane precursors are completed.

Size of alkoxy groups is also effective on hydrolysis process. Hydrolysis is strongly affected by bulkiness of neighboring alkoxy groups that controls the steric hindrance of nucleophilic reactions. Longer or branched alkoxy group usually reins back the reaction. The correlation between reaction rate and alkoxy groups have been successfully confirmed by Voronkov *et al*.[71]

1.1.3.2 Stöber method and derivatives

Stöber method has been widely used for synthesizing silica nanoparticles because of their size uniformity and the size tunability. In 1968, Stöber *et al.* have reported that monodisperse silica nanoparticles formed in basic aqueous solution containing ethanol molecules.[72] Two important factors are indispensable in this method. One is the presence of rich amount of ethanol. Second is the dilute concentration of silica sources. Particle size was precisely controlled by composition, pH value and reaction time of precursor solution, in which the effect of each parameters on the product has been investigated in detail by many researchers.[73,74]

There has been two prevailing formation mechanisms of silica nanoparticles by Stöber method. One is the deposition mechanism of LaMer model,[75,76] and the other is the agglomeration mechanism.[77,78] Deposition mechanism consists of two separate phases consisting of nucleation phase and nuclear growth phase, as illustrated in Figure 1.10a. When solute concentration in solution exceeds the critical supersaturation value, the nucleation phase is dominant. Once the solute concentration falls below the value, the grow phase turns preferential instead. If nucleation phase is limited to short period, all the nanoparticles can grow at the same time, resulted in the formation of

monodisperse silica nanoparticles. On the other hand, agglomeration mechanism is the model, in which primary nanoparticles of solute aggregates associate the larger nanoparticles (Figure 1.10b).

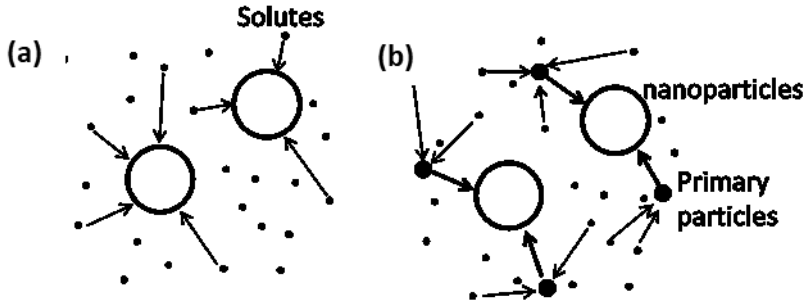

Figure 1.10. Schematic of (a) deposition and (b) agglomeration mechanism.

Stöber method has been arranged for achieving smaller sizes. Recently, Yokoi *et al.* have fabricated monodisperse silica nanoparticles of 8-35 nm in size.[79,80] The nanoparticles were synthesized from TEOS in the aqueous solution containing certain amount of octane and L-lysine. TEOS was slowly hydrolyzed at the water/oil interface, followed by voluntarily moved into the water phase. The primitive nucleus of ~4 nm in size existed in water phase at the early stage of synthesis. Then, the hydrolyzed monomers were consumed not to form a new nucleus but to grow an existing nucleus. Interestingly, the monodisperse nanoparticles were likely to be arranged with cubic closed packing structure after solvent evaporation. The nucleation phase of Yokoi method has also been investigated in detail by C. C. M. C. Carcouët *et al*.[81] Small nanoparticles of smaller than 5 nm in size actually existed at the primary stage of particle formation, but they rapidly associated to form larger nanoparticles due to the deficient stability of the small sizes (Figure 1.11). Wiesner group has modified Stöber method to develop fluorescent silica nanoparticles with color variation, named as “C

dots", for biological application.[82,83,42] Small sized nanoparticles ~3 nm in size have been prepared by termination of particle growth by in-situ surface modification with polyethylene glycol in order to avoid undesirable aggregation. Fluorescent dyes were contained in ultra-small silica nanoparticles, where their particle size is small enough for cellular uptake (Figure 1.12).

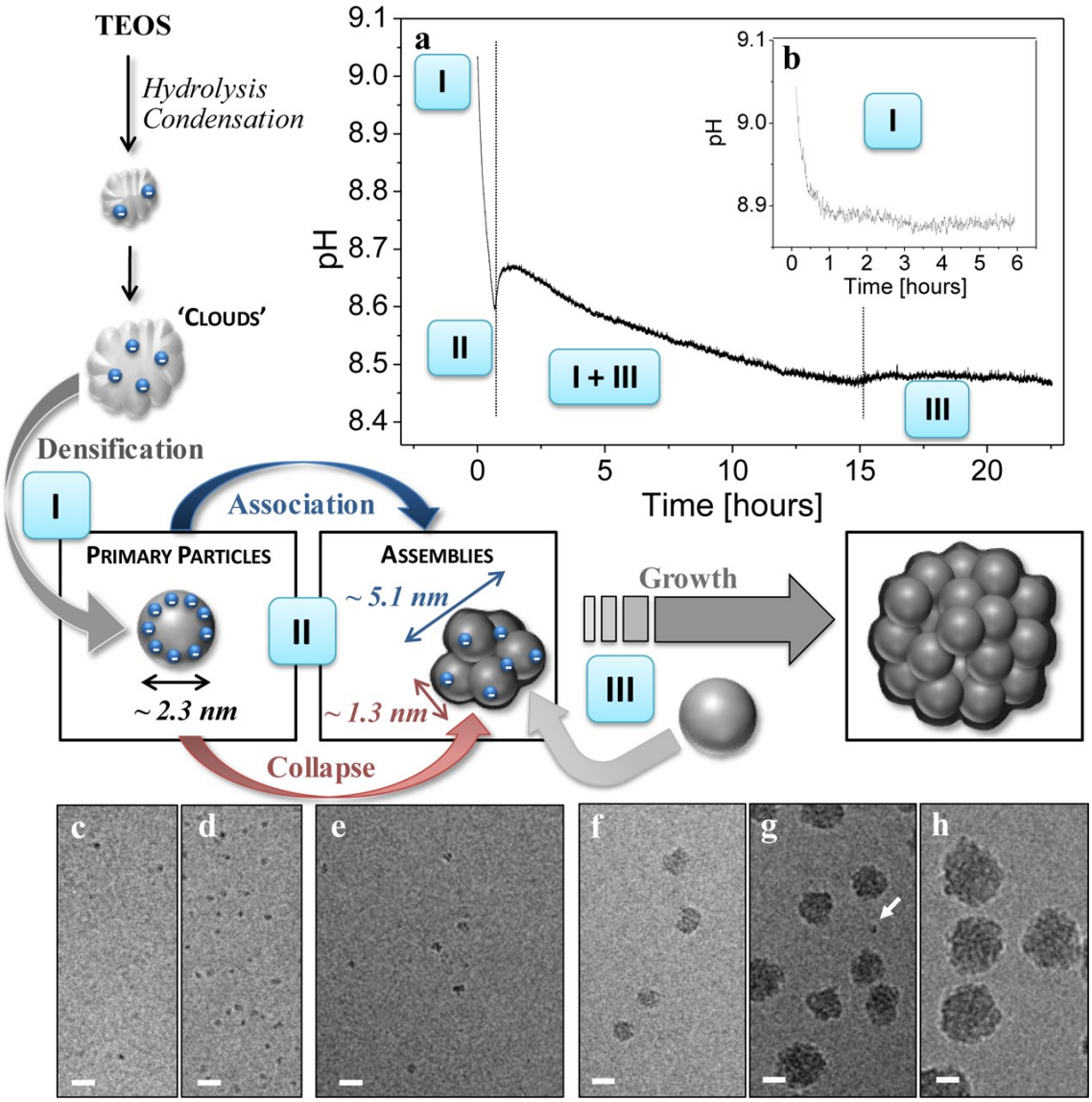

Figure 1.11. Schematic representation of the formation mechanism, combined with (a,b) pH monitoring during particle formation and (c-h) Cryo-TEM images of the dispersion at several reaction times of (c) 30 min, (d) 40 min, (e) 45 min, (f) 2 h, (g) 7 h,

and (h) 24 h. Scale bars: 10 nm. Reprinted with permission from C. C. M. C. Carcouët, M. W. P. van de Put, B. Mezari, P. C. M. M. Magusin, J. Laven, P. H. H. Bomans, H. Friedrich, A. C. C. Esteves, N. A. J. M. Sommerdijk, R. A. T. M. Benthem, and G. With, "Nucleation and Growth of Monodisperse Silica Nanoparticles", *Nano Lett.* **2014**, *14*, 1433. Copyright 2006 American Chemical Society.

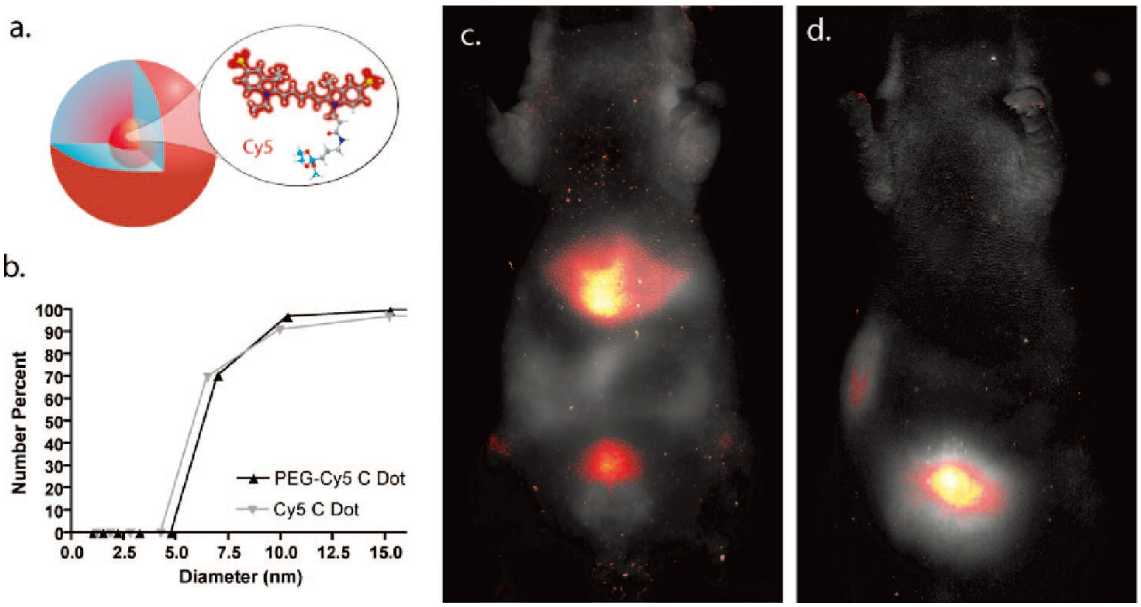

Figure 1.12. (a) Schematic representation of C dots. (b) Dynamic light scattering profile of C dots. (c, d) In vivo imaging of fluorescence in C dots overlaid on nude mice, where the surface of C dots was bare silica (c), and preliminarily modified with polyethylene glycol (d). Reprinted with permission from A. A. Burns, J. Vider, H. Ow, E. Herz, O. Penate-Medina, M. Baumgart, S. M. Larson, U. Wiesner and M. Bradbury, "Fluorescent Silica Nanoparticles with Efficient Urinary Excretion for Nanomedicine", *Nano Lett.* **2009,** 9, 442. Copyright 2009 American Chemical Society.

1.1.3.3 Reverse micelle method and derivatives

Water and oil phases can coexist in the presence of surfactants, where the water phase is entrapped inside surfactant micelles. This nanoscale organization is called W/O (water in oil) emulsion. It is possible to apply the confined space of water phase to a template of silica nanoparticle formation.[84] Good dispersibility and size uniformity of the resulting nanoparticles are derived from the surface surfactants and the stability of

emulsion templates, respectively. In a typical emulsion consisting of sodium sulfosuccinate surfactants in co-solvent of water/*n*-heptane, the size is adjustable by tuning the water/surfactant ratio. K. S. Finnie *et al.* have investigated the formation mechanism of silica nanoparticles using emulsion of nonylphenyl ether (C_9H_{19}-C_6H_4-$(OCH_2CH_2)_5OH$).[85] Silica precursors of tetramethoxy silane (TMOS) diffused into a preferentially formed emulsion, and quickly hydrolyzed to form silica nanoparticles of ~5 nm in size in pH 1.05. In contrast, the slow hydrolysis after the diffusion of TMOS into an emulsion resulted in the formation of silica nanoparticles of ~11 nm in size in pH 10.85. The stability of emulsion was confirmed by no precipitation in the acidic solution after retention of 48 h.

This method is also available for the surface coverage with silica shell around various nanoparticles. Koole *et al.* have synthesized quantum dots (QDs)@SiO_2 core-shell nanoparticles.[86] After surface ligands of QDs were replaced with hydrolyzed silica monomers, the QDs diffused into an emulsion, followed by silica shell formation (Figure 1.13). Interestingly, the location of QDs were shifted outwards when adhesive ligands were chosen as a protection layer of QDs.

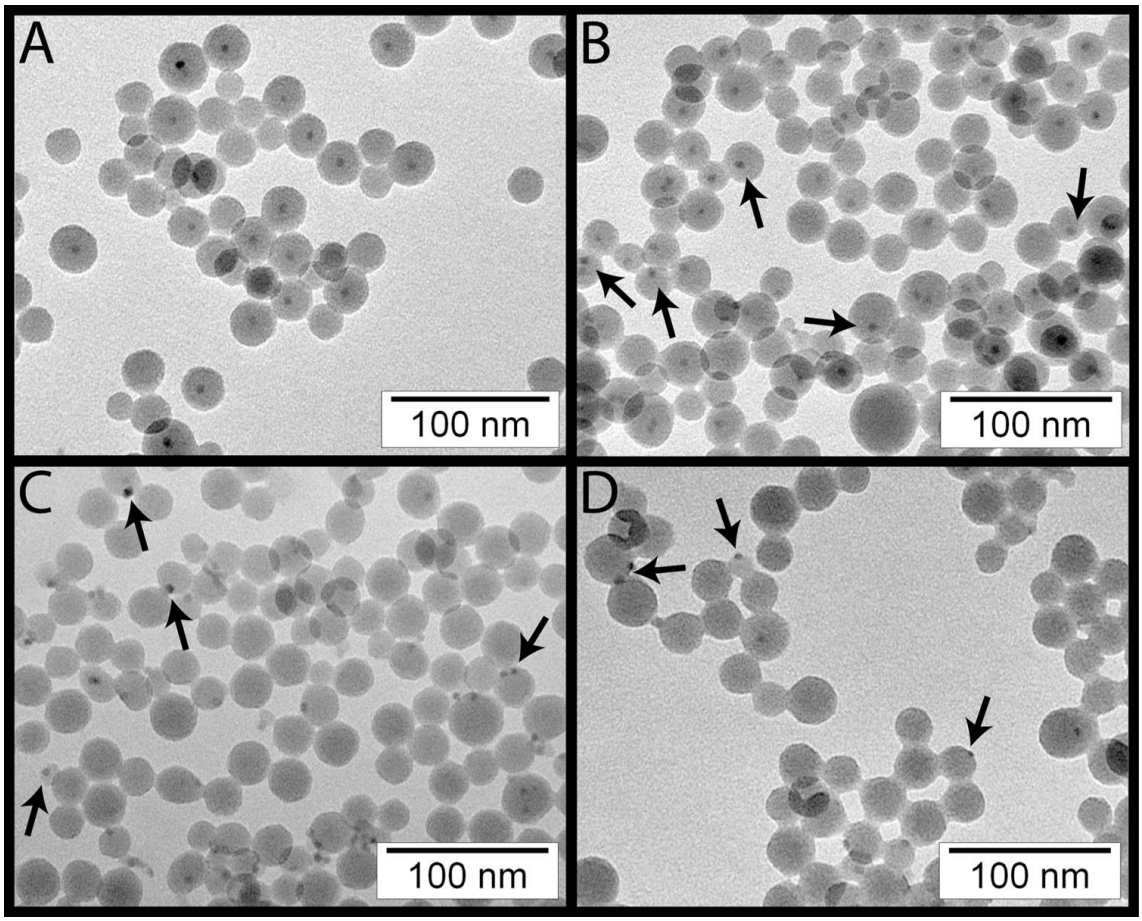

Figure 1.13. TEM images of QDs@SiO_2 nanoparticles synthesized in W/O emulsion. An adhesive ligand of dodecylthiol was added corresponding to (A) 0, (B) 10, (C) 100, or (D) 500 monolayers to the QDs before core-shell formation. Reprinted with permission from R. Koole, M. M. Schooneveld, J. Hilhorst, C. M. Donegá, D. C. Hart, A. Blaaderen, D. Vanmaekelbergh and A. Meijerink, "On the Incorporation Mechanism of Hydrophobic Quantum Dots in Silica Spheres by a Reverse Microemulsion Method", *Chem. Mater.* **2008**, 20, 2503. Copyright 2008 American Chemical Society.

1.1.3.4 Other synthetic methods to silica nanoparticles

There has emerged new techniques to produce silica nanoparticles bearing unique shapes and functionalities. Here are the introductions of other synthetic approaches to monodisperse silica nanoparticles.

Top-down approach is a smart technique for synthesizing a unique silica nanoparticle, which is based on destruction of hierarchical structures. Li *et al.* have

fabricated silica nanoparticles by disassembling a mesoporous silica that was a replica of an opal colloidal crystal in weak acidic condition (Figure 1.14).[87] The nanoparticle shape was uniquely cubic, which was not accessible by the conventional methods. Remarkably, the crystallinity of hierarchical structures is retained to the resulting nanoparticles in this method.[88, 89] Lee *et al.* have synthesized zeolite nanoparticles of 10-40 nm in size by ultrasonic treatment of mesoporous zeolite (silicalite-1). The crystalline nanoparticle was useful as a seed for the epitaxial growth of silicalite-1 thick film, by spreading nanocrystals on alumina foundation and following secondary growth of the crystal.

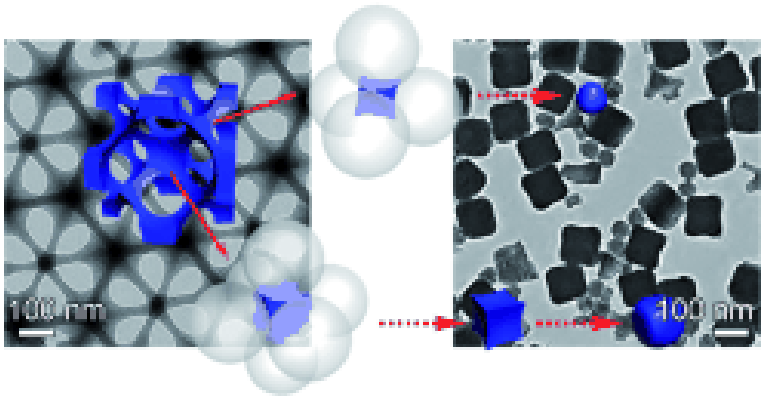

Figure 1.14. TEM images of (left) the silica replica of a colloidal crystal, and (right) the resulting nanoparticles after the destruction. Reprinted with permission from F. Li, Z. Wang, A. Stein, "Shaping Mesoporous Silica Nanoparticles by Disassembly of Hierarchically Porous Structures", *Angew. Chem. Int. Ed.* **2007**, 46, 1885. Copyright 2006 Wiley-VCH Verlag GmbH & Co. KGaA.

Block copolymers consisting of two or more different segments transform into core-shell or core-shell-corona spheres in specific solvents. The size and structure of these spheres are tuned by designing chain length and hydrophilic/hydrophobic nature of each segment in a block copolymer. These block copolymer spheres have been

employed as a template of silica nanoparticle formation. Huo *et al.* have first proposed this method for fabricating silica nanoparticles of ~10 nm in size using F127 as a core-shell template.[90] The release rate of incorporated drugs from the silica nanoparticle was slower than the case of the silica-free core-shell structure. Khanal *et al.* have prepared silica hollow nanoparticles by the selective deposition of silica in the shell region of the poly(styrene-*b*-2-vinylpyridine-*b*-ethylene oxide) (PS-PVP-PEO) core/shell/corona structure, in which PVP acted as an acidic catalyst for silica formation. (Figure 1.15).[91]

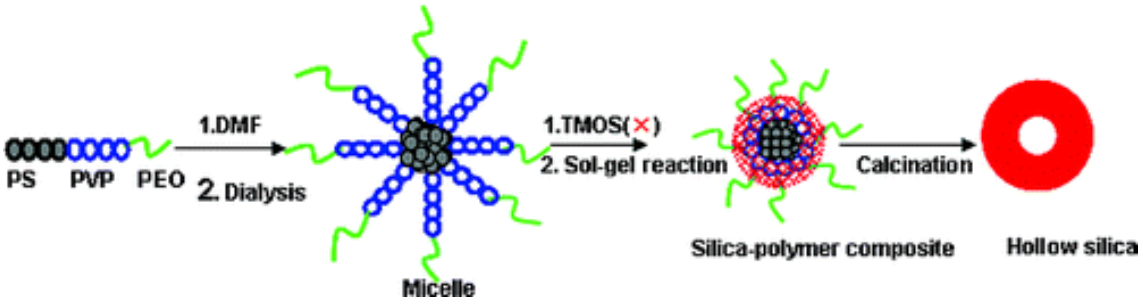

Figure 1.15. Schematic representation of forming hollow silica nanoparticles using PS-PVP-PEO core-shell-corona templates. Reprinted with permission from A. Khanal , Y. Inoue , M. Yada , and K. Nakashima, "Synthesis of Silica Hollow Nanoparticles Templated by Polymeric Micelle with Core−Shell−Corona Structure", *J. Am. Chem. Soc.* **2007**, 129, 1534. Copyright 2007 American Chemical Society.

When using a template for the synthesis of silica nanoparticles, the size uniformity of templates decides the dispersity of silica nanoparticles. Suzuki *et al.* demonstrated the use of metal-organic-frameworks (MOFs) containing molecularly defined nanospaces inside as a template (Figure 1.16).[92] The size uniformity of the resulting nanoparticle was determined on the basis of the M_w/M_n value of < 1.01. The amount of SiO_2 units was calculated to be 170 in one nanoparticle of 2.9 nm in

diameter.

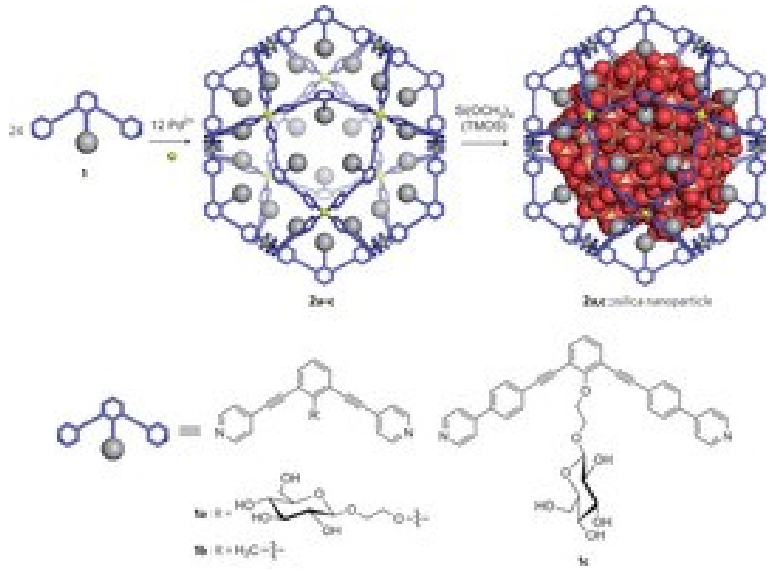

Figure 1.16. Synthetic scheme of monodisperse silica nanoparticles using a MOFs template of a glucose derivative with 12 metal ions and 24 bispyridyl ligands. Reprinted with permission from K. Suzuki, S. Sato, and M. Fujita, "Template synthesis of precisely monodisperse silica nanoparticles within self-assembled organometallic spheres", *Nat. Chem.* **2010**, 2, 25. Copyright 2010 Macmillan Publishers Limited.

Organic chemistry permits the bottom-up synthesis of silica-based nanoparticles with molecularly designed architectures. Du *et al.* proposed a branched dendrimer-like hybrid nanoparticles, which showed excellent biocompatibility and high surface area.[93] Different size of drugs and genes were simultaneously incorporated into the bimodal pores of the dendrimer-like nanoparticles. Kawahara *et al.* reported crystal-like nanoparticles by the stepwise silylation of polyhedral oligomeric silsesquioxanes (POSSs).[94] Unfortunately, there is inconvenience in synthesizing the larger sizes (>2 nm) due to their synthetic difficulty.

Crystalline nanoparticles can be prepared by the conversion of amorphous silica nanoparticles. Awala *et al.* have fabricated zeolite nanoparticles of 10-15 nm in

size by reacting amorphous silica nanoparticles with aluminum powder in basic solution.[95] Thanks to high surface area and thermal stability, the nanoparticle exhibited large micropore volume (0.30 cm^3/g), catalytic performance on dealkylation reaction of 1,3,5-triisopropylbenzen, and good dispersibility in a solvent (Figure 1.17).

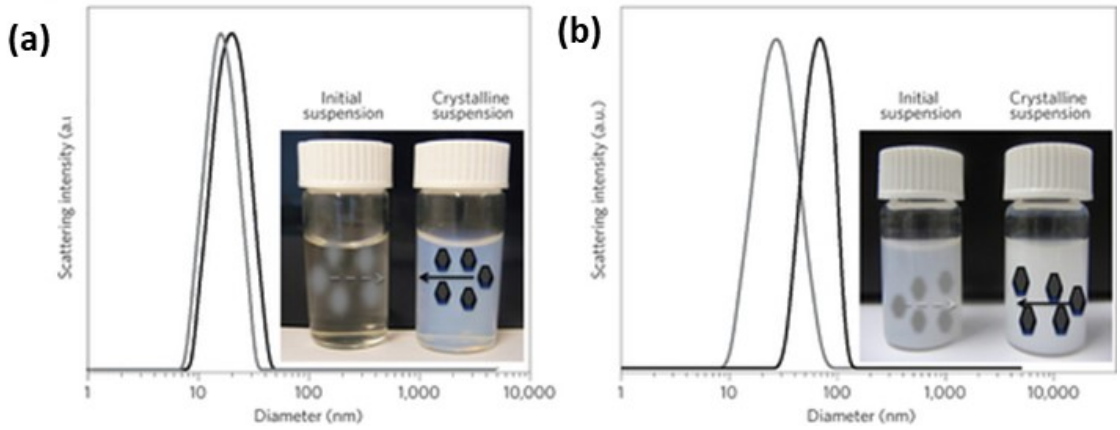

Figure 1.17. Dynamic light scattering curves of the primary (grey line) and crystalline (black line) nanoparticle suspensions of (a) 10 nm and (b) 70 nm in size. Inset is the photographs. Reprinted with permission from H. Awala, J. -P. Gilson, R. Retoux, P. Boullay, J. -M. Goupil, V. Valtchev, and S. Mintova, "Template-free nanosized faujasite-type zeolites", *Nat. Mater.* **2015**, 14, 447. Copyright 2015 Macmillan Publishers Limited.

As described above, there have been many reports about the formation of monodisperse silica nanoparticles and their derivatives such as mesoporous silica nanoparticles, hollow silica nanoparticles, cubic silica nanoparticles, and crystalline nanoparticles. The conventional synthetic routes such as Stöber method and reverse-micelle method cannot achieve silica nanoparticles smaller than 5 nm in diameter. In contrast, there has been some solution to break through the size limitation using metal-organic framework templates[92] or *in-situ* surface silylation.[42] Unfortunately, however, it is necessary to overcome the synthetic difficulty and the limitation of composition for facile use of the small silica nanoparticles. This thesis newly proposes a

convenient and simple synthetic procedure to such a small silica nanoparticle, by using a reverse-type mesostructure as an intermediate. In the next section, variations and formation mechanisms of conventional mesostructures are summarized for basic understanding of a reverse-type mesostructure.

1.2 Silica mesostructure

1.2.1 Silica mesostructure

Since the discovery of silica mesostructures in the end of 1980's, up to date an enormous amount of relevant studies have been carried out all over the world. Two kinds of matured technologies have been integrated to establish this new material concept. One is the solution process of synthesizing inorganic ceramics, and the other is the micelle formation of organic amphiphiles. The synthetic approach to silica mesostructructure is based on cooperative self-organization behavior of amphiphiles and silica precursors. Assembling behavior of amphiphiles are suitably explained using a geometrical packing parameter of steric structures.[96] This parameter is calculated through the formula of $g = v / l_c a_0$, in which g, v, l_c, and a_0 indicate packing parameters, occupied volume of hydrophobic area, hydrophobic length, and surface area of hydrophilic head, respectively (Figure 1.18). Amphiphiles are assembled into four different structures on the basis of the packing parameter, as shown in Figure 1.19. Silica mesostructures have been synthesized by the formation of polysiloxane networks in the hydrophilic moiety of the periodically arranged micelles. Surfactants have been majorly utilized as a micellar template of the cooperative self-organization with silica precursors, while organosilane molecules have self-organized into mesostructures without surfactants via the self-templating.

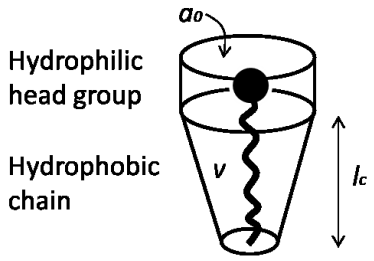

Figure 1.18. Schematic image of a packing parameter.

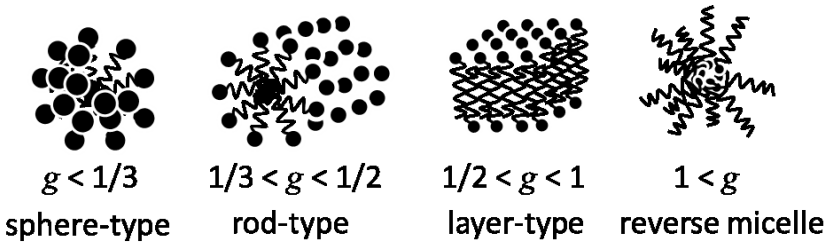

Figure 1.19. Relationship between packing parameter and assembling structures of amphiphiles.

1.2.2 Cooperative self-assembly of silica precursors and surfactants

Yanagisawa *et al.* have first fabricated a silica mesostructure ahead of other reports in the world. A layered silicate of kanemite was fragmented after the intercalation of alkyltrimethylammonium salts, and subsequently formed silica mesostructure through the cooperative self-organization of the salts and the fragmented silicate species.[97,98] Shortly thereafter, Kresge *et al.* have proposed convenient procedure using alkoxysilanes as a precursor for the formation of M41S family including MCM-41, 48, 50.[99-100] Until now, various types of mesostructures have been established by arranging surfactant species and composition of precursor solutions (Figure 1.20).[101]

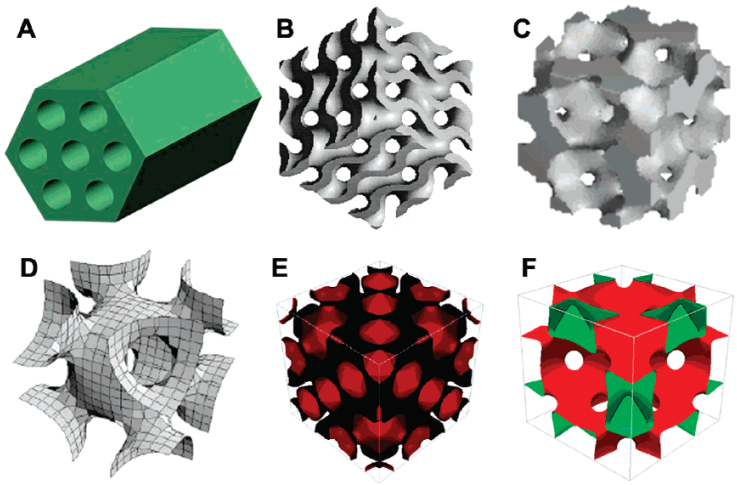

Figure 1.20. 3D modelling of various mesostructures; (A) *p6mm*, (B) $Ia\bar{3}d$, (C) $Pm\bar{3}n$, (D) $Im\bar{3}m$, (E) $Fd\bar{3}m$, and (F) $Fm\bar{3}m$. Reprinted with permission from Y. Wan, and D. Zhao "On the Controllable Soft-Templating Approach to Mesoporous Silicates", *Chem. Rev.* **2007**, 107, 2821. Copyright 2007 American Chemical Society.

1.2.2.1 Formation mechanism of silica mesostructure

Surfactant species can form various liquid-crystalline phases, which are periodic arrangements of surfactant micelles, depending on the geometrical packing parameter. Silica mesostructures are formed after polysiloxane formation in the hydrophilic moiety of the liquid-crystalline phases. Until now, there have been many reports about the formation mechanism of such a periodic mesostructure using analytical techniques, such as nuclear magnetic resonance (NMR) and small-angle X-ray scattering (SAXS). Beck *et al.* have proposed two hypothese about the formation mechanism of a typical rod-type mesostructure (MCM-41).[100] One was multistep route. Rod-type assembly consisting of only surfactants is aligned with six-fold symmetry, and then anionic silica precursors are penetrated into the cationic area in liquid-crystalline phase for the charge compensation (Figure 1.21(a)). The other was the cooperative self-organization route. Anionic silica precursors and cationic surfactants are

concertedly self-organized into periodic structures (Figure 1.21(b)). Liquid crystal phases are not observed in the precursor solution as a result of *in-situ* ^{14}N NMR analysis. On the other hand, J.Frasch *et al.* have concluded that the polysiloxane formed near surfactant micelles. Here, the surfactant micelles are not a template but a source of surfactants for the concerted self-organization.[102] As well, M. Adachi *et al.* have proposed the multistep route, comprising the primary formation of silica cylinders in random configurations and subsequent alignment of the cylinders (Figure 1.22).[103] Nowadays, the concerted self-organization route has been supported as the possible formation mechanism.[104]

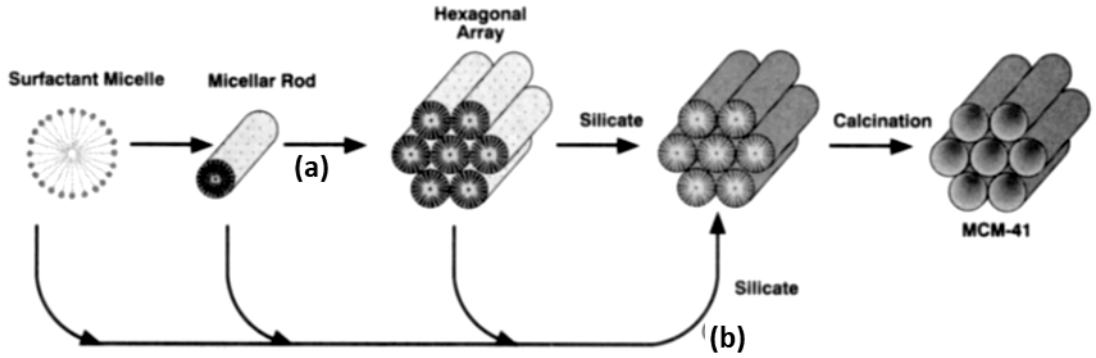

Figure 1.21. Possible formation mechanism of silica mesostructure with 2D hexagonal phase. Reprinted with permission from J. S. Beck, J. C. Vartuli, W. J. Roth, M. E. Leonowicz, C. T. Kresge, K. D. Schmitt, C. T. W. Chu, D. H. Olson, E. W. Sheppard, S. B. McCullen, J. B. Higgins and J. L. Schlenker, "A new family of mesoporous molecular sieves prepared with liquid crystal templates", *J. Am. Chem. Soc.*, **1992**, *114*, 10834. Copyright 1992 American Chemical Society.

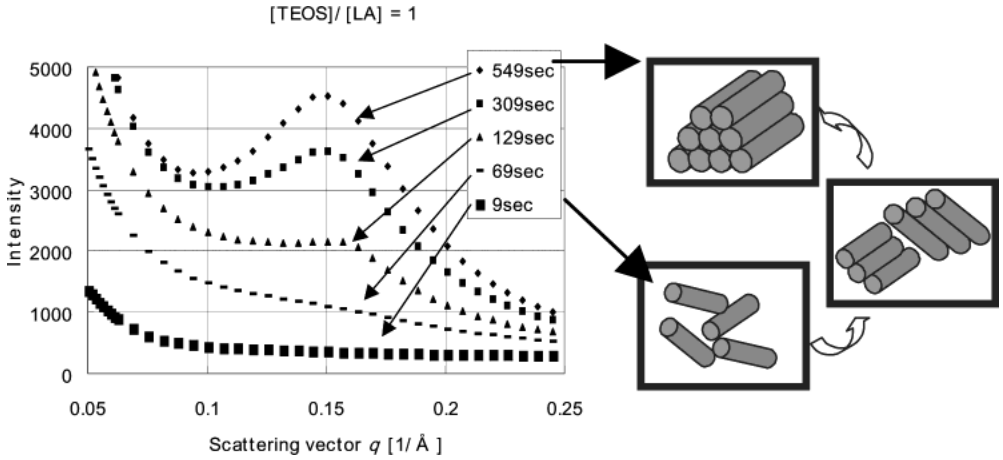

Figure 1.22. SAXS patterns at various reaction time, and considerable formation mechanism of silica mesostructure of silica. Reprinted with permission from J. S. Beck, M. Adachi, Y. Murata, K. Sago, and K. Nakagawa, "Formation Processes of the Integrated Ordered Mesostructure of Silica at Liquid-Liquid Interface Using Synchrotron Radiation X-rays" *Langmuir*, **2004**, *20*, 5965. Copyright 2004 American Chemical Society.

1.2.2.2 Variety of silica mesostructures

New types of mesostructures have been identified by structural characterization. Similar to the conventional crystallography, combination of X-ray diffraction (XRD) and transmission electron microscope (TEM) has been frequently utilized for the identification. Figure 1.23 is a typical example of structural characterization of an intricate cubic phase on the basis of TEM observation, which was further characterized by scanning electron microscope (SEM), argon gas adsorption, 3D modelling, and XRD.[105] Terasaki group has been engaged in the structural analysis of newly emerging mesostructures using an excellent microscope technique.[106-108]

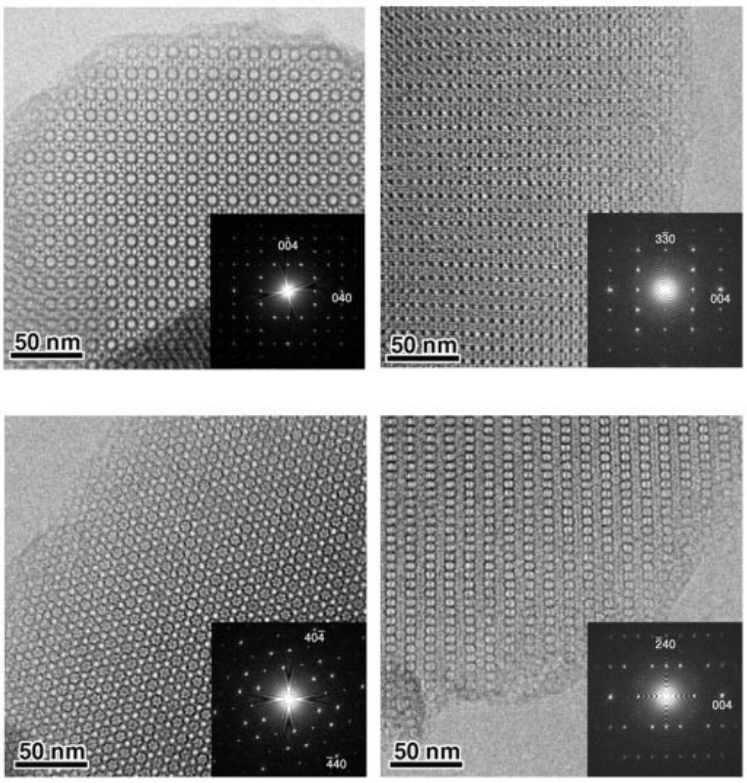

Figure 1.23. TEM images of four different crystal planes in SBA-6. Reprinted with permission from Y. Sakamoto, M. Kaneda, O. Terasaki, D. Y. Zhao, J. M. Kim, G. Stucky, H. J. Shin, and R. Ryoo, "Direct imaging of the pores and cages of three-dimensional mesoporous materials", *Nature.* **2000**, *408*, 449. Copyright 2000 Macmillan Publishers Limited.

Diagram is a facile approach for schematic understanding of the relationship between a composition of precursor solution and a resulting mesostructure. Figure 1.24 is a typical example of TEOS/NaOH/CTAB three composition diagram, reported by Firouzi *et al.*[109] Here, CTAB (cetyltrimethylammonium bromide) is one of the most familiar surfactants. Under the fixed ratio of TEOS:NaOH = 8:2, resulting mesostructures were stably shifted towards higher curvature from lamellar to gyroid and finally 2D hexagonal during the increasing TEOS/CTAB ratio of precursor solution. This was theoretically explained by expansion of hydrophilic area with hydrolyzed silica precursors. Whereas, under the fixed ratio of TEOS:NaOH = 6:4, resulting

mesostructures were conversely shifted from 2D hexagonal to lamellar for the large TEOS/CTAB ratio. In order to explain this phenomenon, other parameters should be considered. It is necessary to understand the influential parameters on the concerted self-organization for the rational design of various mesostructures.

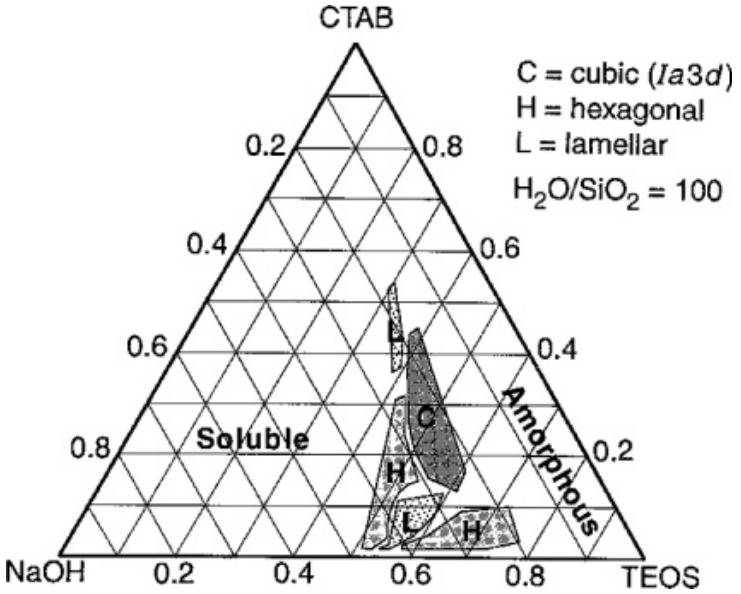

Figure 1.24. Phase diagram of mesostructures in TEOS/NaOH/CTAB three composition system. Reprinted with permission from A. Firouzi, D. Kumar, L. M. Bull, T. Besier, P. Sieger, Q. Huo, S. A. Walker, J. A. Zasadzinski, C. Glinka, J. Nicol, D. Margolese,G. D. Stucky, and B. F. Chmelka "Cooperative organization of inorganic-surfactant and biomimetic assemblies", *Science,* **1995**, *267*, 1138. Copyright 1995 American Association for the Advancement of Science.

As described above, the packing parameter of surfactants is the definitive factor on the self-organization. Wan *et al*. have summarized the relationship between *g* value of surfactants and resulting mesostructures, as shown in Table 1.1.[101] In case of $g < 1/3$, three dimensional mesostructure with a periodic arrangement of spherical micelles is formed predominantly. As the *g* value increased, the resulting mesostructure changes from rod-type assembly (2D Hexagonal; $1/3 < g < 1/2$) to 3D bicontinuous assembly

(gyroid; 1/2 < *g* < 2/3), layer-type assembly (Lamellar; *g* =1), and finally reverse micelles assembly (1 > *g*). Note that no example was introduced as a reverse-type mesostructure.

Table 1.1. Relationship between packing parameter of surfactants and resulting mesostructures. Reprinted with permission from Y. Wan, and D. Zhao "On the Controllable Soft-Templating Approach to Mesoporous Silicates", *Chem. Rev.* **2007**, *107*, 2821. Copyright 2007 American Chemical Society.

$g = V/a_0 l \rightarrow$					
$<1/3$		$1/3 < 1/2$	$1/2 < 2/3$	1	>1
spherical micelles single-chain surfactants with large headgroups, e.g., $C_nH_{2n+1}N(C_2H_5)_3X$ ($n = 12-18$), $18B_{4-3-1}$, C_{n-s-1} ($n = 12-18$)		cylindrical micelles single-chain surfactants with small headgroups, e.g., $C_nH_{2n+1}N(CH_3)_3X$ ($n = 8-18$)	3D cylindrical micelles single-chain surfactants with small headgroups, e.g., CTAB special surfactants with large hydrophobic polar head and double-chain surfactants with large headgroups and flexible chains, e.g., $C_{16}H_{33}(CH_3)_2N(CH_2)(C_6H_5)$, Gemini C_{m-12-m}	lamellar micelles double-chain surfactants with small headgroups or rigid, immobile chains, e.g., $C_nH_{2n+1}N(CH_3)_3X$ ($n = 20, 22$), $C_{16-2-16}$	reversed micelles double-chain surfactants with small groups
			Basic Synthesis		
SBA-6 (cubic $Pm\bar{3}n$)	SBA-7 (3D hexagonal $P6_3/mmc$)	MCM-41 (2D hexagonal $p6mm$)	MCM-48 (cubic $Ia\bar{3}d$)	MCM-50 (lamellar structure)	
			Acidic Synthesis		
SBA-1 (cubic $Pm\bar{3}n$)	SBA-2 (3D hexagonal $P6_3/mmc$)	SBA-3 (2D hexagonal $p6mmc$		SBA-4 (lamellar structure)	

The packing parameter of surfactants can be controlled by their molecular design. Huo *et al.* have investigated the effects of molecular structures on their self-organization by comparing cetyltrimethyl ammonium ions with the analogous surfactants bearing a dimer head, a larger head, a bifunctional chain, and a longer chain.[110]. The result was good agreement with the theory of the packing parameter, as shown in Table 1.2.

Table 1.2. Relationship between the packing parameter of various cationic surfactants and resulting mesostructures. Reprinted with permission from Q. Huo, D. I. Margolese and G. D. Stucky, "Surfactant Control of Phases in the Synthesis of Mesoporous Silica-Based Materials", *Chem. Mater.* **1996**, *8*, 1147. Copyright 1996 American Chemical Society.

	Surfactant		Composition (mole, $SiO_2 = 1.0$)					product
no.	R	trait	R	HX (or MOH)	H_2O	additive	temp/time	phase
1	$C_{16-10-16}$	dimer	0.06	4.9 HCl	130		RT/1 h	SBA-3
2	$C_{16-12-16}$	dimer	0.05	0.62NaOH	115		100 °C/10 days	MCM-48
3	$C_{16}TMA^+$	normal	0.12	9.2 HCl	130		RT/1 h	SBA-3
4	C16TMA$^+$	normal	0.12	4.9 HBr	130		RT/1 h	SBA-3
5	$C_{16}H_{33}N(C_3H_7)_3^+$	big head group	0.12	4.9 HBr	130		RT/1 h	SBA-3
6	$C_{16}H_{33}N(C_2H_5)_3^+$	big head group	0.13	10.4 HCl	130		RT/1 h	SBA-1
7	$C_{16}H_{33}N(C_2H_5)_3^+$	with additive	0.13	10.4 HCl	130	0.61 *t*-AmOH	RT/1 h	SBA-3
8	$C_{20}TMA^+$	long chain	0.12	4.9 HCl	130		RT/1 h	lamellar
9	$(C_{12}H_{25})_2N(CH_3)_2^+$	bichain	0.12	6.2 HCl	150		RT/1 h	lamellar
10	$(C_{12}H_{25})_2N(CH_3)_2^+$	bichain	0.12	0.7 NaOH	150		100 °C/10 days	MCM-50
11	$C_{16}TMA^+$	normal	0.28	0.29 TMAOH	80		100 °C/16 h	MCM-41
12	$C_{16}TMA^+$	with additive	0.28	0.29 TMAOH	80	0.29 TMB	100 °C/6 h	MCM-50

Surfactants are often categorized into three types on the basis of the polarity of a head group; cationic,[99, 111-115] anionic,[116-120] and nonionic surfactants.[121-126] Some mesostructures indicate the distinctive properties that are derived from the surfactant types. In the case of nonionic surfactant templates, there existed micropores in the framework of mesoporous silica after the removal of surfactants by calcination or extraction.[124] Hydrophilic heads of nonionic surfactants are penetrated into the silica framework. In the meantime, when using anionic surfactants possessing chiral center, the resulting mesostructure appeared distinctive helical morphologies.[119]

The self-organization behavior is also adjusted by sault addition. Ions can compensate the charge of surfactants and accordingly reduce the apparent size of head groups, resulted in the preferential formation of mesostructures with lower curvature. Che *et al.* confirmed that the effect of salts was larger in the order corresponding to Hofmeister series of NO_3^- > Cl^- > SO_4^{2-} when using a cationic surfactant as a template.[127]

Ionization degree of head group in surfactants can be tuned by pH value. Gao

et al. proved that the alkalinity of solution was a decisive factor for consequent mesostructures in an anionic surfactant system.[128] Meanwhile, polycondensation reaction is accompanied by a reverse reaction to form silanol groups in the basic condition, which can also affect the self-organization behavior.

An organic additive acts as an expander of the hydrophobic moiety in a self-organized mesostructure. The location of such an additives depends on the molecular size. Small additives are likely to accumulate at the interface between water and oil phases, on the other hand large additives exist in hydrophobic moieties of surfactant assemblies. In the case of some alcohol additives, the periodicity of resulting mesostructures was well-ordered because there emerges the enough time for self-organization by slowing the condensation reaction. Kleitz *et al.* expanded the composition window for successful synthesis of cubic mesoporous silica by adding butanol as a phase-controlling agent in the presence of nonionic blockcopolymer templates (Figure 1.25).[129]

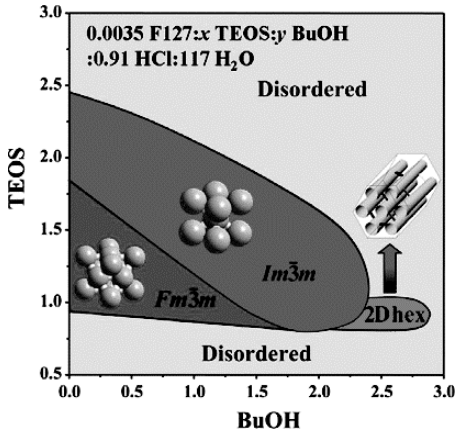

Figure 1.25. Phase diagram of mesostructures in TEOS/BuOH two composition system in F127/TEOS/BuOH/HCl/H_2O system. Reprinted with permission from F. Kleitz , T. W. Kim, and R. Ryoo, "Phase Domain of the Cubic $Im\bar{3}m$ Mesoporous Silica in the $EO_{106}PO_{70}EO_{106}$−Butanol−H_2O System", *Langmuir,* **2006**, 22, 440. Copyright 1996 American Chemical Society.

Many mesoporous silica materials have been synthesized by hydrothermal treatment, which induces the precipitation of a silica mesostructure in uniform water-based solution. While, evaporation induced self-assembly (EISA) is another convenient procedure of the synthesis. A micelle formation is induced by the increasing concentration of compositions including silica precursors and surfactants during the solvent evaporation. Grosso *et al.* characterized the *in-situ* phase transition of mesostructures in EISA process by SAXS annalysis.[130] In the process to form a cubic $Pm\overline{3}n$ mesostructure, lamellar and 2D Hexagonal phases existed at the interface of air-side, and 3D Hex phase existed at the interface of substrate-side, as shown in Figure 1.26. This phenomenon was derived from the heterogeneity of surfactant concentrations during solvent evaporation.

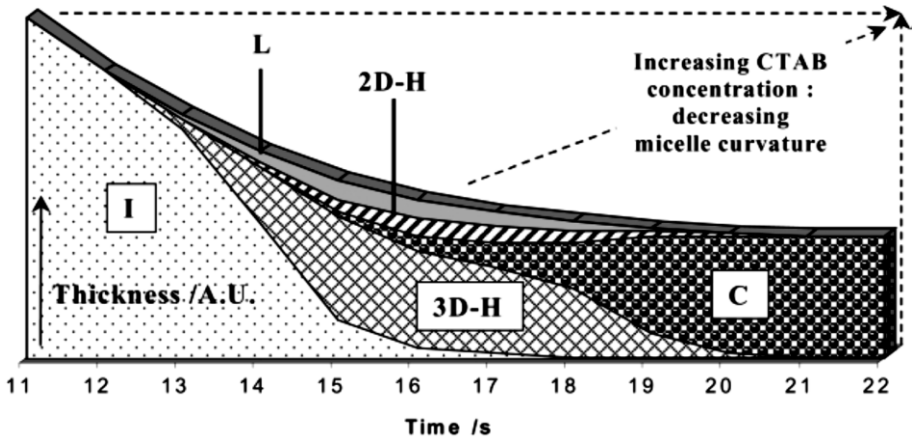

Figure 1.26. Diagram of the mesophase transition during the EISA process. **L**, **2D-H**, **3D-H**, and **C** represents the mesophases of lamellar, 2D hexagonal, 3D hexagonal, and cubic, respectively. Reprinted with permission from D. Grosso, F. Babonneau, G. J. A. A. Soler-Illia, P. -A. Albouy and H. Amenitsch , "Phase transformation during cubic mesostructured silica film formation", *Chem. Commun.* **2002**, 0, 748. Copyright 2002 Royal Society of Chemistry.

1.2.3 Self-assembly of organoalkoxysilanes

Partial organoalkoxysilanes, where hydrophobic organic groups and alkoxygroups are covalently bonded to Si atom, are converted into amphiphiles after hydrolysis of alkoxy groups. The amphiphiles are subsequently self-organized without structure-directing agents of surfactants, and polycondensed to form a silica-organic hybrid mesostructures. Until today, various organoalkoxysilanes have been demonstrated to self-organize into silica-organic hybrid mesostructures.

Shimojima *et al.* have studied the self-organization of diverse organoalkoxysilane molecules bearing a long saturated alkyl chain. Alkyltriethoxysilanes have self-organized into a lamellar structure, and the repeating pitch of the mesostructure was well correlated with the alkyl chain length of starting molecules.[131] When using the precursors bearing a larger head group of $-Si(OSi(OCH_3)_3)_3$, mesostructures with high curvature (2D hexagonal and 2D monoclinic) were formed as shown in Figure 1.27.[132-134] When using precursors bearing a longer alkyl chain, the lamellar mesostructure with the lower curvature was formed instead. Consequently, self-organization of organoalkoxysilane molecules depended on the packing parameter similar to the surfactant system. It's notable that the formation of a 2D monoclinic mesostructure has not been prepared by cooperative self-organization of silica precursor and surfactants. The 2D monoclinic mesostructure seems to be stably formed, owing to the limited mobility of covalently-connected alkyl chain and oligosiloxane head.

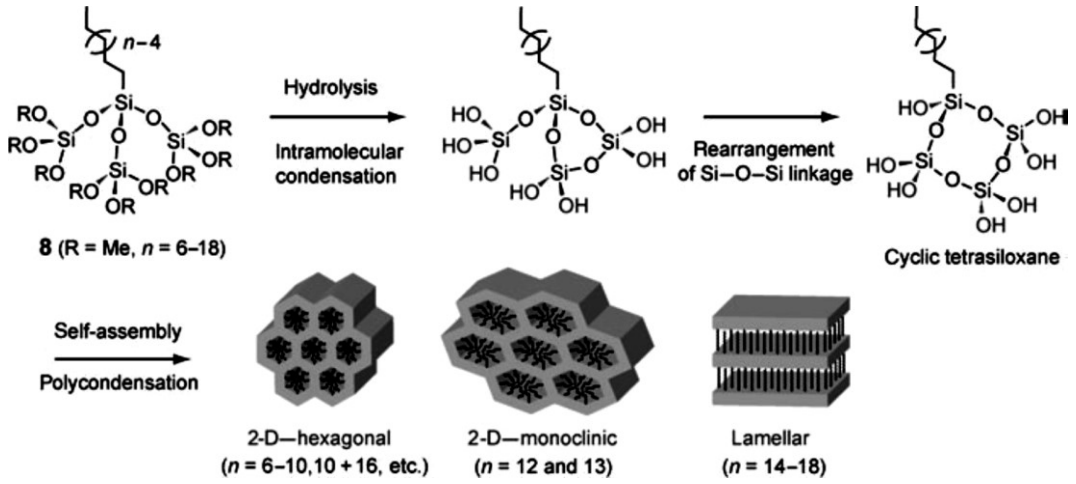

Figure 1.27. Reaction and self-organization scheme of alkyltetrasiloxane molecules. Reprinted with permission from A. Shimojima and K. Kuroda "Designed synthesis of nanostructured siloxane‐organic hybrids from amphiphilic silicon-based precursors" *Chem. Rec.* **2006**, *6*, 53. Copyright 2006 John Wiley & Sons, Inc.

Organically bridged alkoxysilanes ($(RO)_3Si$-R'-$Si(OR)_3$, OR is an alkoxy group, and R' is an organic bridge) have also self-organized to form hybrid mesostructures. In addition to the hydrophobic/hydrophilic interaction in amphiphiles, the interaction between adjacent organic bridges affects their structuring. Moreau *et al.* have exhibited the impact of hydrogen bonds on the formation of lamellar mesostructure using precursors bearing urea moieties in alkylene bridges.[135] Novel properties can be macroscopically induced by the orientation of organic bridges. Brinker *et al.* have demonstrated the utility of well-aligned azobenzene bridges in a lamellar mesostructure.[136] The d_{100} value of diffraction peak in the XRD pattern reversibly changed under the ultra-violet (UV) light and visible (Vis) light irradiation, indicative of variable interlayer spacing corresponding to the *cis*/*trans* photoisomerization of azobenzene bridges (Figure 1.28).

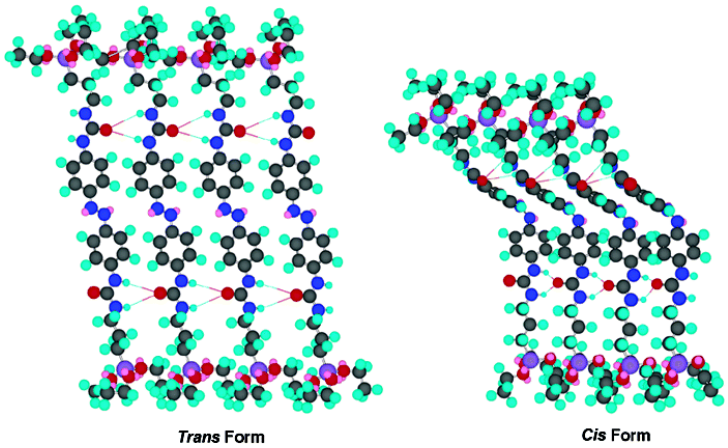

Figure 1.28. Illustrations of two different supramolecular structures, which were prepared by hydrolysis and subsequent solvent-evaporation of organically bridged alkoxysilanes bearing an azobenezene group. Reprinted with permission from N. Liu, K. Yu, B. Smarsly, D. R. Dunphy, Y. -B. Jiang, and C. J. Brinker "Self-Directed Assembly of Photoactive Hybrid Silicates Derived from an Azobenzene-Bridged Silsesquioxane" *J. Am. Chem. Soc.* **2002**, *124*, 14540. Copyright 2002 American Chemical Society.

1.2.4 Reverse micelle type mesostructures

Most of silica mesostructures are composed of well-arranged micelles with hydrophobic core and outer silica network, in which each micelles are covalently connected to each other. On the other hand, silica network is isolated within every micelles in reverse micelle type mesostructures. Micelles are retained by the weak van der Waals force between individual organic shells, therefore readily dissociated to form silica nanoparticles in an organic solvent. Size uniformity and small sizes are expected to thus prepared nanoparticles on the basis of the periodicity and repeating pitch of individual micelles in the mesostructure. Garcia *et al.* have successfully synthesized the silica/alumina nanoparticle using a reverse micelle type mesostructure as a template of inorganic nanoparticle formation.[137] The mesostructure was prepared by EISA process of diblock copolymer (poly(isoplane-*b*-ethylene oxide)). Formation of reverse micelle type mesostructures has been limited to the case of polymer templates.[137-139]

Unfortunately, polymer templates tend to leave micropores in silica networks after removing the template, and there is a difficulty in synthesizing single-digit nanometer scale nanoparticles due to their large repeating pitch. If such a reverse micelle type mesostructure is synthesized by self-organization of organoalkoxysilanes or cooperative self-organization of surfactants and silica precursors, monodisperse silica nanoparticles smaller than 5 nm in size can be readily prepared.

1.3 References

1 S. Sivasankar and S. Chu, *Nano Lett*. **2007**, *7,* 3031.

2 Y. Hoshikawa, H. Yabe, A. Nomura, T. Yamaki, A. Shimojima, and T. Okubo, *Chem. Mater.* **2010**, *22*, 12.

3 Y. -S. Chen, W. Frey, S. Kim, P. Kruizinga, K. Homan, and S. Emelianov, *Nano Lett.* **2011**, *11*, 348.

4 G. Lapadula, A. Bourdolle, F. Allouche, M. P. Conley, I. d. Rosal, L. Maron, W. W. Lukens, Y. Guyot, C. Andraud, S. Brasselet, C. Copéret, O. Maury, and R. A. Andersen, *Chem. Mater.* **2014**, *26*, 1062.

5 Y. Sonnefraud, H. G. Sinclair, Y. Sivan, M. R. Foreman, C. W. Dunsby, M. A. A. Neil, P. M. French, and S. A. Maier, *Nano Lett.* **2014**, *14*, 4449.

6 S. H. Joo, J. Y. Park, C. -K. Tsung, Y. Yamada, P. Yang, and G. A. Somorjai, *Nat. Mater*. **2009**, *8*, 126.

7 K. X. Yao and H. C. Zeng, *Chem. Mater*. **2012**, *24*, 140.

8 W. -J. Zhou, L. Fang, Z. Fan, B. Albela, L. Bonneviot, F. D. Campo, M. Pera-Titus, and J. -M. Clacens, *J. Am. Chem. Soc.* **2014**, *136*, 4869.

9 B. Küstner, M. Gellner, M. Schütz, F. Schöppler, A. Marx, P. Ströbel, P. Adam, C. Schmuck, and S. Schlücker, *Angew. Chem. Int. Ed.* **2009**, *48*, 1950.

10 V. L. Schmit, R. Martoglio, B. Scott, A. D. Strickland, and K. T. Carron, *J. Am. Chem. Soc.* **2012**, *134*, 59.

11 D. Rodríguez-Fernández, J. Langer, M. Henriksen-Lacey, and L. M. Liz-Marzán, *Chem. Mater.* **2015**, *27*, 2540.

12 I. Makarovsky, Y. Boguslavsky, M. Alesker, J. Lellouche, E Banin, and J. -P. Lellouch, *Adv. Funct. Mater.* **2011**, *21*, 4295.

13 Y. Tao, E. Ju, J. Ren, and X. Qu, *Adv. Mater.* **2015**, *27*, 1097.

14 F. Tang, L. Li, and D. Chen, *Adv. Mater.* **2012**, *24*, 1504.

15 S. Angelos, Y. -W. Yang, N. M. Khashab, J. F. Stoddart, and J. I. Zink, *J. Am. Chem. Soc.* **2009**, *131*, 11344.

16 V. Cauda, H. Engelke, A. Sauer, D. Arcizet, C. Bräuchle, J. Rädler, and T. Bein, *Nano Lett.* **2010**, *10*, 2484.

17 L. Pan, J. Liu, and J. Shi, *Adv. Funct. Mater.* **2014**, *24*, 7318.

18 M. A. Malvindi, A. Greco, F. Conversano, A. Figuerola, M. Corti, M. Bonora, A. Lascialfari, H. A. Doumari, M. Moscardini, R. Cingolani, G. Gigli, S. Casciaro, T. Pellegrino, and A. Ragusa, *Adv. Funct. Mater.* **2011**, *21*, 2548.

19 T. Kim, E. Momin, J. Choi, K. Yuan, H. Zaidi, J. Kim, M. Park, N. Lee, M. T. McMahon, A. Quinones-Hinojosa, J. W. M. Bulte, T. Hyeon, and A. A. Gilad, *J. Am. Chem. Soc.* **2011**, *133*, 2955.

20 H. Matsushita, S. Mizukami, F. Sugihara, Y. Nakanishi, Y. Yoshioka, and K. Kikuchi, *Angew. Chem. Int. Ed.* **2015**, *54*, 1007.

21 C. -H. Lee, S. -H. Cheng, Y. -J. Wang, Y. -C. Chen, N. -T. Chen, J. Souris, C. -T. Chen, C. -Y. Mou, C. -S. Yang, and L. -W. Lo, *Adv. Funct. Mater.* **2009**, *19*, 215.

22 Li Tang, X. Yang, L. W. Dobrucki, I. Chaudhury, Q. Yin, C. Yao, S. Lezmi, W. G. Helferich, T. M. Fan, and J. Cheng, *Angew. Chem. Int. Ed.* **2012**, *51*, 12721.

23 S. Shinde, Z. El-Schich, A. Malakpour, W. Wan, N. Dizeyi, R. Mohammadi, K. Rurack, A. G. Wingren, and B. Sellergren, *J. Am. Chem. Soc.* **2015**, *137*, 13908.

24 D. R. Larson, H. Ow, H. D. Vishwasrao, A. A. Heikal, U. Wiesner, and W. W. Webb, *Chem. Mater.* **2008**, *20*, 2677.

25 J. Malinge, C. Allain, A. Brosseau, and P. Audebert, *Angew. Chem. Int. Ed.* **2012**, *51*, 8534.

26 J. Jeong, M. Cho, Y. T. Lim, N. W. Song, and B. H. Chung, *Angew. Chem. Int. Ed.* **2009**, *48*, 5296.

27 N. R. Jana, C. Earhart, and J. Y. Ying, *Chem. Mater.* **2007**, *19*, 5074.

28 T. Chen, Y. Hu, Y. Cen, X. Chu, Y. Lu, *J. Am. Chem. Soc.* **2013**, *135*, 11595.

29 J. S. Kim, W. J. Rieter, K. M. L. Taylor, H. An, W. Lin, and W. Lin, *J. Am. Chem. Soc.* **2007**, *129*, 8962.

30 C. A. Barnes, A. Elsaesser, J. Arkusz, A. Smok, J. Palus, A. Leśniak, A. Salvati, J. P. Hanrahan, W. H. de Jong, E. Dziubałtowska, M. Stępnik, K. Rydzyński, G. McKerr, I. Lynch, K. A. Dawson, and C. V. Howard, *Nano Lett.* **2008**, *8*, 3069.

31 M. A. Malfatti, H. A. Palko, E. A. Kuhn, and K. W. Turteltaub, *Nano Lett.* **2012**, *12*, 5532.

32 Z. Zhelev , H. Ohba , and R. Bakalova, *J. Am. Chem. Soc.* **2006**, *128*, 6324.

33 G. A. Sotiriou, T. Sannomiya, A. Teleki, F.Krumeich, J. Vörös, and S. E. Pratsinis, *Adv. Funct. Mater.* **2010**, *20*, 4250.

34 X. Meng, K. Fujita, S. Murai, T. Matoba, and K. Tanaka, *Nano Lett.* **2011**, *11*, 1374.

35 S. Ceylan, C. Friese, C. Lammel, K. Mazac, and A. Kirschning, *Angew. Chem. Int. Ed.* **2008**, *47*, 8950.

36 J. Shi, Y. Jiang, X. Wang, H. Wu, D. Yang, F. Pan, Y. Suad, and Z. Jiang, *Chem. Soc. Rev.* **2014**, *43*, 5192.

37 I. I. Slowing , B. G. Trewyn , and V. S. -Y. Lin, *J. Am. Chem. Soc.* **2007**, *129*, 8845.

38 F. Tang, L. Li, and D. Chen, *Adv. Mater.* **2012**, 24, 1504.

39 C. Park, K. Oh, S. C. Lee, and C. Kim, *Angew. Chem. Int. Ed.* **2007**, 46, 1455.

40 Z. -A. Qiao, P. Zhang, S. -H. Chai, M. Chi, G. M. Veith, N. C. Gallego, and M. Kidder, S. Dai, *J. Am. Chem. Soc.* **2014**, *136*, 11260.

41 W. Shang , J. H. Nuffer, J. S. Dordick , and R. W. Siegel, *Nano Lett.* **2007**, *7*, 1991.

42 A. A. Burns, J. Vider, H. Ow, E. Herz, O. Penate-Medina, M. Baumgart, S. M. Larson, U. Wiesner, and M. Bradbury, *Nano Lett.* **2009**, *9*, 442.

43 F. Li, D. P. Josephson, and A. Stein, *Angew. Chem. Int. Ed.* **2011**, *50*, 360.

44 N. Vogel, M. Retsch, C. -A. Fustin, A. Campo, and U. Jonas, *Chem. Rev.* **2015**, *115*, 6265.

45 H. Zou, S. Wu, and J. Shen, *Chem. Rev.* **2008**, *108*, 3893.

46 D. Lee, M. F. Rubner, and R. E. Cohen, *Nano Lett.* **2006**, *6*, 2305.

47 S. Sunny, N. Vogel, C. Howell, T. L. Vu, and J. Aizenberg, *Adv. Funct. Mater.* **2014**, *24*, 6658.

48 A. Bansal, H. Yang, C. Li, K. Cho, B. C. Benicewicz, S. K. Kumar, and L. S. Schadler, *Nat. Mater.* **2005**, *4*, 693.

49 P. Rittigstein, R. D. Priestley, L. J. Broadbelt, and J. M. Torkelson, *Nat. Mater.* **2007**, *6*, 278.

50 P. Akcora, H. Liu, S. K. Kumar, J. Moll, Y. Li, B. C. Benicewicz, L. S. Schadler, D. Acehan, A. Z. Panagiotopoulos, V. Pryamitsyn, V. Ganesan, J. Ilavsky, P. Thiyagarajan, R. H. Colby, and J. F. Douglas, *Nat. Mater.* **2009**, *8*, 354.

51 B. Nijs, S. Dussi, F. Smallenburg, J. D. Meeldijk, D. J. Groenendijk, L. Filion, A. Imhof, A. Blaaderen, and M. Dijkstra, *Nat. Mater.* **2015**, *14*, 56.

52 P. Agarwal, M. Chopra, and L. A. Archer, *Angew. Chem. Int. Ed.* **2011**, *50*,

8670.
53 D. Ge, E. Lee, L. Yang, Y. Cho, M. Li, D. S. Gianola, and S. Yang, *Adv. Mater.* **2015**, *27*, 2489.
54 H. Zhou, H. Wang, H. Niu, A. Gestos, X. Wang, and T. Lin, *Adv. Mater.* **2012**, *24*, 2409.
55 D. Lin, W. Liu, Y. Liu, H. R. Lee, P. -C. Hsu, K. Liu, and Y. Cui, *Nano Lett.* **2016**, *16*, 459.
56 S. Rose, A. Prevoteau, P. Elzière, D. Hourdet, A. Marcellan, and L. Leibler, *Nature*, **2014**, *505*, 382.
57 N. C. Su, Z. P. Smith, B. D. Freeman, and J. J. Urban, *Chem. Mater.* **2015**, *27*, 2421.
58 W. Heni, L. Vonna, and H. Haidara, *Nano Lett.* **2015**, *15*, 442.
59 J. G. Vail, *J. Soc. Chem. Ind.* **1925**, *44*, 214.
60 R. K. Iler. *Soil Science*, **1955**, *80*, 86.
61 R. K. Iler. *J. Colloid Interface Sci.* **1966**, *21*, 569..
62 赤崎忠行、福永登志一, *TOSOH Research & Technology Review*, **2001**, *45*, 65.
63 I. A. Rahman and V. Padavettan, *J. Nanomaterials*, **2012**, 8.
64 小松通郎、西田広泰, SEN'I GAKKAISHI (繊維と工業), **2004**, *60*, 376.
65 A. B. Descalzo, R. Martínez-Máñez, F. Sancenón, K. Hoffmann, and K. Rurack *Angew. Chem. Int. Ed.* **2006**, *45*, 5924.
66 作花済夫, ゾル - ゲル法の応用, アグネ承風, 1997.
67 C. J. Brinker, and G. W. Scherer, Sol-Gel Science, Hydrolysis and Condensation II: Silicates, Chapter 3, Academic Press, Tokyo, **1990**.
68 M. Yamane, S. Inoue and A. Yasumori, *J. Non-Cryst. Solids*, **1984**, *63*, 13.
69 H. Shmidt, H. Scholze, and A. Kaiser, *J. Non-Cryst.* Solids, **1984**, *63*, 1.
70 J. Zarzycki, M. Prassas and J. Phalippou, *J. Mater. Sci.* **1982**, *17*, 3371.
71 M. G. Voronkov, V. P. Mileshkevich, and Y. A. Yuzhelevski, The Siloxane Bond, Consultant Bureau, New York, 1978.
72 W. Stöber, A. Fink, and E. Bohn, *J. Colloid Interface Sci*. **1968**, *1*, 62.
73 T. Sugimoto, *Adv. Colloid Interf. Sci.* **1987**, *28*, 65.
74 G.H. Bogush, M.A. Tracy, and C.F. Zukoski IV, *J. Non-Cryst. Solids*, **1988**, *104*, 95.
75 T. Matsoukas, and E. Gulari, *J. Colloid Interface Sci.* **1988**, *124*, 252.
76 T. Matsoukas, and E. Gulari, *J. Colloid Interface Sci.* **1989**, *132*, 13.
77 G.H Bogush, and C.F Zukoski IV, *J. Colloid Interface Sci.* **1991**, *142*, 1.
78 G.H Bogush, and C.F Zukoski IV, *J. Colloid Interface Sci.* **1991**, *142*, 19.

79 T. Yokoi, Y. Sakamoto, O. Terasaki, Y. Kubota, T. Okubo, and T. Tatsumi, *J. Am. Chem. Soc.* **2006**, *128*, 13664.

80 T. Yokoi, J. Wakabayashi, Y. Otsuka, W. Fan, M. Iwama, R. Watanabe, K. Aramaki, A. Shimojima, T. Tatsumi, and T. Okubo, *Chem. Mater.* **2009**, *21*, 3719.

81 C. C. M. C. Carcouët, M. W. P. van de Put, B. Mezari, P. C. M. M. Magusin, J. Laven, P. H. H. Bomans, H. Friedrich, A. C. C. Esteves, N. A. J. M. Sommerdijk, R. A. T. M. Benthem, and G. With, *Nano Lett.* **2014**, *14*, 1433.

82 A. Burns, H. Ow, and U. Wiesner, *Chem. Soc. Rev.* **2006**, *35*, 1028.

83 H. Ow , D. R. Larson, M. Srivastava, B. A. Baird, W. W. Webb, and U. Wiesner, *Nano Lett.* **2005**, *5*, 113.

84 M. Boutonnet, J. Kizling, and P. Stenius, *Colloids and Surfaces*, **1982**, *5*, 209.

85 K. S. Finnie, J. R. Bartlett, C. J. A. Barbé, and L. Kong, *Langmuir*, **2007**, 23, 3017.

86 R. Koole, M. M. Schooneveld, J. Hilhorst, C. M. Donegá, D. C. 't Hart, A. van Blaaderen, D. Vanmaekelbergh, and A. Meijerink, *Chem. Mater.* **2008**, *20*, 2503.

87 F. Li, Z. Wang, and A. Stein, *Angew. Chem. Int. Ed.* **2007**, *46*, 1885.

88 J. Perez-Ramirez, S. Abello, L. A. Villaescusa, and A. Bonilla, *Angew. Chem. Int. Ed.* **2008**, *47*, 7913.

89 Pyung-Soo Lee, X. Zhang, J. A. Stoeger, A. Malek, W. Fan, S. Kumar, W. C. Yoo, S. A. Hashimi, R. L. Penn, A. Stein, and M. Tsapatsis, *J. Am. Chem. Soc.* **2011**, *133*, 493.

90 Q. Huo, J. Liu , Li-Qiong Wang , Y. Jiang, T. N. Lambert, and E. Fang, *J. Am. Chem. Soc.* **2006**, *128*, 6447.

91 A. Khanal , Y. Inoue , M. Yada , and K. Nakashima, *J. Am. Chem. Soc.* **2007**, *129*, 1534.

92 K. Suzuki, S. Sato, and M. Fujita, *Nat. Chem.* **2010**, *2*, 25.

93 X. Du, B. Shi, J. Liang, J. Bi, S. Dai, and S. Z. Qiao, *Adv. Mater.* **2013**, *25*, 5981.

94 K. Kawahara, Y. Hagiwara, A. Shimojima, and K. Kuroda, *J. Mater. Chem.* **2008**, *18*, 3193.

95 H. Awala, J. –P. Gilson, R. Retoux, P. Boullay, J. –M. Goupil, V. Valtchev, and S. Mintova, *Nat. Mater.* **2015**, *14*, 447.

96 D. J. Mitchell, and B. W. Ninham, *J. Chem. Soc. Faraday Trans.* **1981**, *277*, 601.

97 T. Yanagisawa, T. Shimizu, and K. Kuroda, C. Kato, *Bull. Chem. Soc. Jpn.* **1990**, *63*, 988.

98 T. Yanagisawa, T. Shimizu, K. Kuroda, and C. Kato, *Bull. Chem. Soc. Jpn.* **1990**, *63*, 1535.

99 C. T. Kresge, M. E. Leonowicz, W. J. Roth, and J. C. Vartuli, J. S. Beck, *Nature*, **1992**, *359*, 710.

100 J. S. Beck, J. C. Vartuli, W. J. Roth, M. E. Leonowicz, C. T. Kresge, K. D. Schimitt, C. T-W. Chu, D. H. Olson, E. W. Sheppard, S. B. McCullen, J. B. Higgins, and J. L. Schlenker, *J. Am. Chem. Soc.* **1992**, *114,* 10834.

101 Y. Wan and D. Zhao, *Chem. Rev.* **2007**, *107*, 2821.

102 J. Frasch, B. Lebeau, M. Soulard, and J. Patarin, *Langmuir* **2000**, *16*, 9049.

103 M. Adachi, Y. Murata, K. Sago, and K. Nakagawa, *Langmuir*, **2004**, *20*, 5965.

104 Q. Huo, D. I. Margolese, U. Ciesla, D. G. Demuth, P. Feng, T. E. Gier, P. Sieger, A. Firouzi, B. F. Chmelka, F. Schuth, and G. D. Stucky, *Chem. Mater.* **1994**, *6*, 1176.

105 Y. Sakamoto, M. Kaneda, O. Terasaki, D. Y. Zhao, J. M. Kim, G. Stucky, H. J. Shin, and R. Ryoo, *Nature*, **2000**, *408*, 449.

106 C. Xiao, N. Fujita, K. Miyasaka, Y. Sakamoto, and O. Terasaki, *Nature*, **2012**, *487*, 349.

107 S. Che, Z. Liu, T. Ohsuna, K. Sakamoto, O Terasaki, and T Tatsumi, *Nature*, **2004**, *429*, 281.

108 M. Choi, K. Na, J. Kim, Y. Sakamoto, O. Terasaki, and R. Ryoo, *Nature*, **2009**, *461*, 246.

109 A. Firouzi, D. Kumar, L. M. Bull, T. Besier, P. Sieger, Q. Huo, S. A. Walker, J. A. Zasadzinski, C. Glinka, J. Nicol, D. Margolese,G. D. Stucky, and B. F. Chmelka, *Science*, **1995**, *267*, 1138.

110 Q. Huo, D. I. Margolese, and G. D. Stucky, *Chem. Mater.* **1996**, *8*, 1147.

111 K. Beneke, and G. Lagaly, *Am. Miner.* **1977**, *62*, 763.

112 S. Inagaki, Y. Fukushima, and K. Kuroda, *J. Chem. Soc. Chem. Commun.* **1993**, 680.

113 S. Inagaki, A. Koiwai, N. Suzuki, Y. Fukushima, and K. Kuroda, *Bull. Chem. Soc. Jpn.* **1996**, *69*, 1449.

114 Q. Huo, R. Leon, P. M. Petroff, and G. D. Stucky, *Science*, **1995**, *268*, 1324.

115 T. Kimura, T. Kamata, M. Fuzisawa, Y. Takano, M. Kaneda, Y. Sakamoto, O. Terasaki, Y. Sugahara, and K. Kuroda, *Angew. Chem. Int. Ed.* **2000**, *39*, 3855.

116 M. H. Huang, B. S. Dunn, H. Soyez, and J. I. Zink, *Langmuir*, **1998**, *14*, 7331.

117 M. H. Huang, B. S. Dunn, and J. I. Zink, *J. Am. Chem. Soc.* **2000**, *122*, 3739.

118 T. Yokoi, H. Yoshitake, and T. Tatsumi, *Chem. Mater*. **2003**, *15*, 4536.

119 S. Che, A. G-Bennett, T. Yokoi, K. Sakamoto, H. Kunieda, O. Terasaki, and T. Tatsumi, *Nat. Mater.*, **2003**, *2*, 801.

120 A. E. Garcia-Bannett, K. Miyasaka, and O. Terasaki, *Chem. Mater.* **2004**, *16*, 3597.

121 S. A. Bagshaw, E. Prouzet, and T. J. Pinnavaia, *Science*, **1995**, *269*, 1242.

122 G. S. Attard, Joanna C. Glyde, and C. G. Göltner, *Nature*, **1995**, *378*, 366.

123 N. R. B. Coleman, and G. S. Attard, *Micropor. Mesopor. Mater.* **2001**, *44*, 73.

124 D.Zhao, Q.Huo, J.Feng, B.F.Chmelka, and G. D.Stucky, *J. Am. Chem. Soc.* **1998**, *120*, 6024.

125 W. Zhang, B. Glomski, T. R. Pauly, and T. J. Pinnavaia, *Chem. Comm*. **1999**, 1803.

126 J. L. Blin, A. Lèonard, and B. L. Su, *Chem. Mater.* **2001**, *13*, 3542.

127 S. Che , H. Li, S. Lim, Y. Sakamoto, O. Terasaki, and T. Tatsumi, *Chem. Mater.* **2005**, *17*, 4103.

128 C. B. Gao, H. B. Qiu, W. Zeng, Y. Sakamoto, O. Terasaki, K. Sakamoto, Q. Chen, and S. Che, A. *Chem. Mater.* **2006**, *18*, 3904.

129 F. Kleitz , T. W. Kim, and R. Ryoo, *Langmuir*, **2006**, *22*, 440.

130 D. Grosso, F. Babonneau, G. J. A. A. Soler-Illia, P. –A. Albouy, and H. Amenitsch, *Chem. Commun*. **2002**, 748.

131 A. Shimojima, Y. Sugahara, and K. Kuroda, *J. Am. Chem. Soc.* **1998**, *120*, 4528.

132 A. Shimojima, and K. Kuroda, *Angew. Chem. Int. Ed.* **2003**, *42*, 4057.

133 A. Shimojima, Z. Liu, T. Ohsuna, O. Terasaki, and K. Kuroda, *J. Am. Chem. Soc.* **2005**, *127*, 14108.

134 A. Shimojima, and K. Kuroda, *Chem. Rec.* **2006**, *6*, 53.

135 J. J. E. Moreau, L. Vellutini, M. W. C. Man, C. Bied, J. L. Bantignies, P. Dieudonne, and J. L. Sauvajol, *J. Am. Chem. Soc.* **2001**, *123*, 7957.

136 N. Liu, K. Yu, B. Smarsly, D. R. Dunphy, Y.-B. Jiang, and C. J. Brinker, *J. Am. Chem. Soc.* **2002**, *124*, 14540.

137 C. B. W. Garcia, Y. Zhang, S. Mahajan, F. DiSalvo, and U. Wiesner, *J. Am. Chem. Soc.* **2003**, *125*, 13311.

138 R. Ulrich, AD. Chesne, M. Templin, and U. Wiesner, *Adv. Mater.* **1999**, *11*, 141.

139 K. Yu, A. J. Hurd, A. Eisenberg, and C. J. Brinker, *Langmuir*, **2001**, *17*, 7961.

Chapter 2

Formation of Two- and Three-Dimensional Hybrid Mesostructures from Branched Siloxane Molecules

Adapted with permission from S. Sakamoto, A. Shimojima, K. Miyasaka, J. Ruan, O. Terasaki, and K. Kuroda, "Formation of Two- and Three-Dimensional Hybrid Mesostructures from Branched Siloxane Molecules", *J. Am. Chem. Soc.* **2009**, 131, 9634–9635. Copyright 2009 American Chemical Society.

2.1 Abstract

We report the design of a new precursor having three branching disiloxane units capable of forming 3D mesostructures with a cubic *Pm*-3*n* and its orthorhombic and tetragonal variants *Cmmm* and $P4_2/mnm$, in addition to a conventional 2D hexagonal (*p6mm*) mesostructure, thus creating a novel research area of mesostructural design in silica-organic nanohybrid materials.

2.2 Introduction

The self-assembly route to hybrid inorganic-organic solids is of significant interest not only for fundamental research but also for the production of novel functional materials.[1-3] Recently, ordered silica-based hybrid materials have been synthesized from organoalkoxysilanes by taking advantage of their intermolecular interactions and ability to form siloxane network by hydrolysis and polycondensation.[4,5] The molecular design based on rich organosilicon chemistry would permit fine-tuning of compositions, structures, and properties of the products. The design of amphiphilic siloxane-based molecules is promising for producing hybrid mesostructures with a long-range order. The structure can be controlled in part by varying the size of the siloxane head as well as the alkyl chain length.[4,6] For example, trialkoxy- or trichloro-(alkyl)silanes form lamellar solids via hydrolysis and polycondensation,[6] whereas tris(trialkoxysilyloxy)-(alkyl)silanes ($C_nH_{2n+1}Si(OSi(OMe)_3)_3$, n = 6-13 (hereafter called "tetrasiloxane precursors"), can form mesophases consisting of rod-like assemblies such as 2D hexagonal phase.[7] In view of the geometrical packing parameter,[6a,8] further enlargement of the siloxane head should favor the formation of spherical assemblies, leading to structural diversity and complexity arising from packing variations; however, no such higher curvature mesophases have been observed

for amphiphilic organosiloxanes without the aid of surfactants. Here we report the design of a new precursor having three branching disiloxane units (**1** in Scheme 2.1) capable of forming 3D mesostructures with a cubic *Pm*-3*n* and its orthorhombic and tetragonal variants *Cmmm* and $P4_2/mnm$. A 2D hexagonal (*p6mm*) mesostructure was also formed by control of water content during self-assembly. The large, branched siloxane head of **1** is essential for the formation of such 3D mesophases, which have only been found in organic molecules and block copolymers with specific geometries,[9] thus creating a novel research area of mesostructural design in silica-organic nanohybrid materials.

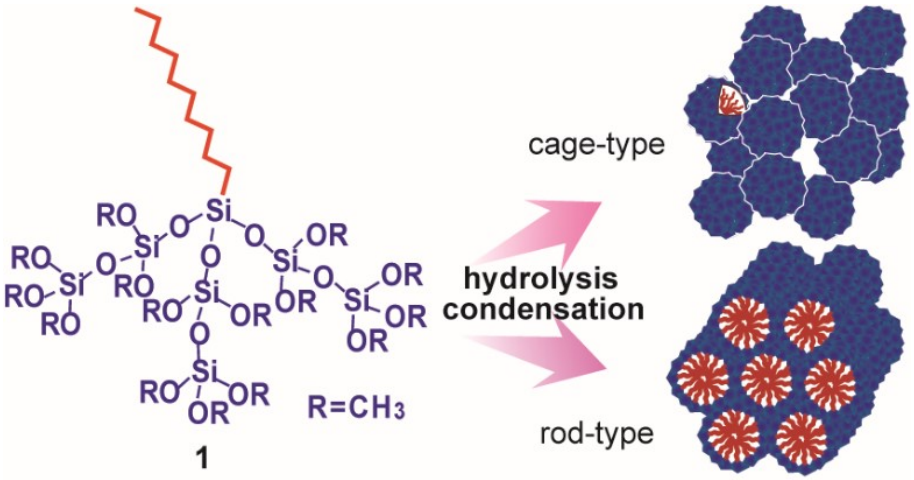

Scheme 2.1. Self-Assembly of the Precursor **1** into Two Types of Hybrid Mesostructures

2.3 Experimental

2.3.1 Synthesis of Compound 1

Compound **1** ($C_{10}H_{21}Si(OSi(OMe)_2OSi(OMe)_3)_3$) was synthesized by silylation of decylsilanetriol[8] with a disiloxane bearing one Si–Cl group. All reactions were performed under nitrogen atmosphere using standard Schlenk techniques. The

disiloxane was synthesized by adding H_2O (17.5 mL) and 6N HCl (12.5 mL) into the mixture of tetramethoxysilane (TMOS, 500 g) and tetrahydrofuran (THF, 300 mL) followed by refluxing for 3 h. After removal of solvents and unreacted TMOS in vacuo, hexamethoxydisiloxane ($(CH_3O)_3SiOSi(OCH_3)_3$, HMDS) was isolated by vacuum distillation. Partial replacement of -OMe with -Cl was then performed by stirring the mixture of HMDS (35.4 g), tetrachlorosilane ($SiCl_4$, 7.7 g), and $AlCl_3$ (0.31 g) at room temperature for 3 days. Removal of $AlCl_3$ and monomeric silanes ($SiCl_n(OMe)_{4-n}$) followed by vacuum distillation gave a mixture of HMDS, $(CH_3O)_3SiOSiCl(OCH_3)_2$, and $(CH_3O)_2ClSiOSiCl(OCH_3)_2$ (approximate molar ratio of 0.60:1.0:0.17, as evidenced by ^{29}Si NMR), which was used as the silylating agent without further separation. Decylsilanetriol (4.7g) dissolved in THF (200 mL) was added to a stirred mixture of the silylating agent (101 g), pyridine (5.6 mL) and THF (100 mL), and the mixture was stirred at 60 °C for 2 h. To eliminate the residual -Cl groups, methanol and pyridine were subsequently added to the mixture. After removal of pyridine hydrochloride by filtration, the residue was vacuum distilled to yield **1** as a clear, colorless liquid (yield: >60% based on decylsilantriol).

Tris(pentamethoxydisilyloxy)(decyl)silane ($C_{10}H_{21}Si(OSi(OMe)_2OSi(OMe)_3)_3$). ^1H NMR (500 MHz, $CDCl_3$): δ (ppm) 0.68–0.80 (m, 2H), 0.85–0.91 (t, 3H; CH_3), 1.20–1.38 (m, 14H), 1.42–1.52 (m, 2H), 3.59 (s, 45H; OCH_3); ^{13}C NMR (125.7 MHz, $CDCl_3$): δ (ppm) 13.03, 14.01, 22.55, 29.37, 29.41, 31.98, S2 33.36, 50.93, 50.49 ; ^{29}Si NMR (99.3 MHz, $CDCl_3$): δ (ppm) –94.37 (Q^2), –86.04 (Q^1), –67.43 (T^3) ; MS(FAB): m/z = 921.

2.3.2 Synthesis of pentasiloxane precursor

The pentasiloxane precursor ($C_{10}H_{21}SiCH_3(OSi(OMe)_2OSi(OMe)_3)_2$) was

synthesized by silylation of decylmethylsilanediol with the above mentioned silylating agent.

Bis(pentamethoxydisilyloxy)(decyl)(methyl)silane ($C_{10}H_{21}SiCH_3(OSi(OMe)_2OSi(OMe)_3)_2$). ^{1}H NMR (500 MHz, $CDCl_3$): δ (ppm) 0.21 (s, 3H), 0.65–0.68 (t, 2H), 0.87–0.90 (t, 3H), 1.27 (m, 14H), 1.43 (m, 2H), 3.58–3.59 (s, 45H; OCH_3) ; ^{13}C NMR (125.7 MHz, $CDCl_3$): δ (ppm) –1.28, 14.14, 16.86, 22.66, 22.83, 29.52, 29.76, 29.86, 32.10, 33.48, 50.96, 51.12 ; ^{29}Si NMR (99.3 MHz, $CDCl_3$): δ (ppm) –93.41 (Q^2), –85.97 (Q^1), –18.17 (D^2).

2.3.3 Synthesis of hybrid mesostructures $1H_A$ and $1H_B$

Hydrolysis and polycondensation of **1** were performed in a mixture with the molar ratio of 1:THF:H_2O:HCl = 1:50:30:0.002. The mixture was stirred at room temperature for 3 h, and then diluted with THF (and H_2O) to the final molar ratios of 1:THF:H_2O:HCl = 1:75:50:0.002 for synthesizing $\mathbf{1H_A}$ and 1:75:30:0.002 for synthesizing $\mathbf{1H_B}$, respectively. These two solutions were cast on glass substrates and air-dried at room temperature for two days. The resulting thick films were scraped off from the substrates and pulverized before characterization.

2.3.4 Characterization

Liquid-state ^{29}Si NMR spectra were recorded on a JEOL Lambda-500 spectrometer at a resonance frequency of 99.3 MHz with a pulse width of 6.5 μs and a recycle delay of 10 s or 20 s. The solution was put in a 5-mm glass tube, where $CDCl_3$ or [D_8]THF was used for obtaining lock signals, and a small amount of chromium(III) acetylacetonate was added for the relaxation of ^{29}Si nuclei. Liquid-state ^{1}H and ^{13}C NMR spectra were recorded on the same spectrometer at resonance frequencies of 500

MHz and 125.7 MHz, respectively. Solid-state ^{29}Si MAS NMR spectra were recorded on a JEOL JNM-CMX-400 spectrometer at a resonance frequency of 79.42 MHz with a recycle delay of 200 s. Samples were put into 7.5-mm zirconia rotors and spun at 5 kHz. The powder XRD patterns of the mesostructured hybrid materials were recorded on a Mac Science M03XHF22 diffractometer with Mn-filtered Fe Kα radiation (40 kV, 20 mA). Synchrotron powder XRD was measured at BL02B2 in SPring-8, Japan. The wavelength used was 0.100 nm. Diffraction profiles were recorded by a Debye-Scherrer-type camera with an imaging plate. Nitrogen adsorption and desorption measurements were performed on an Autosorb 1 instrument (Quantachrome Instruments) at 77 K. TEM studies were carried out on a JEOL JEM-3010 electron microscope operated at 300 kV (point resolution 0.17 nm, Cs = 0.6 mm) or on a JEOL JEM-2010 electron microscope operated at 200 kV. Samples were crushed in an agate mortar, suspended in the ethanol using ultrasoncating and then dropped onto the carbon grid.

2.4 Results and discussion

2.4.1 Characterization of hybrid mesostructures $\mathbf{1H_A}$ and $\mathbf{1H_B}$

We have developed a facile route to the heptasiloxane precursor **1** by one-step silylation of decylsilanetriol[7] with disiloxane species where -OMe groups of hexamethoxydisiloxane ($(MeO)_3SiOSi(OMe)_3$) are partly replaced by more reactive -Cl groups. Successful synthesis of **1** was confirmed by NMR and MS (Figure 2.1 and 2.2). Hydrolysis of **1** proceeded almost completely under acidic conditions in THF as confirmed by disappearance of the $SiOCH_3$ signals in the ^{13}C NMR spectrum. After diluting this hydrolyzed solution with more THF and water, the solution was cast and dried on a glass substrate to give a xerogel film ($\mathbf{1H_A}$). Similarly, a hybrid solid, $\mathbf{1H_B}$,

was prepared by diluting with only THF under otherwise identical conditions.

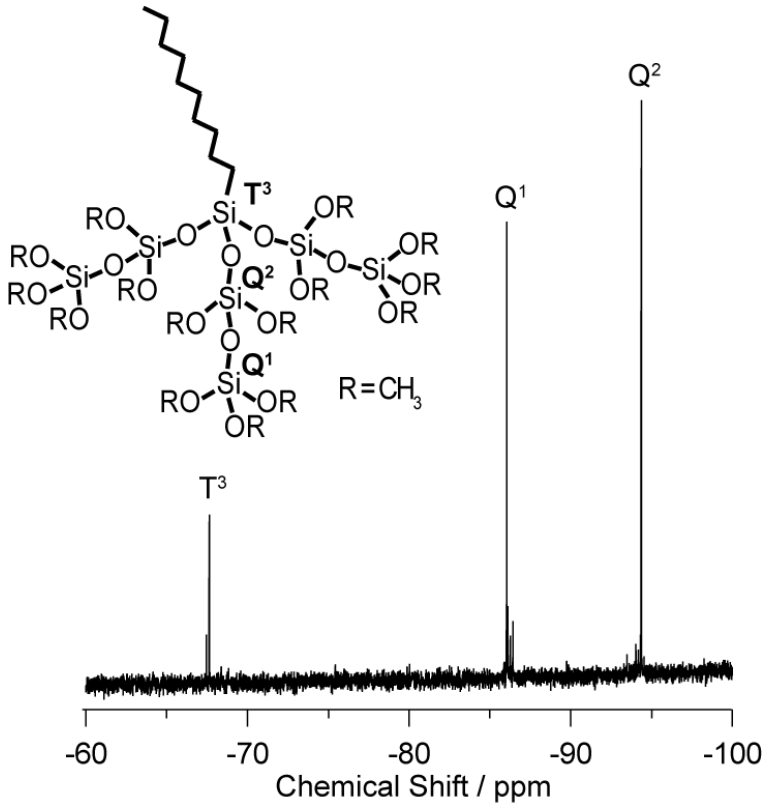

Figure 2.1. Liquid-state ^{29}Si NMR spectrum of **1** in $CDCl_3$, showing three signals corresponding to the T^3, Q^1 and Q^2 sites (T_x: $CSi(OSi)_x(OH)_{3-x}$, Q_y: $Si(OSi)_y(OH)_{4-y}$) with the integral intensity ratios of 1:3:3, respectively.

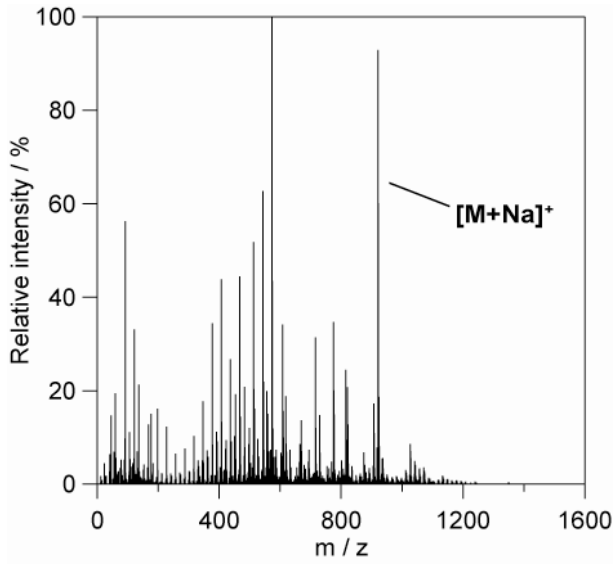

Figure 2.2. Fast atom bombardment (FAB) mass spectrum of **1**.

The powder XRD pattern of **1H$_A$** (Figure 2.3a) shows several peaks due to mesoscale periodicity. The TEM images (Figure 2.4) show that the material comprises different packing domains of cages with space groups of $P4_2/mnm$, $Pm\text{-}3n$, and their modulated mixture, among which the $P4_2/mnm$ is dominant. The packing of the cage domains is very coherent, which is evidenced by the FFT diffractograms (insets of Figure 2.4) that display well-resolved spots despite the presence of the mesostructural modulation and the relevant stacking faults (Figure 2.5). On the basis of the prevailing $P4_2/mnm$ symmetry, the lattice constants of the unit cell calculated from the FFT are a = 12.8 nm and c = 5.3 nm. These lattice constants are presumed to give the indexing of the present XRD peaks in Figure 2.3a. The packings with $P4_2/mnm$ and *Cmmm* are explained from that with $Pm\text{-}3n$ by the occurrence of two-dimensionally periodic planar faults.[10] This same packing behavior and the relationship have since been described for liquid crystals9a and a mesoporous silica (AMS-9) prepared with anionic surfactants and costructure directing agents.[11]

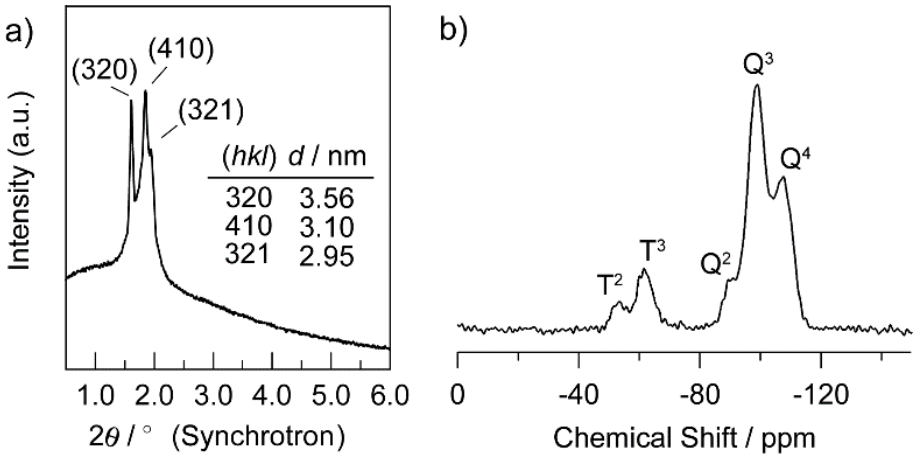

Figure 2.3. (a) Powder XRD pattern (collected in Spring-8, Japan) of **1H$_A$**, which is indexed based on the cell parameter determined from TEM observation. (b) ^{29}Si MAS NMR spectrum of **1H$_A$**.

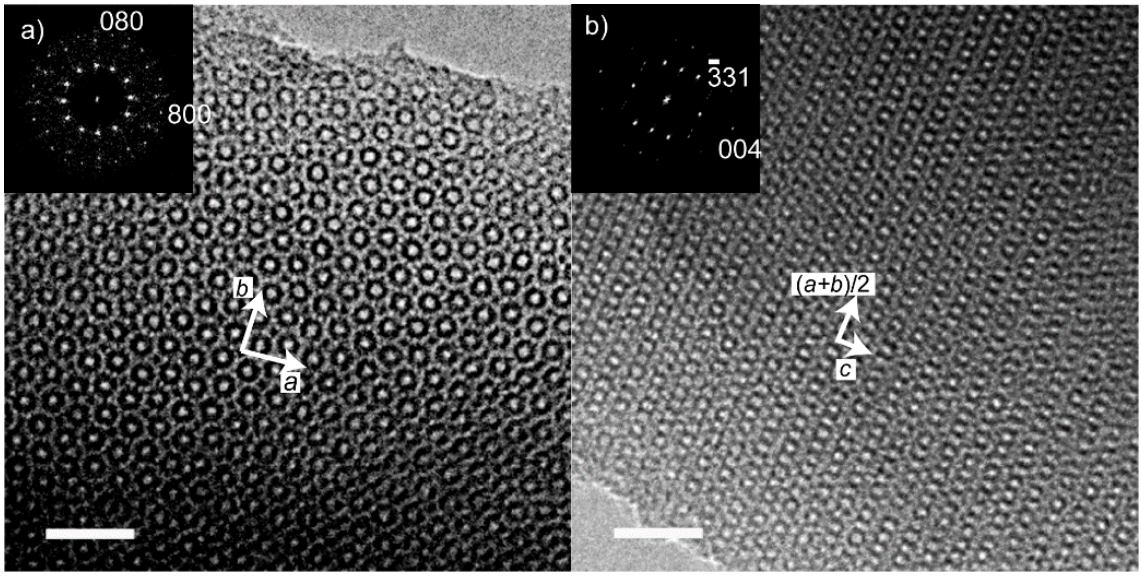

Figure 2.4. TEM images and FFT diffractograms of **1H$_A$** taken by a JEM-3010 microscope; (a) [001] and (b) [110] directions of $P4_2/mnm$ space group. The italic symbols indicate the lattice vectors of the tetragonal lattice. Scale bar: 20 nm.

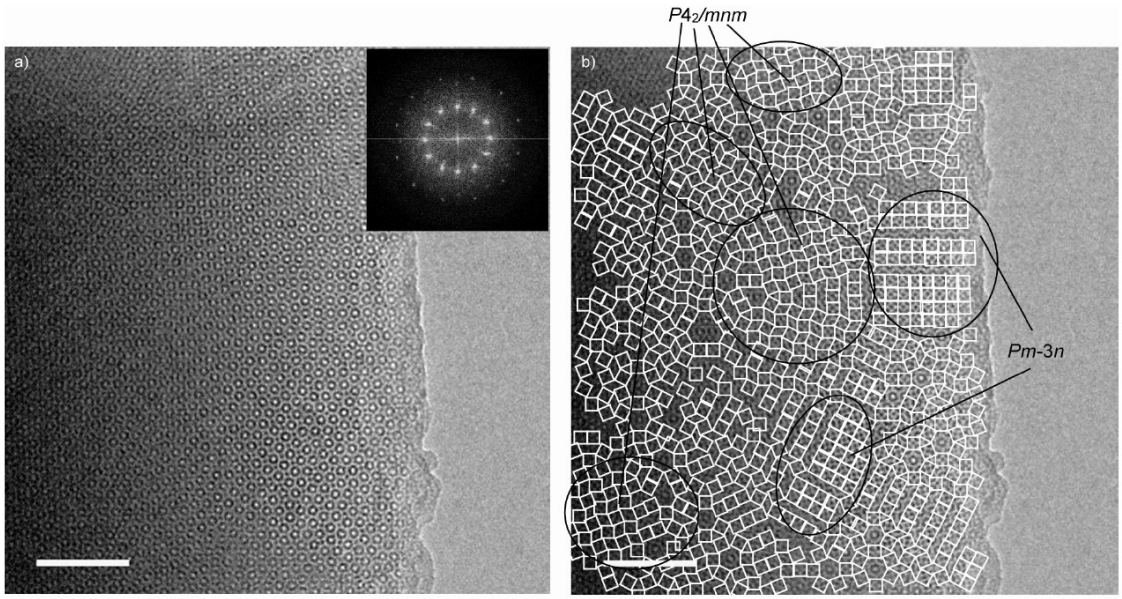

Figure 2.5. (a) Typical TEM image of **1H$_A$** with the corresponding FFT diffractogram and (b) the same image in which the bright spots are connected to each other with white lines, showing many squares and regular triangles with the same sizes. The square corresponds to a unit cell of *Pm*-3*n*. Scale bar, 50 nm.

In contrast, the 2D hexagonal (*p6mm*) structure of **1H$_B$** was revealed by XRD and TEM showing either honeycomb or striped patterns depending on the electron incidents (Figure 2.6). The d_{10} spacing (2.69 nm) is smaller than that for the 2D hexagonal structure derived from the tetrasiloxane precursor with the same chain length (d_{10} = 2.92 nm),[7] suggesting that **1H$_B$** has a smaller diameter of the rodlike assemblies. Although the larger siloxane head of **1** should lead to a thicker siloxane wall, the internal diameter should decrease because of the increased lateral distance and therefore lowered density of alkyl chains in the rods. These structural features were actually confirmed by nitrogen sorption data of the porous silica samples obtained by calcination (Figure 2.7).

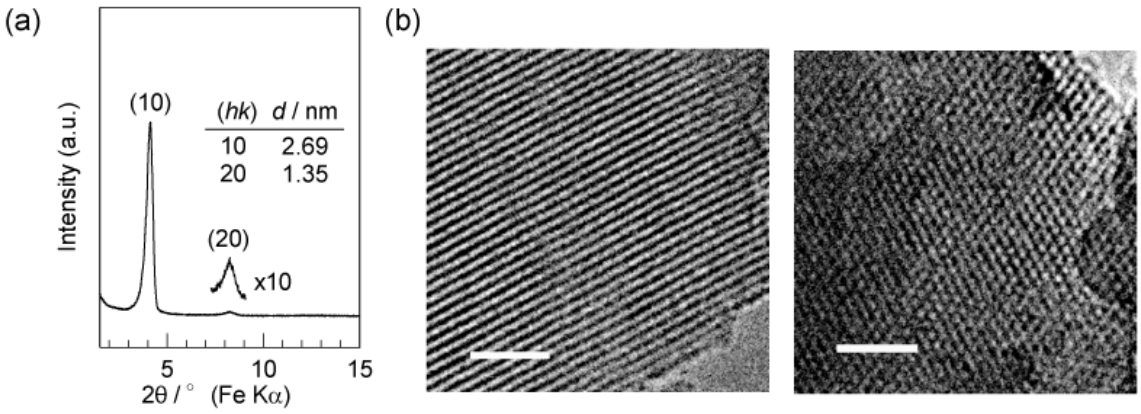

Figure 2.6. (a) Powder XRD pattern and (b) typical TEM images of **1H$_B$**. The XRD pattern was obtained using a FeKα X-ray source. The absence of the (11) peak is probably due to the parallel alignment of the cylinders within the plate-like particles. The TEM images were taken by a JEOL JEM-2010 microscope operated at 200 kV. Scale bar 20 nm.

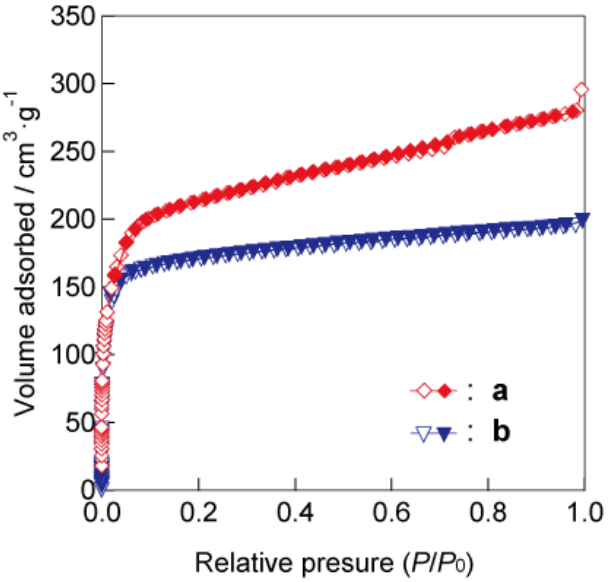

Figure 2.7. Nitrogen adsorption-desorption isotherms of (a) the product derived from the pentasiloxane precursor and (b) **1H$_B$** after calcination at 500 °C for 8 h. The open symbols and the filled symbols denote adsorption and desorption, respectively. The BET surface areas are 820 and 610 m^2 g^{-1} for (a) and (b), respectively. In addition, the average pore sizes calculated by NLDFT are 2.0 nm and 1.6 nm for (a) and (b), respectively.

In both **1H$_A$** and **1H$_B$**, alkyl chains are in a similarly disordered state with mixed trans-gauche conformations, as suggested by the position of the $\nu_{as}(>CH_2)$ bands (2930 cm^{-1}) in the IR spectra (Figure 2.8). Also, no difference was observed in the local structures of the siloxane networks. The solid-state ^{29}Si MAS NMR show similar spectra consisting of the T^2, T^3, Q^2, Q^3, and Q^4 signals (T^x: $CSi(OSi)_x(OH)_{3-x}$; Q_y: $Si(OSi)_y(OH)_{4-y}$; see Figure 2.3b for **1H$_A$**, Table 2.1). The presence of the T^2 signal indicates the partial cleavage of the Si-O-Si bonds in **1** during the synthesis. Nevertheless, the liquid-state ^{29}Si NMR spectrum of the hydrolyzed solution (data not shown) mainly showed the T^3 signal, suggesting that uncleaved species were still predominant at this stage.

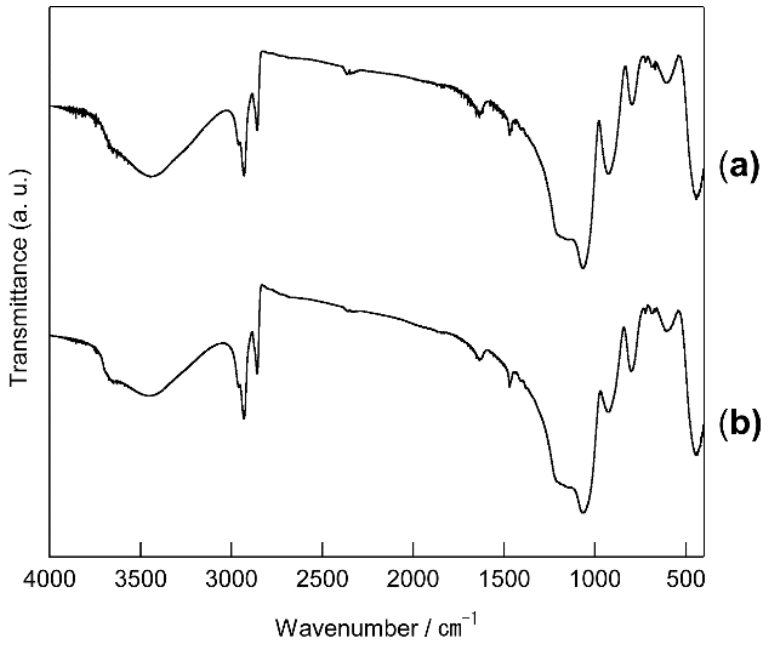

Figure 2.8. IR spectra of (a) **1H$_A$** and (b) **1H$_B$**.

Table 2.1 Chemical shifts and relative intensity ratios of the signals observed in the ^{29}Si MAS NMR spectra of **1H$_A$** and **1H$_B$**

Sample	Relative intensity ratios [%]					Degree of condensation [%]	
	T^2	T^3	Q^2	Q^3	Q^4	T^a	Q^b
1H$_A$	5	10	9	46	30	88	81
	(-53.6)	(-62.4)	(-91.0)	(-99.4)	(-108.0)		
1H$_B$	8	12	9	44	26	86	80
	(-53.8)	(-62.8)	(-90.9)	(-99.5)	(-108.5)		

a Evaluated by the equation, $(2 \times T^2 + 3 \times T^3)/((T^2 + T^3) \times 3) \times 100$

b Evaluated by the equation, $(2 \times Q^2 + 3 \times Q^3 + 4 \times Q^4) / ((Q^2 + Q^3 + Q^4) \times 4) \times 100$

c The values in the parenthesis are the chemical shifts of the signals [ppm]

The variation of the mesostructures (**1H$_A$** and **1H$_B$**) with the water content in the precursor solution should be associated with the difference in the concentration of the hydrolyzed species after preferential evaporation of THF. Similar behavior has been found for silica-surfactant mesostructured films prepared by evaporation-induced self-assembly (EISA) processes.[12]

2.4.2 Characterization of hybrid mesostructure prepared with pentasiloxane siloxane precursor

We also examined the use of a pentasiloxane precursor ($C_{10}H_{21}SiMe(OSi(OMe)_2OSi(OMe)_3)_2$), where one branching disiloxane unit of **1** is replaced with a methyl group. This precursor exclusively formed a 2D hexagonal phase as confirmed by XRD and TEM (Figure 2.9). The d_{10} spacing (3.04 nm) is larger by 0.35 nm than that of $\mathbf{1H_B}$, which is explained by the smaller lateral distance of alkyl chains in the rods.

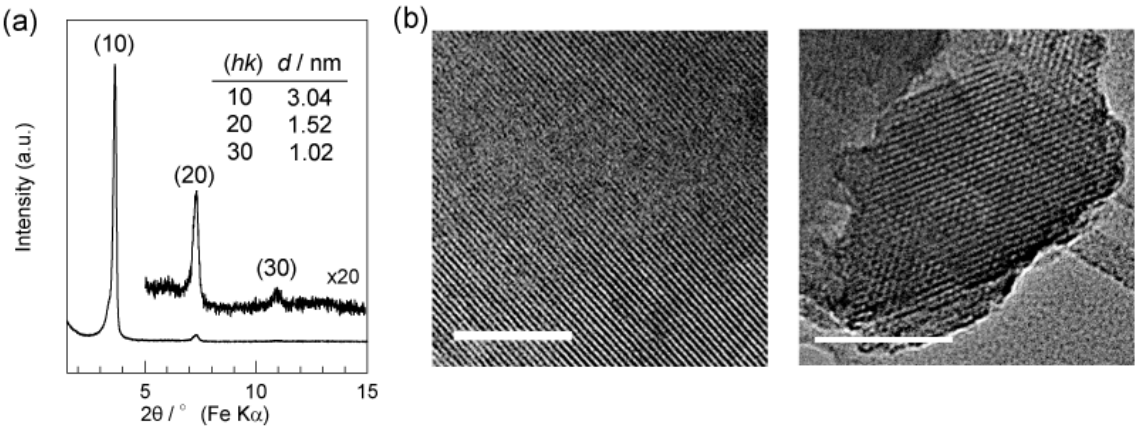

Figure 2.9. (a) Powder XRD pattern and (b) typical TEM images of the hybrid derived from pentasiloxane precursor. The pattern was obtained using a FeKα X-ray source. The TEM images were taken by a JEOL JEM-2010 microscope operated at 200 kV. Scale bar 50 nm.

2.4.3 Influence of head group architecture on mesostructure.

The present results suggest that alkylsiloxane mesophase is governed by both the size and configuration of the siloxane head. In contrast to the formation of well-ordered 3D mesophases from **1**, cubic-octasiloxane precursors ($CnH_{2n+1}Si_8O_{12}(OEt)_7$) yielded 2D hexagonal phases when n = 16-20 and the structure became disordered upon decreasing the chain length to n = 10.[13] Although the number

of Si atoms is similar among these two precursors, major differences exist in the rigidity and the number of hydrolysable alkoxy groups. The maximum number of -OH groups generated by hydrolysis is much larger for **1** (15 -OH per molecule) than for the octasiloxane precursors (7 -OH per molecule). Thus, the hydrolyzed **1** should be more amphiphilic and, hence, capable of forming well-ordered mesostructures.

2.5 Conclusion

In conclusion, we have demonstrated the formation of 3D tetragonal (and cubic) as well as 2D hexagonal mesostructures from a branched heptasiloxane precursor, providing deeper insight into the relationship between molecular structure and self-assembled mesostructures of alkylsiloxane amphiphiles. The modification of the organic counterpart is under study to achieve more sophisticated structures with specific functions.

2.6 References

1 Colfen, H.; Mann, S. *Angew. Chem., Int. Ed.* **2003**, *42*, 2350.

2 Descalzo, A. B.; Martinez-Manez, R.; Sancenn, F.; Hoffmann, K.; Rurack, K. *Angew. Chem., Int. Ed.* **2006**, *45*, 5924.

3 Hoffmann, F.; Cornelius, M.; Morell, J.; Fro¨ba, M. *Angew. Chem., Int. Ed.* **2006**, *45*, 3216, and references therein.

4 Shimojima, A.; Kuroda, K. *Chem. Rec.* **2006**, *6*, 53.

5 For example,(a) Moreau, J. J. E.; Vellutini, L.; Wong Chi Man, M.; Bied, C. *J. Am. Chem. Soc.* **2001**, *123*, 1509. (b) Boury, B.; Corriu, R. J. P. *Chem. Commun.* **2002**, 795.

6 (a) Huo, Q.; Margolese, D. I.; Stucky, G. D. *Chem. Mater.* **1996**, *8*, 1147. (b)

Parikh, A. N.; Schivley, M. A.; Koo, E.; Seshadri, K.; Aurentz, D.; Mueller, K.; Allara, D. L. *J. Am. Chem. Soc.* **1997**, *119*, 3135. (c) Shimojima, A.; Sugahara, Y.; Kuroda, K. *Bull. Chem. Soc. Jpn.* **1997**, *70*, 2847.

7 Shimojima, A.; Liu, Z.; Ohsuna, T.; Terasaki, O.; Kuroda, K. *J. Am. Chem. Soc.* **2005**, *127*, 14108.

8 Wan, Y.; Zhao, D. *Chem. Rev.* **2007**, *107*, 2821.

9 (a) Ungar, G.; Zeng, X. B. *Soft Matter*, **2005**, *1*, 95. (b) Hayashida, K.; Dotera, T.; Takano, A.; Matsushita, Y. *Phys. Rev. Lett.* **2007**, *98*, 195502. (c) Thomas, E. L.; Anderson, D. M.; Henkee, C. S.; Hoffman, D. *Nature*, **1988**, *334*, 598.

10 Hiraga, K.; Hirabayashi, M.; Terasaki, O.; Watanabe, D. *Acta Crystallogr.* **1982**, *A38*, 269.

11 Garcia-Bennett, A. E.; Kupferschmidt, N.; Sakamoto, Y.; Che, S.; Terasaki, O. *Angew. Chem., Int. Ed.* **2005**, *44*, 5317.

12 Cagnol, F.; Grosso, D.; Soler-Illia, G. J. de A. A.; Crepaldi, E. L.; Babonneau, F.; Amenitschb, H.; Sanchez, C. *J. Mater. Chem.* **2003**, *13*, 61.

13 Shimojima, A.; Goto, R.; Atsumi, N.; Kuroda, K. *Chem.Eur. J.* **2008**, *14*, 8500.

Chapter 3

Molecularly Designed Nanoparticles by Dispersion of Self-Assembled Organosiloxane-Based Mesophases

Adapted with permission from S. Sakamoto, Y. Tamura, H. Hata, Y. Sakamoto, A. Shimojima, and K. Kuroda, "Molecularly Designed Nanoparticles by Dispersion of Self-Assembled Organosiloxane-Based Mesophases", *Angew. Chem. Int. Ed.* **2014**, 53, 9173 –9177. Copyright 2014 Wiley-VCH Verlag GmbH & Co. KGaA.

3.1 Abstract

The design of siloxane-based nanoparticles is important for many applications. Here we show a novel approach to form core–shell silica nanoparticles of a few nanometers in size through the principle of "dispersion of ordered mesostructures into single nanocomponents". Self-assembled siloxane–organic hybrids derived from amphiphilic alkyl-oligosiloxanes were postsynthetically dispersed in organic solvent to yield uniform nanoparticles consisting of dense lipophilic shells and hydrophilic siloxane cores. In-situ encapsulation of fluorescent dyes into the nanoparticles demonstrated their ability to function as nanocarriers.

3.2 Introduction

Functionalized nanoparticles have found many applications including in biomedicine,[1-5] optics,[6, 7] electronics,[8,9] and catalysis.[10] As host or coating matrices, silica is widely utilized because of its transparency, biocompatibility, insulating property, and controllable porosity. Fine control of the particle sizes and surface properties while retaining a high dispersibility is crucial for various new applications. For example, the optimal nanoparticle size for drug delivery systems is limited to the range of 3–7 nm to avoid an inflammatory immune response.[5] Control of these factors is also crucial for the alignment and dispersion of the nanoparticles to provide unique functions for electronic and optical devices.[10] The methodology for the preparation of uniform and stable silica nanoparticles with tailored sizes and surface properties as well as with the ability to accommodate various guest species thus addresses an important need in these fields.

The self-assembly of amphiphilic organosilanes has attracted growing interest as a direct approach to silica–organic hybrid nanomaterials.[11-14] Micellar and vesicular particles have been prepared from lipids or block copolymers bearing $Si(OEt)_3$

groups;[13,14] however, difficulty remains in precisely controlling their dimensions, particularly in the 1–10 nm range. In this context, we focused on the formation of a periodic and extended reverse-type mesophase where siloxane spheres surrounded by an organic shell are arranged periodically to establish a straightforward dispersion process yielding uniform and discrete nanoparticles of a few nanometers in size.

Herein, we report a novel approach to form core–shell silica nanoparticles of a few nanometers in size through the principle of "dispersion of ordered mesostructures into single nanocomponents" (Scheme 3.1). Self-assembled siloxane–organic hybrids derived from amphiphilic trialkyl-substituted oligosiloxanes were postsynthetically dispersed in organic solvent to yield uniform nanoparticles consisting of dense lipophilic shells and hydrophilic siloxane cores. To explore their ability to function as nanocapsules, we demonstrate the in situ encapsulation of hydrophilic dyes into the nanoparticles. The synthetic development of such a molecularly designed nanoparticle is a promising step toward various advanced applications.

This concept has been realized by the design of linear and alkoxylated oligosiloxane precursors, in which three alkyl chains are attached to the terminal Si atom (**1(Si*n*)** in Scheme 3.1). The larger volume of the hydrophobic trialkylsilyl group relative to the linear oligosiloxane chain should favor the formation of reverse micelles and their assemblies. The self-assembly and siloxane network formation are induced by the evaporation of solvent from the solution containing the hydrolyzed precursor, which allows the synthesis of monodisperse silica nanoparticles stabilized against irreversible aggregation by the organic outer shell. This strategy is fundamentally different from the conventional approaches that use reverse micelles or block copolymer assemblies as templates for the confined growth of inorganic nanoparticles.[15, 16]

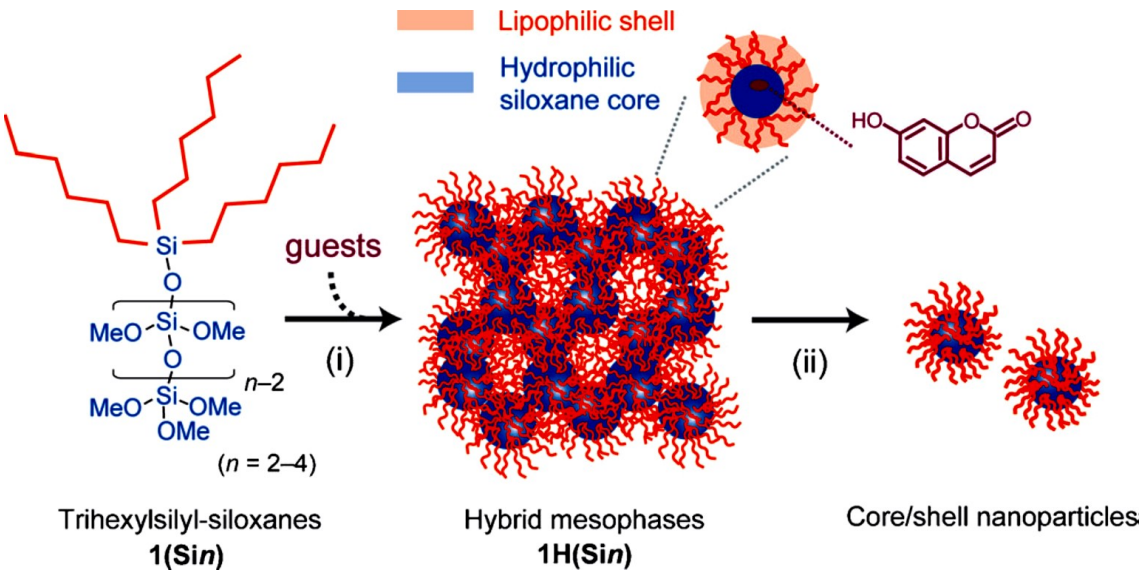

Scheme 3.1. Self-assembly/dispersion approach to organically modified silica nanoparticles: (i) an evaporation-induced self-assembly process involving hydrolysis and polycondensation of **1(Si*n*)**; (ii) dispersion of a hybrid mesophase (**1H(Si*n*)**) in a nonpolar solvent to form single nanoparticles. Hydrophilic guest species can be loaded into the nanoparticles during the self-assembly process.

3.3 Experimental

3.3.1 Synthesis of compound 1(Si4)

All reactions were performed under nitrogen atmosphere using standard Schlenk techniques. The alkoxytrisiloxane was synthesized by adding H_2O (17.5 mL) and 6N HCl (12.5 mL) to a mixture of tetramethoxysilane (TMOS, 500 g) and tetrahydrofuran (THF, 300 mL), followed by heating at reflux for 3 h. After removal of the solvent in vacuo, octamethoxytrisiloxane [$(CH_3O)_3SiOSi(OCH_3)_2OSi(OCH_3)_3$] was isolated by vacuum distillation. Partial replacement of -OMe groups with -Cl was then performed by stirring a mixture of octamethoxytrisiloxane (25 g), tetrachlorosilane ($SiCl_4$; 1.3 mL), and $AlCl_3$ (0.32 g) at RT for 1 day. Removal of $AlCl_3$ followed by vacuum distillation gave a mixture of $(CH_3O)_3SiOSi(OCH_3)_2OSi(OCH_3)_3$ and $(CH_3O)_2ClSiOSi(OCH_3)_2OSi(OCH_3)_3$ (approximate molar ratio of 1:1). Trihexylsilanol

was synthesized by stirring a mixture of trihexylsilane (5.0 g), THF (60 mL), H_2O (2.0 mL), and Pearlman's catalyst (22 mg) for 30 min in an ice bath. The resulting solution was filtered to remove the catalyst and the solvent was evaporated. The resulting solid (trihexylsilanol) was dissolved in hexane (50 mL) and added to a stirred mixture of alkoxytrisiloxane (20 g), pyridine (5.2 mL), and THF (100 mL), and the mixture was stirred at RT. To eliminate the residual -Cl groups, methanol (1.3 mL) was added to the mixture. After removal of pyridine hydrochloride by filtration, the residue was distilled under vacuum to yield **1(Si4)** as a clear, colorless liquid (8.5 g).

1(Si4). ^{1}H NMR (500 MHz, [D8]THF): δ = 0.61-0.64 (m, 2H), 0.88-0.89 (t, 3H; CH_3), 1.31-1.39 (m, 8H), 3.51-3.55 ppm (s, 21H; OCH_3); ^{13}C NMR (125.7 MHz,[D8]THF): δ = 14.42, 15.88, 23.42, 23.73, 32.43, 34.18, 50.96, 51.08, 51.10 ppm; ^{29}Si NMR (99.3 MHz, [D_8]THF): δ = -93.97 (Q^2), -92.76 (Q^2), -86.17 (Q^1), 10.21 ppm (M^1); MS (MALDI-TOF): $[M^+K^+]$ = 672, $[M^+Na^+]$ = 656.

3.3.2 Synthesis of compound 1(Si2) and 1(Si3)

Compounds **1(Si2)** and **1(Si3)** were synthesized by the reaction of trihexylsilanol with monochlorinated alkoxysilane and alkoxydisiloxane, respectively. The silylating agent used for the synthesis of **1(Si2)** was the mixture of $SiCl(OCH_3)_3$ (>60%) and $Si(OCH_3)_4$ obtained by adding methanol dropwise to $SiCl_4$ in a N_2 flow. The silylating agent for **1(Si3)** was the siloxane dimer with a Si-Cl group.[12] Other procedures were the same as those for the synthesis of **1(Si4)**.

1(Si2). ^{1}H NMR (500 MHz, [D_8]THF): δ = 0.60-0.63 (m, 2H), 0.88-0.90 (t, 3H; CH_3), 1.30-1.39 (m, 8H), 3.48 ppm (s, 9H; OCH_3); ^{13}C NMR (125.7 MHz, [D_8]THF): δ = 14.40, 15.90, 23.36, 23.70, 32.39, 34.10, 50.95 ppm; ^{29}Si NMR (99.3 MHz,[D_8]THF): δ = -84.84 (Q^1), 9.93 ppm (M^1).

1(Si3). ^{1}H NMR (500 MHz, [D_8]THF): δ = 0.61 (m, 2H), 0.89 (t, 3H; CH_3), 1.30 (m, 8H), 3.48-3.52 ppm (s, 15H; OCH_3); ^{13}C NMR (125.7 MHz, [D_8]THF): δ =14.35, 15.83, 23.25, 23.58, 32.29, 34.01, 50.82, 51.85, 50.94 ppm; ^{29}Si NMR (99.3 MHz, [D_8]THF): δ = -92.58 (Q^2), -86.15 (Q^1), 10.14 ppm (M^1); MS (MALDI-TOF): [M^+K^+] =566, [M^+Na^+] = 550.

3.3.3 Synthesis of hybrid mesostructures 1H(Si*n*)

Hydrolysis and polycondensation of **1(Si*n*)** were performed in a mixture with the molar ratio of **1(Si*n*)**/THF/H_2O/HCl=1:30:(2*n*-1) × 2:0.01. The mixture was stirred at room temperature until complete hydrolysis was confirmed by liquid-state ^{13}C NMR spectroscopy. In the cases of *n* = 2 and 4, hydrolyzed solutions were diluted with H_2O to the final molar compositions of **1(Si2)**:THF:H_2O:HCl=1:30:12:0.01 and **1(Si4)**:THF:H_2O:HCl=1:30:29:0.01, respectively. These solutions were cast on glass substrates and air-dried at RT for 1 day. In the case of **1H(Si2)**, the film was aged for 1.5 h at 80 °C to form the structure with a better arrangement.

3.3.4 Synthesis of dye-containing hybrid mesostrucrure

7-Hydroxycoumarin was added to the hydrolyzed solution of **1H(Si4)** with the molar ratio of **1(Si4)**:THF:H_2O:HCl:dye=1:30:15:0.002:0.2. The mixture was stirred for 30 min to completely dissolve the dye, and then cast on glass substrates and air-dried.

3.3.5 Dissociation of hybrid materials (1H(Si4)) into nanoparticles

The hybrid materials derived from **1(Si4)** can be well dispersed in hexane (regardless of whether they contain dyes). A tiny amount of undispersed polymeric species was removed by filtration to give clear and colorless solutions.

3.3.6 Characterization

Characterization: Liquid-state ^{29}Si, ^{13}C, and 1H NMR spectra were recorded on a JEOL Lambda-500 spectrometer at resonance frequencies of 99.3, 125.7, and 500 MHz, respectively. The solution was put in a 5 mm glass tube, where a small amount of [D_8]THF was added for obtaining lock signals, and a small amount of chromium(III) acetylacetonate was added for the relaxation of ^{29}Si nuclei. Solid-state ^{29}Si MAS NMR and ^{13}C CP/MAS NMR spectra were recorded on a JEOL JNM-CMX-400 spectrometer at resonance frequencies of 79.42 and 100.5 MHz with recycle delays of 100 s and 12 s, respectively. The θ–2θ XRD patterns of the mesostructured hybrid materials were recorded on a Mac Science M03XHF22 diffractometer with Mn-filtered Fe Kα radiation or on a Rigaku RINT 2000 diffractometer with Ni-filtered Cu Ka radiation. TEM studies were carried out on a JEOL JEM-2010 electron microscope operated at 200 kV. SEM observation was carried out on a HITACHI S-5500 microscope operated at 30 kV. For TEM and SEM observation, mesostructures were directly formed by applying drops of the hydrolyzed solution on a carbon-supported grid. In the case of the particle observation, the hexane solutions of particles were applied dropwise onto the same grid and air-dried. UV/Vis absorption spectra were obtained with a Shimadzu UV-3100PC instrument. Fluorescence spectra were recorded on a Hitachi F-4500 spectrofluorophotometer at the excitation wavelength of 327 nm. For spectroscopic data, transparent hexane solutions were measured, after filtration of the solution with a 0.2 mm filter. MALDI-TOF mass analysis was carried out with a Shimadzu AXIMACFR instrument. The matrix of 1,8,9-anthracenetriol and the sample in hexane were spotted on the MALDI-TOF MS source target and allowed to dry in air prior to analysis.

3.4 Results and discussion

3.4.1 Characterization of hybrid mesostructure 1H(Si4)

The precursors **1(Si*n*)** were synthesized by the reaction of trihexyl(hydroxy)silane with alkoxylated oligosiloxanes and were hydrolyzed in tetrahydrofuran (THF) under acidic conditions. After complete hydrolysis of the constituent Si-OMe groups, the solutions were cast onto a glass substrate to evaporate the volatile components so that self-assembly of the hydrolyzed molecules and the concomitant polysiloxane formation could proceed. The resulting film was solid, but exhibited some plasticity. The resulting hybrid material **1H(Si4)** from the **1(Si4)** precursor was characterized in detail by electron microscopy, X-ray diffraction (XRD), and solid-state NMR spectroscopy.

The scanning electron microscopy (SEM) imaging of the surface of the cast film revealed hexagonally arranged spherical particles with a uniform diameter of ca. 3.3 nm (Figure 3.1a). The particle size roughly corresponds to twice the extended molecular length of **1(Si4)** (ca. 1.7 nm). This film exhibits an XRD peak corresponding to a *d* spacing of 2.7 nm (Figure 3.1b). Assuming that this peak is assigned to the (111) plane of a face-centered cubic structure, the calculated particle size (3.3 nm) is in good agreement with that determined by SEM. The solid-state ^{29}Si magic-angle spinning (MAS) NMR spectrum of **1H(Si4)** shows the Q^3 and Q^4 signals along with the M^1 and Q^2 signals (Q^m: $Si(OSi)_m(OH)_{4-m}$, M^1: $C_3Si(OSi)$; Figure 3.1c), confirming the formation of crosslinked siloxane networks with a certain degree of uncondensed silanols. The presence of the alkyl chains as well as the elimination of alkoxy groups were confirmed by ^{13}C cross-polarization magic-angle spinning (CP-MAS) NMR spectroscopy.

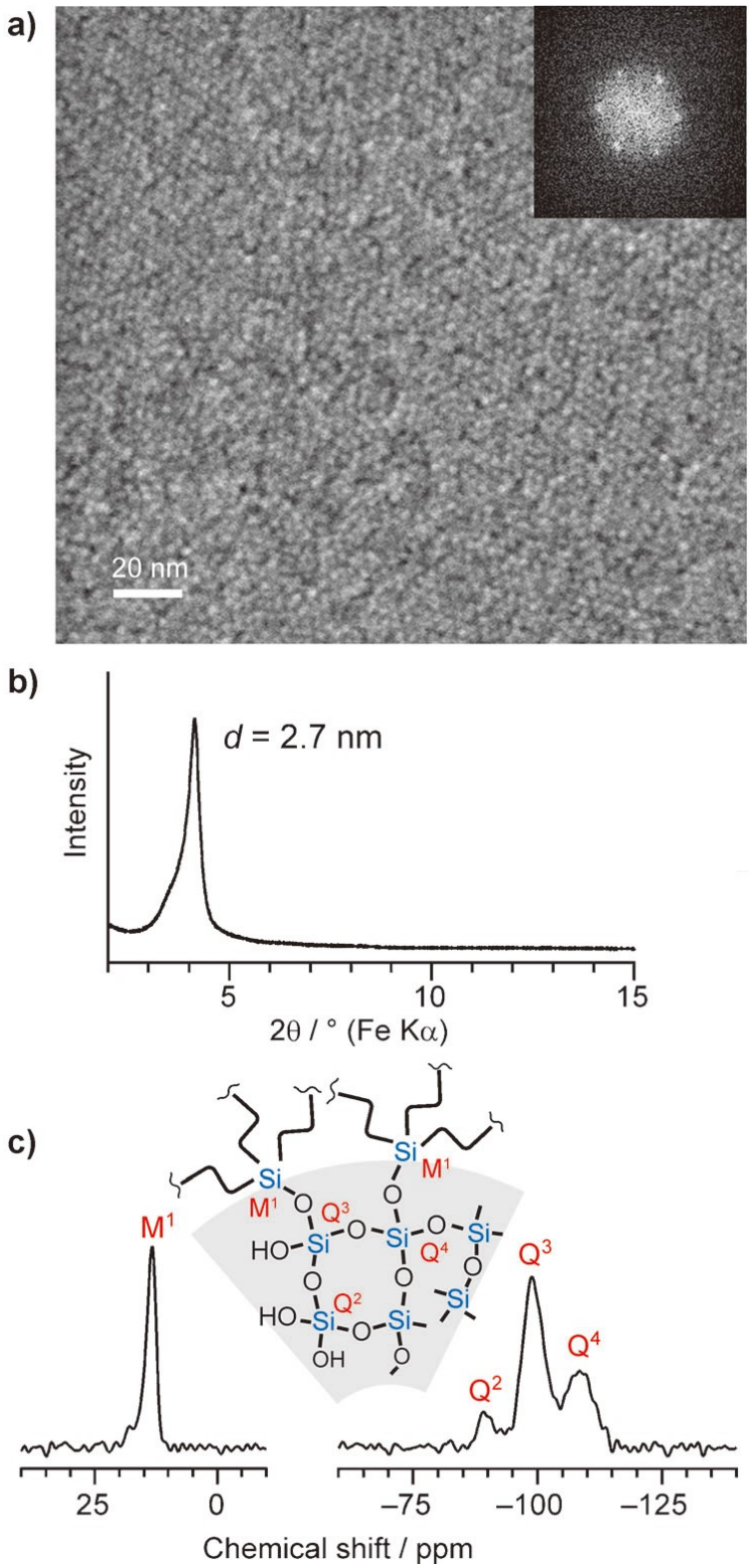

Figure 3.1. a) Typical SEM micrograph and its Fourier transform image of the hybrid mesostructure **1H(Si4)**. The sample was imaged without prior deposition of a conductive metal top-coat. b) XRD pattern and c) solid-state ^{29}Si MAS NMR spectrum

of **1H(Si4)**.

3.4.2 Characterization of nanoparticles derived from 1H(Si4)

The hybrid material **1H(Si4)** was readily dispersed in hexane to give a colloidal solution. When the clear solution is allowed to dry, island-shaped aggregates (Figure 3.2a) and discrete nanoparticles (Figure 3.2b) are clearly observed by SEM and the relative proportion of these two forms depends on the dilution ratio. The discrete particles are also observed by transmission electron microscopy (TEM) (inset of Figure 3.2b). The affinity of these nanoparticles to the nonpolar solvent strongly suggests that they have a reverse micellar structure with the alkyl chains facing outward and the hydrophilic silanol groups inward. Furthermore, these nanoparticles can be re-assembled into various macroscopic morphologies, such as spherical particles (ca. 200 nm in diameter) through the addition of ethanol to the hexane solution (Figure 3.3), and as thin films by coating the hexane solution onto substrates. These secondary structures can again be re-dispersed in hexane. The ability of these nanoparticles to undergo reversible assembly/dispersion illustrates their chemical stability.

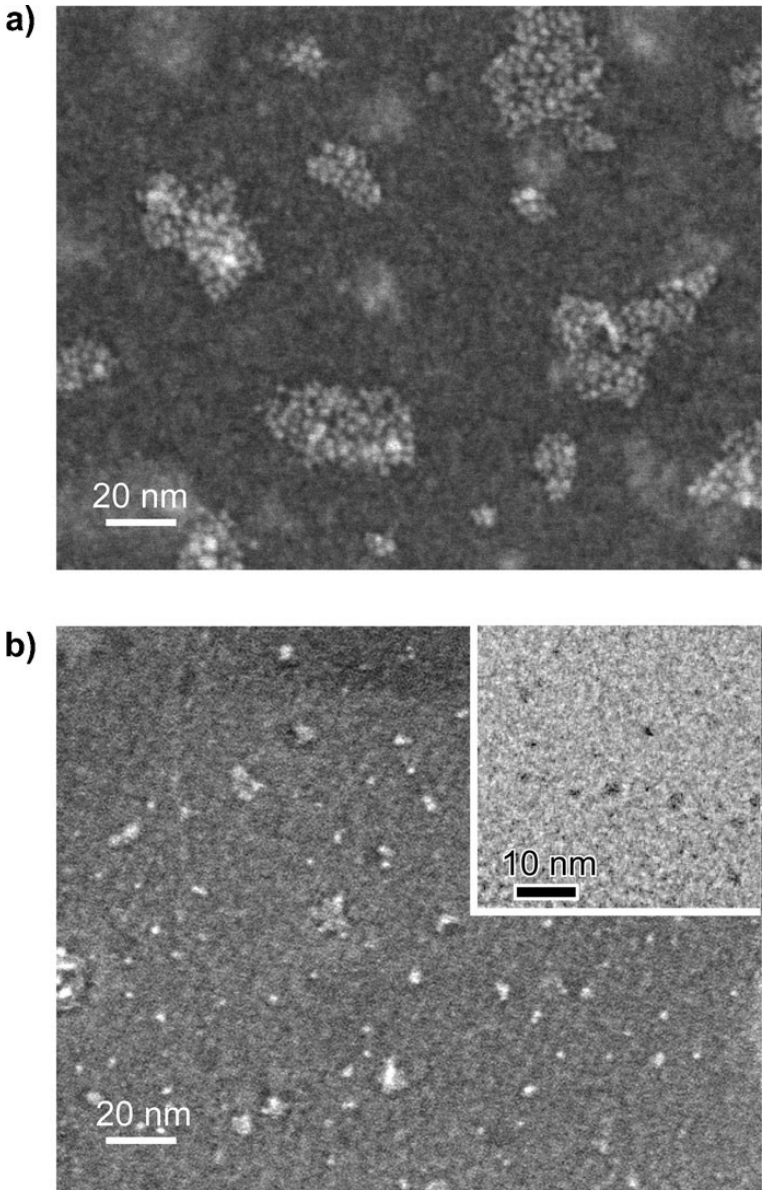

Figure 3.2. Direct observation of the nanoparticles deposited from a hexane solution. SEM images of a) island-shaped aggregates and b) discrete nanoparticles. The samples were prepared by applying drops of the solutions on copper TEM grids followed by drying in air. The inset of b) shows the TEM image of the discrete nanoparticles.

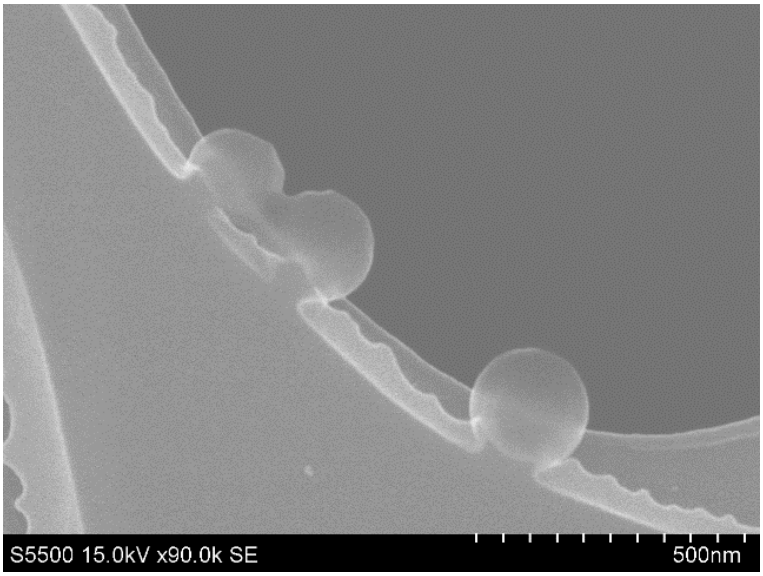

Figure 3.3. SEM image of the spherical aggregates. These spheres were prepared by addition of ethanol to the hexane dispersion of the nanoparticles. The size distribution can be estimated briefly around 200 ± 150 nm.

Thus, core–shell hybrid nanoparticles as small as 3.3 nm in diameter have been obtained. The maximum thickness of the organic shell is ca. 0.7 nm when the C6 chains are in an extended state, and the diameter of the siloxane core is then calculated to be ca. 1.9 nm. A recent report on the templated synthesis of silica nanospheres in metal complex capsules confirmed that a nanosphere of 2.9 nm in diameter is composed of roughly 170 SiO_2 units.[17] Considering that our nanoparticles have a similar degree of condensation (i.e. Q^3 unit is predominant), as confirmed by ^{29}Si MAS NMR spectroscopy, the number of SiO_2 units in our case is estimated to be 48. Therefore, each nanoparticle of **1H(Si4)** is presumed to be composed of at least 12 molecules of **1(Si4)**.

3.4.3 Influence of oligosiloxane length of precursor on mesostructure.

Our previous studies have shown that the structural periodicity of the

alkylsiloxane mesophase is dependent on the alkyl chain length of the precursors.[11] In the present case, precise size control of the nanoparticles can be achieved by varying the length of the oligosiloxane chains in the presence of trihexyl groups. Homologous precursors with a disiloxane unit, **1(Si2)**, as well as a linear trisiloxane unit, **1(Si3)**, form mesophases with smaller *d* spacings (Figure 3.4), which indicates a decrease of the resultant particle size. These mesophases were fully dispersible in hexane. Notably, **1H(Si2)** was a viscous liquid mainly consisting of the trimer of hydrolyzed **1(Si2)** having a cyclic trisiloxane core, as confirmed by liquid-state ^{29}Si NMR spectroscopy and matrix assisted laser desorption/ionization time-of-flight mass spectrometry (MALDI-TOF-MS) (Figure 3.5). The smaller number of crosslinkable units available with this disiloxane precursor should result in a decreased number of the molecular components in a particle. Hence, the direct observation of individual nanoparticles has not been achieved mainly because of their extremely small numbers of SiO_2 units.

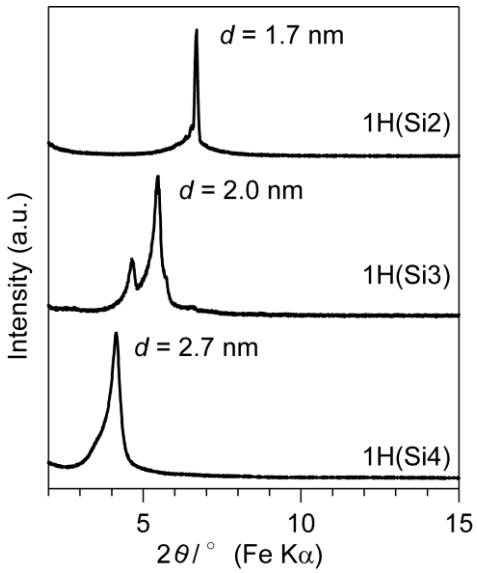

Figure 3.4. XRD patterns of the **1H(Si*n*)** films of varying siloxane chain length. The additional small peak at lower angle in the XRD pattern observed for **1H(Si3)** might be due to a co-existed another mesophase, which is unclear so far.

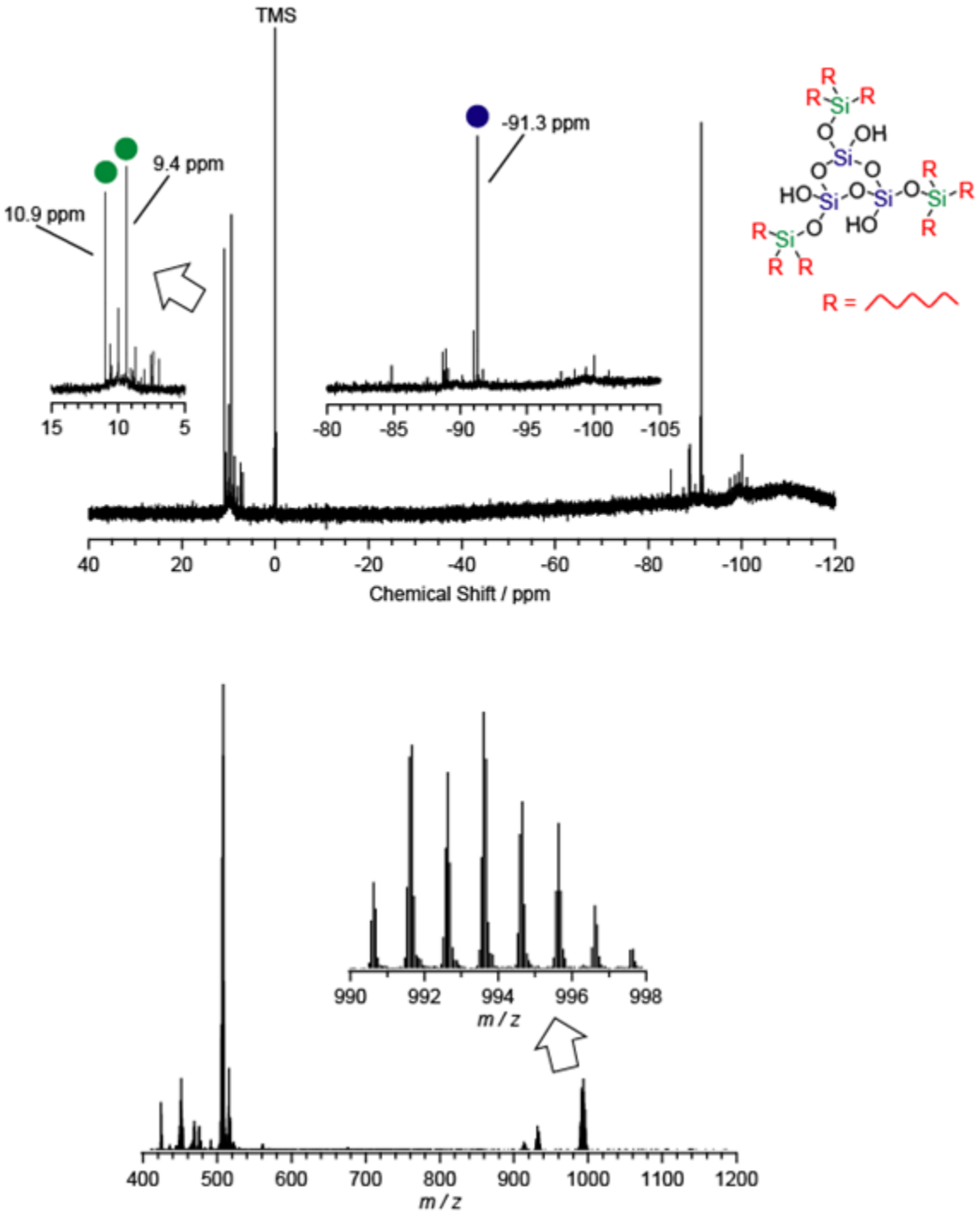

Figure 3.5. Liquid-state ^{29}Si NMR spectrum and MALDI-TOF-MS spectrum of the hybrid mesostructure **1H(Si2)** dissolved in hexane. Main three signals in the NMR spectrum can be assigned to each silicon atoms of the expected molecule. Also, peaks in MS around m/z = 994 can be assigned to the expected molecule derivatives ($[M\text{-}C_6H_{13}]^+$) from liquid-state ^{29}Si NMR spectrum.

3.4.4 Introduction of vinyl group into organic shells

Varying the chemical composition of the outer organic layer plays a key role in tuning the surface and therefore the nanoparticles' properties with regard to interparticle interactions, solubility, and functionality.[19, 20] As an example, we performed the reaction of the precursor bearing C=C bonds at the terminus of the hexyl groups forming a periodic structure that exhibits an XRD peak at d = 2.3 nm. The slightly shorter periodicity compared to that of **1H(Si4)** aggregates may be attributed to the different packing due to the presence of C=C bonds. The C=C bonds should allow further reactions, such as hydrosilylation, coupling reactions, and radical polymerizations. For biomedical applications, grafting of hydrophilic PEG chains to the terminal C=C bonds is of great significance. Our direct-assembly method thus provides a versatile route for the production of organically modified nanoparticles. This is superior to the conventional method based on the postsynthetic modification of bare silica nanoparticles,[18, 19] which is often complicated by self-condensation of the silylating agents and/or irreversible aggregation of the nanoparticles during modification.

3.4.5 Characterization of dye-containing nanoparticles

To demonstrate the ability of our silica nanoparticles to serve as nanocapsules, we investigated the encapsulation of a hydrophilic fluorescent dye, 7-hydroxycoumarin, into the siloxane core by dissolving the dye in the solution of hydrolyzed **1(Si4)** prior to evaporation-induced self-assembly. The obtained particles can be dispersed in hexane, and the resulting clear solution exhibits absorption at λ_{max} = 327 nm (Figure 3.6), suggesting that the dyes are incorporated in the nanoparticles. The fluorescent peak at 390 nm suggests that the incorporated dye molecules are not aggregated and in their neutral state,[20] implying that the dyes are fixed to the siloxane core through a weak

hydrophilic interaction and/or hydrogen bonding. This represents a new method to "dissolve" hydrophilic dyes in nonpolar solvents and such an encapsulation of dyes in silica matrices is expected to enhance their stability against degradation.[21] Similar results were observed for different types of hydrophilic dyes, confirming that this encapsulation capability is of general versatility.

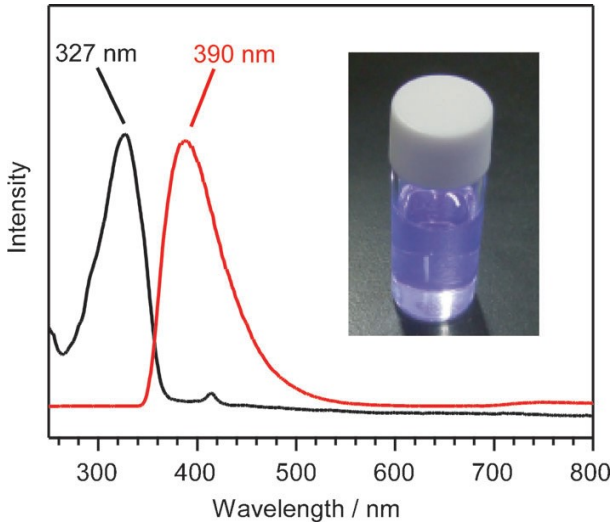

Figure 3.6. UV/Vis spectrum (black line) and fluorescence spectrum (red line, excitation wavelength: 327 nm) of the hexane dispersion of 7-hydroxycoumarin-containing **1H(Si4)**. The inset shows the photograph of the dispersion under UV irradiation (365 nm).

3.5 Conclusion

In conclusion, we have developed a novel route to organically modified silica nanoparticles with diameters of a few nanometers from well-defined single-molecule precursors. The small silica core is covered with a dense layer of alkyl chains, which allows for the dispersion of the bulk mesophase into its individual nanoparticle building blocks without the occurrence of irreversible nanoparticle aggregation. Furthermore, we succeeded in encapsulating a fluorescent dye into the siloxane cores. This study paves

the way to new possibilities for designing functionalized hybrid nanoparticles through the targeted tailoring of the chemical and physical properties of the core and shell components.

3.6 References

1 D. Knopp, D. Tang, R. Niessner, *Anal. Chim. Acta.* **2009**, *647*, 14.

2 A. Burns, H. Ow, U. Wiesner, *Chem. Soc. Rev.* **2006**, *35*, 1028.

3 M. A. Noginov, G. Zhu, A. M. Belgrave, R. Bakker, V. M. Shalaev, E. E. Narimanov, S. Stout, E. Herz, T. Suteewong, U. Wiesner, *Nature*, **2009**, *460*, 1110.

4 H. Ow, D. R. Larson, M. Srivastava, B. A. Baird, W. W. Webb, U. Wiesner, *Nano Lett.* **2005**, *5*, 113.

5 A. B. Andrew, J. Vider, H. Ow, E. Herz, O. Penate-Medina, M. Baumgart, S. M. Larson, U. Wiesner, M. Bradbury, *Nano Lett.* **2009**, *9*, 442.

6 X. Zhao, R. P. Bagwe, W. Tan, *Adv. Mater.* **2004**, *16*, 173.

7 E. Rampazzo, S. Bonacchi, M. Montalti, L. Prodi, N. Zaccheroni, *J. Am. Chem. Soc.* **2007**, *129*, 14251.

8 H. Fan, K. Yang, D. M. Boye, T. Sigmon, K. J. Malloy, H. Xu, G. P. López, C. J. Brinker, *Science*, **2004**, *304*, 567.

9 P. Mulvaney, L. M. Liz-Marzán, M. Giersigc, T. Ung, *J. Mater. Chem.* **2000**, *10*, 1259.

10 S. H. Joo, J. Y. Park, C.-K. Tsung, Y. Yamada, P. Yang, G. A. Somorjai, *Nat. Mater.* **2009**, *8*, 126.

11 A. Shimojima, K. Kuroda, *Chem. Rec.* **2006**, *6*, 53.

12 S. Sakamoto, A. Shimojima, K. Miyasaka, J. Ruan, O. Terasaki, K. Kuroda, *J.*

Am. Chem. Soc. **2009**, *131*, 9634.

13 K. Katagiri, M. Hashizume, K. Ariga, T. Terashima, J. Kikuchi, *Chem. Eur. J.* **2007**, *13*, 5272.

14 J. Du, Y. Chen, *Angew. Chem.* **2004**, *116*, 5194; *Angew. Chem. Int. Ed.* **2004**, *43*, 5084.

15 F. J. Arriagada, K. Osseo-Asare, *J. Colloid Interface Sci.* **1995**, *170,* 8.

16 C. B. W. Garcia, Y. Zhang, S. Mahajan, F. DiSalvo, U.Wiesner, *J. Am. Chem. Soc.* **2003**, *125*, 13310.

17 K. Suzuki, S. Sato, M. Fujita, *Nat. Chem.* **2010**, *2*, 25.

18 A. B. Descalzo, R. Martínez-Máñez, F. Sancenón, K. Hoffmann, K. Rurack, *Angew. Chem.* **2006**, *118*, 6068; *Angew. Chem. Int. Ed.* **2006**, *45*, 5924.

19 F. Santoyo-Gonzalez, F. Hernandez-Mateo, *Chem. Soc. Rev.* **2009**, *38*, 3449.

20 Y. Tsuru, T. Sawada, H. Kamada, *Bunseki Kagaku*, **1975**, *24*, 594.

21 D. Avnir, V. R. Kaufman, R. Reisfeld, *J. Non-Cryst. Solids*, **1985**, *74*, 395.

Chapter 4

Formation of Single-Digit Nanometer Scale Silica Nanoparticles by Evaporation-Induced Self-Assembly

Adapted with permission from S. Sakamoto, M. Yoshikawa, K. Ozawa, Y. Kuroda, A. Shimojima, and K. Kuroda, "Formation of Single-Digit Nanometer Scale Silica Nanoparticles by Evaporation-Induced Self-Assembly", *Langmuir* **2018**, 34, 1711−1717.
Copyright 2009 American Chemical Society.

4.1 Abstract

There are emerging demands for single-digit nanoscale particles in multidisciplinary fields, such as nanomedicine, optics, catalysis, and sensors, to create new functional materials. Here, we report a novel route to prepare silica nanoparticles less than 3 nm in size via the evaporation-induced self-assembly of silicate species and quaternary trialkylmethylammonium surfactants, which usually form reverse micelles. The solvent evaporation induces a local concentration increase and simultaneous polycondensation of silicate species within the hydrophilic region of the surfactant mesophases. Extremely small silica nanoparticles in the silica−surfactant mesostructures can be stably dispersed in organic solvents by destroying the mesostructure, which is in clear contrast to the preparation of silica nanoparticles using the conventional reverse micelle method. The surface chemical modification of the formed silica nanoparticles is easily performed by trimethylsilylation. The particle size is adjustable by changing the ratio of the surfactants to the silica source because the hydrophobic/hydrophilic ratio determines the curvature and diameter of the resulting spherical silica−surfactant domains in the mesostructure. The versatility of this method is demonstrated by the fabrication of very small titania nanoparticles. These findings will increase the designability of oxide nanoparticles at the single-digit nanoscale because conventional methods based on the generation and growth of nuclei in a solution cannot produce such nanoparticles with highly regulated sizes.

4.2 Introduction

Currently, silica nanoparticles are important ingredients in the materials industry. In addition to their high stability, biocompatibility, and transparency, silica nanoparticles can be chemically modified at their surfaces, and their sizes can be

precisely controlled. Furthermore, a variety of substances can be introduced to the particles, and pores can be added, depending on the requirements of the final product. These features make silica nanoparticles useful for various applications, such as polymer fillers,[1] abrasives,[2] catalysts,[3] and drug delivery carriers.[4] One of the recent trends in nanoparticle technology research is how to reduce the particle size. A convex and high-curvature surface in smaller nanoparticles is advantageous for the adsorption of bulky molecules,[5,6] for enhancing the mechanical stability of nanoparticle coatings,[7] and for avoiding unwanted Rayleigh scattering.[8] In addition, there is a size threshold of less than 10 nm for efficient renal clearance in bioengineering applications.[9,10]

From the viewpoints of size uniformity and dispersity, the Stöber method,[11] in which tetraethoxysilane (TEOS) is hydrolyzed in a water−ethanol−ammonia mixture, has been favored for the fabrication of monodisperse silica nanoparticles of several tens of nanometers in diameter. More recently, Yokoi and co-workers reported the preparation of monodisperse silica nanoparticles around 10 nm in diameter by the reaction of TEOS in water containing basic amino acids.[12,13] Plausible mechanisms for the formation of such silica nanoparticles have been proposed to be nucleation followed by seed growth[12−14] or the association of nuclei.[14,15] In any case, nuclei of sub-5 nm size are formed in the primary stage.[13,15] To terminate particle growth, the capping of the surface silanol groups on the primary nuclei is an effective approach. Ma et al. reported the fine size control of silica nanoparticles at the single-digit nanoscale (2.4−7.3 nm).[16] The success of this procedure depends on surface modification with a polyethylene glycol (PEG)-modified silane. However, if such surface modification is not required, many applications can be achieved through functionalization by postchemical modification. In addition, the procedure requires the precise control of the reaction conditions with low Si concentrations, which is unfavorable for large-scale production.

The size control of silica nanoparticles can also be achieved by using amphiphilic molecules and polymers as structuredirecting agents or templates. Water-in-oil (w/o) microemulsion methods, including the reverse micelle method, are typical for preparing silica and metal oxide nanoparticles; however, it has proven difficult to achieve particle sizes less than 5 nm because the particle size can easily be increased by seed growth or the collision of nanoparticles in microemulsions.[17] Another method is based on the deconstruction of inorganic−organic nanocomposites with reverse-type mesostructures where silica species exist in the hydrophilic regions surrounded by the continuous hydrophobic moieties. Amphiphilic block copolymers are available to form such reverse-type mesostructures through evaporation-induced self-assembly (EISA) or microphase separation.[18,19] Silica nanoparticles have been produced by the fine-tuning of polymer architectures, but an essential problem that remains to be solved is that the size range of the formed nanoparticles is always greater than 10 nm. Recently, we have reported the formation of silica nanoparticles ca. 3 nm in size with dense outer alkyl chains through the self-assembly of oligosiloxane compounds possessing a trialkylsilyl group.[20] The large hydrophobic moiety covalently bonded to the hydrophilic oligosiloxane favors the formation of reverse-type silica-organic hybrid mesostructures by the EISA process, and the mesostructures can be successfully dispersed into discrete nanoparticles in hexane. However, the synthesis of such precursors is rather complicated, and the outer surfaces of the resulting particles cannot be postmodified.

Herein, we propose a facile route to monodisperse silica nanoparticles with diameters of less than 3 nm, on the basis of the self-assembly of small surfactant molecules and silica sources. Upon solvent-evaporation, the surfactants are assembled into reverse micelles, and hydrophilic silicate species are automatically accumulated in

the center of micelles, forming silica nanoparticles (Figure 4.1a, ii). The silica nanoparticles are covered with the surfactant molecules and are accordingly well dispersed in the organic solvents (Figure 4.1a, iii). This synthetic process is essentially different from the conventional reverse micelle method in that nanoparticles are formed as a constituent unit of a solid-state mesostructure, while the conventional reverse micelle method depends on particle growth inside the confined space of micelles in solution (Figure 4.1b). On the basis of the theory of micelle formation, a quaternary ammonium ion bearing three hydrophobic tails, which has a large packing parameter, was chosen as a surfactant.[21] Such triple-chain quaternary ammonium surfactants have been used as pore expanders for mesoporous silica,[22,23] but their use as structure-directing agents in the EISA process has not been reported. There are three unique features of nanoparticles prepared by this method. The first is the small particle sizes less than 3 nm in diameter. The second is the presence of silanol groups on the surface that allow postmodification with organic functional groups. The third is the high stability against aggregation both in the solid state and in the solution state, which is convenient for industrial use. Importantly, the applicability of this method to other compositions was demonstrated by the preparation of titanium oxide nanoparticles.

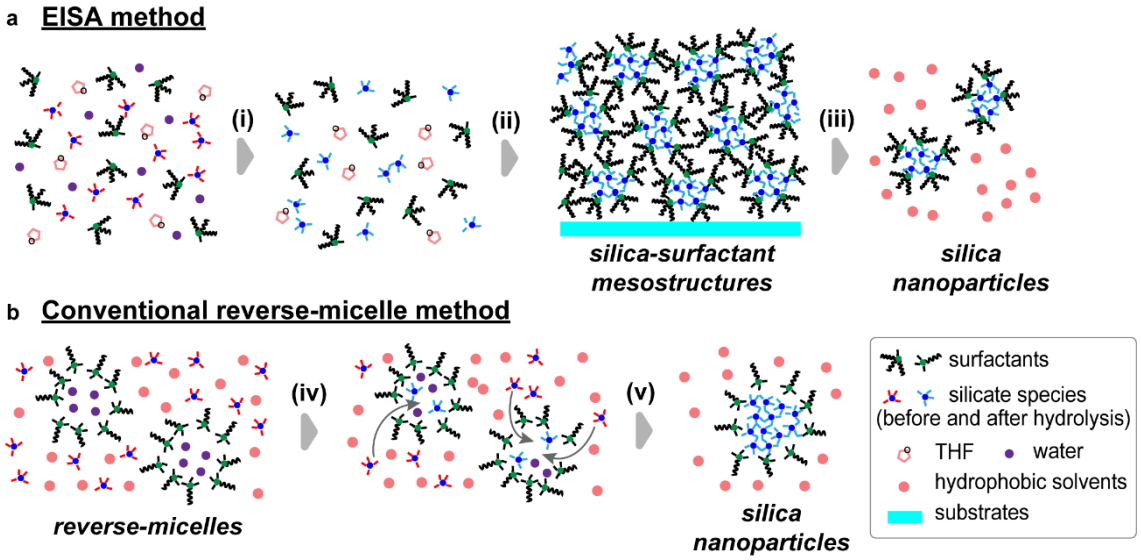

Figure 4.1. Schematic representation of synthetic routes to silica nanoparticles. (a) The newly proposed EISA method consisting of (i) the hydrolysis of TEOS, (ii) evaporation-induced self-assembly with surfactant on a glass substrate, and (iii) the subsequent dispersion in an organic solvent. (b) The conventional reverse-micelle method based on (iv) the transfer of silicate species into reverse micelles and (v) the polycondensation of hydrolyzed silicate species in water-in-oil microemulsion solution.[17]

4.3 Experimental

4.3.1 Materials

Toluene (super dehydrated), tetrahydrofuran (THF, super dehydrated, stabilizer free), ethanol (super dehydrated), hexane, 0.01 mol/L hydrochloric acid, and hydrochloric acid (35.0−37.0%) were purchased from Wako Pure Chemical Industries, Ltd. Tetraethoxysilane ($Si(OCH_2CH_3)_4$, >97.0%), chlorotrimethylsilane (>98.0%), methyltri-*n*-octylammonium chloride (3C8MAC, >95.0%), and titanium tetraisopropoxide ($Ti(OCH(CH_3)_2)_4$; TTIP) were purchased from Tokyo Chemical Industry Co., Ltd. These chemicals were used as received. Glass substrates (48 × 24 mm, Matsunami Glass Ind., Ltd.) were used after washing with deionized water by ultrasonication for 10 min.

4.3.2 Synthesis of silica mesostructure (SNP-as)

3C8MAC was used for the formation of a silica−surfactant mesostructure consisting of reverse-type micelles. The hydrolysis of TEOS was performed in a mixture with the molar composition of TEOS/THF/H_2O/HCl = 1.0:3.5:4.1:7.5 × 10^{-4}. The mixture was stirred at room temperature for 3 h. Then, a THF solution of 3C8MAC was added into the hydrolyzed solution. The final molar ratio of Si/THF/3C8MAC was 1.0:30:0.39. After being stirred for an additional 10 min, the mixture was cast on a glass substrate and was air-dried at room temperature for 1 day. The resulting colorless transparent film is denoted as **SNP-as**. Please note that the ratio of 3C8MAC over TEOS is higher than those used in the conventional EISA method.

4.3.3 Synthesis of Trimethylsilylated Silica Nanoparticles (SNP-TMS)

In a typical synthesis, 200 μL of chlorotrimethylsilane was added to a solution of **SNP-as** (0.20 g of **SNP-as** in 2 mL of THF) with vigorous stirring at room temperature. After stirring for 10 min, ethanol was added for the ethoxylation of unreacted Si−Cl groups. After the evaporation of the volatile components at 60 °C, hexane was poured into the vessel to extract the trimethylsilylated nanoparticles under ultrasonication for 5 min. The supernatant solution was separated from the precipitates of the surfactants and was dried in a Petri dish at 60 °C. The resulting solid was pulverized into a white powder, which is denoted **SNP-TMS**.

4.3.4 Synthesis of titania mesostructure (TNP-as)

Hydrolysis of TTIP was performed in a mixture with the molar ratio of TTIP/THF/H2O/HCl = 1.0:14:3.2:1.2. The mixture was stirred at room temperature for

1 h, followed by the addition of a THF solution of 3C8MAC. The final molar ratio of Ti/THF/3C8MAC was 1.0:28:0.30. After being stirred for an additional 10 min, the mixture was cast on a glass substrate and was air-dried at room temperature for 1 day to give a colorless, transparent thick film (**TNP-as**).

4.3.5 Characterization

Liquid-state ^{13}C and ^{29}Si nuclear magnetic resonance (NMR) spectra were recorded on a JEOL JNM-ECZ 500 spectrometer with resonance frequencies of 125.76 and 99.36 MHz, respectively. The solution was placed in a 5 mm glass tube, where THF-d_8 was used to obtain lock signals, and a small amount of chromium(III) acetylacetonate was added for the relaxation of the ^{29}Si nuclei. Tetramethylsilane was used as an internal reference at 0 ppm. The ^{13}C and ^{29}Si NMR spectra were measured with recycling delays of 2 and 10 s, respectively. Solid-state ^{29}Si magic-angle spinning (MAS) NMR spectra were recorded on a JEOL JNM-ECX-400 spectrometer at a resonance frequency of 79.42 MHz with a 45° pulse and a recycle delay of 150 s. A 4 mm zirconia rotor at a spinning frequency of 5 kHz was used. The chemical shifts were externally referenced to the silicon atoms of poly(dimethylsilane) at −33.8 ppm. The solid-state ^{13}C cross polarization (CP)/MAS NMR spectra were also recorded on a JNMECX 400 spectrometer at a resonance frequency of 99.5 MHz with a recycle delay of 10 s and a contact time of 5 ms. The samples were put in a 4 mm silicon nitride tube and were spun at 10 kHz. The chemical shifts were externally referenced to the methyl groups of hexamethylbenzene at 17.4 ppm. The θ–2θ X-ray diffraction (XRD) patterns were recorded on a Rigaku Ultima IV parallel beam diffractometer using monochromated Fe Kα radiation (40 kV, 30 mA). Scanning electron microscopy (SEM) observation was carried out on a HITACHI S-5500 microscope operated at 30 kV. For

the observation, nanoparticles were arbitrarily diluted in THF, followed by dropping on carbon supported Cu grids and air-drying. Small-angle Xray scattering (SAXS) measurements were performed on a Rigaku Nanoviewer apparatus at 40 kV and 30 mA using a Pilatus 2D detector. The camera length was 100 mm.

4.4 Results and discussion

4.4.1 Characterization of silica mesostructure (SNP-as)

Partial oligomerization of the hydrolyzed species derived from TEOS was confirmed by ^{29}Si NMR measurements of the solution after the hydrolysis of TEOS in THF under acidic conditions for 3 h (Figure 4.2). The signals corresponding to the Q^1, Q^2, and Q^3 units (Q^x:$Si(OSi)_x(OH)_{4-x}$) were observed in addition to the Q^0 signals of hydrolyzed monomers. Cooperative self-organization of the silicate species and 3C8MAC upon evaporation of the solvent gave **SNP-as** as a colorless and transparent thick film that was soft and slightly sticky.

The solid-state ^{29}Si MAS NMR spectrum of **SNP-as** showed the Q^2, Q^3, and Q^4 signals at −90.1, − 99.4, and −109.8 ppm, respectively, indicating the formation of siloxane networks (Figure 5a). The integral intensity ratio was Q^2:Q^3:Q^4 = 1.0:3.6:2.2. The degree of condensation ($(2 \times Q^2 + 3 \times Q^3 + 4 \times Q^4)/((Q^2 + Q^3 + Q^4) \times 4) \times 100$) was calculated to be 79%. The mesoscale periodicity in **SNP-as** was confirmed by the diffraction peak with a d spacing of 2.5 nm in the XRD pattern (Figure 4.3b, i). The single broad peak suggested that the mesostructure consisting of disordered assembly of nanoparticles was formed. Similar diffraction results were reported for assembled crystalline TiO_2 and SnO_2 nanoparticles,[24] though the preparative method was different. A high-resolution SEM image of the film showed a rough surface morphology with some white dots approximately 2 nm in size, implying that **SNP-as** consisted of

randomly aggregated nanoparticles (Figure 4.4).

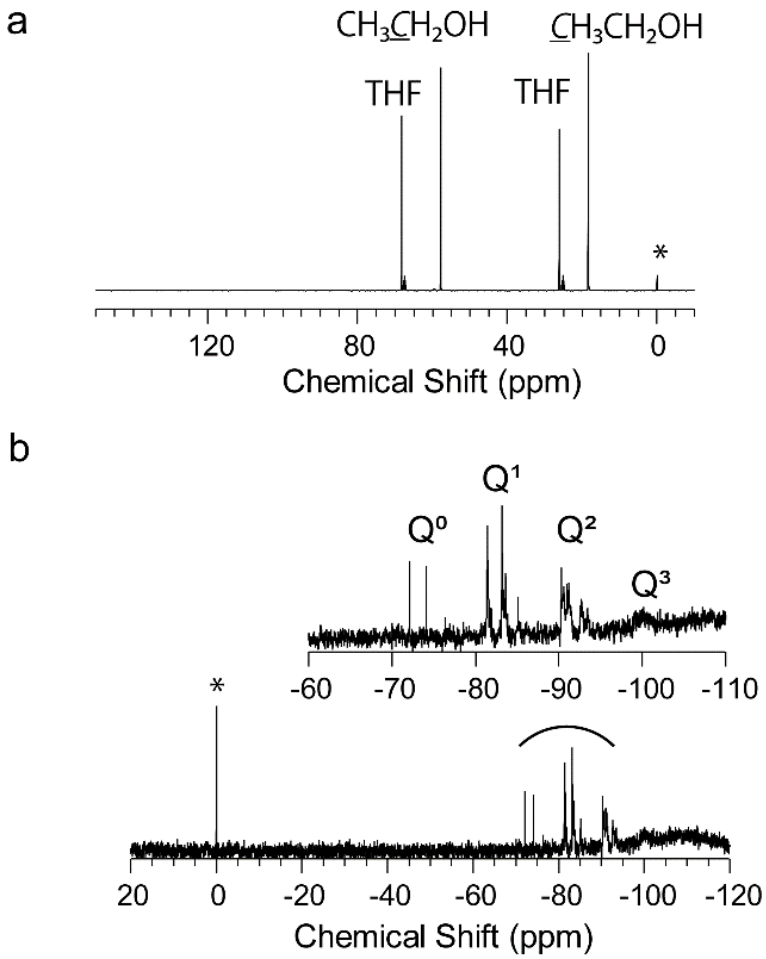

Figure 4.2. Liquid-state NMR spectra of the precursor solution after hydrolysis for 3 h. The ^{13}C NMR spectrum (a) shows the signals assigned to ethanol ($HOCH_2CH_3$) in place of ethoxy groups ($-OCH_2CH_3$), indicating that TEOS is almost hydrolyzed. The ^{29}Si NMR spectrum (b) shows the Q^0, Q^1, Q^2, and Q^3 signals, indicating the presence of oligomeric species along with hydrolyzed monomers. (The asterisk indicates tetramethylsilane.)

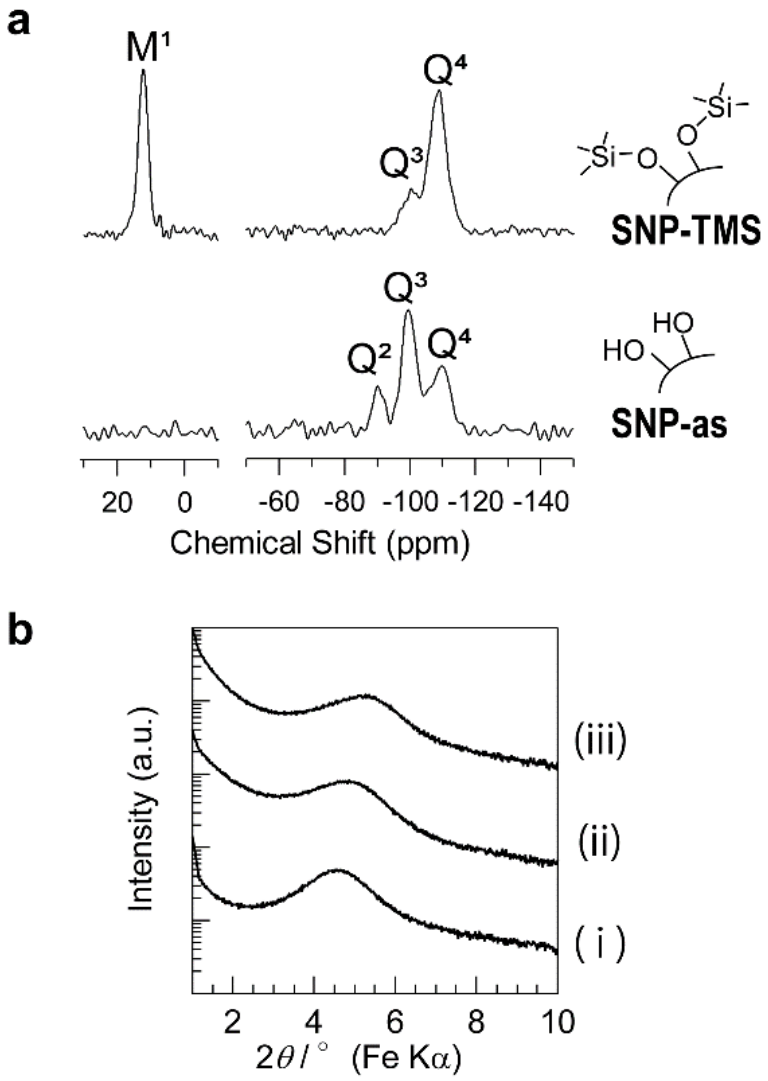

Figure 4.3. (a) Solid-state ^{29}Si MAS NMR spectra of **SNP-as** and **SNP-TMS**. (b) XRD patterns of the samples prepared with different 3C8MAC/TEOS molar ratios of (i) 0.39 (**SNP-as**), (ii) 0.64, and (iii) 1.29.

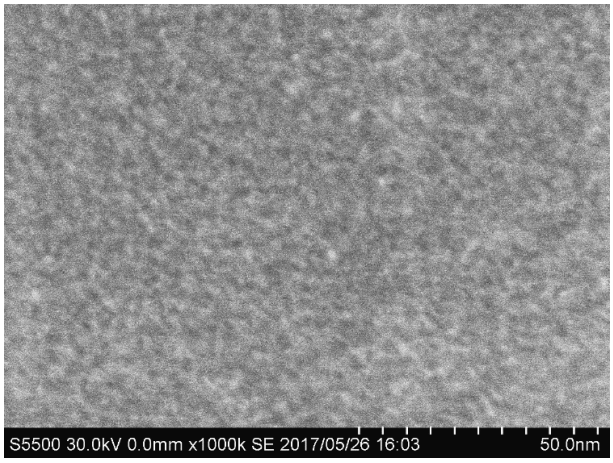

Figure 4.4. High-resolution SEM image of **SNP-as** prepared directly on a Cu-supported carbon grid. The image is not clear probably due to the high content of surfactants.

4.4.2 Characterization of nanoparticles derived from SNP-as

Interestingly, **SNP-as** can be dissolved in organic solvents such as THF and toluene within a few minutes to form a transparent solution by simple mixing. There was no remarkable Rayleigh scattering in the toluene solution against collimated light irradiation at 630−660 nm, which is in clear contrast to the conventional colloidal silica nanoparticles (ca. 9 nm) (Figure 4.5a). The existence of ultrasmall nanoparticles was confirmed by SAXS analysis and SEM observation. The SAXS pattern showed a broad peak at the q values larger than 1.0 nm^{-1} (Figure 4.5b), which is due to the interference of dispersed nanoparticles. The diameter of nanoparticles was roughly calculated to be 2−3 nm on the basis of the Guinier approximation,[25] which is in good agreement with the dspacing of the XRD pattern of **SNP-as** (Figure 4.3b, i). In addition, dots of approximately 2 nm in size that were isolated or partially aggregated on carbon grids were clearly observed by SEM (Figure 4.5c). Transmission electron microscopy (TEM) observation to determine the particle size was unsuccessful probably because of the too small size of the particles, the instability under electron beam irradiation, and the

appearance similar to the surface of a carbon grid. The relatively high intensity ratios of Q^2 and Q^3 signals to that of Q^4 in the solidstate ^{29}Si MAS NMR spectrum of **SNP-as**, mentioned earlier, are also consistent with the very small size. These results indicate that a reverse-type mesostructure consisting of silica nanoparticles was formed by the EISA process. The high colloidal stability of the dispersed silica nanoparticles was confirmed by the lack of precipitation in the solution even after 1 month. It is plausible that the ammonium groups of 3C8MAC were electrostatically adsorbed on the surfaces of the silica nanoparticles and that the outward trialkyl groups played an important role in the separation and stabilization of each nanoparticle. This novel synthetic pathway can produce a large amount of well-dispersed, ultrasmall silica nanoparticles by a simple procedure. **SNP-as** was stable even in the solid state, and it could be dispersed in organic solvents even after the preservation at room temperature for 3 months in air. This finding indicates that the nanoparticles are highly stabilized against interparticle condensation by the presence of the surfactant.

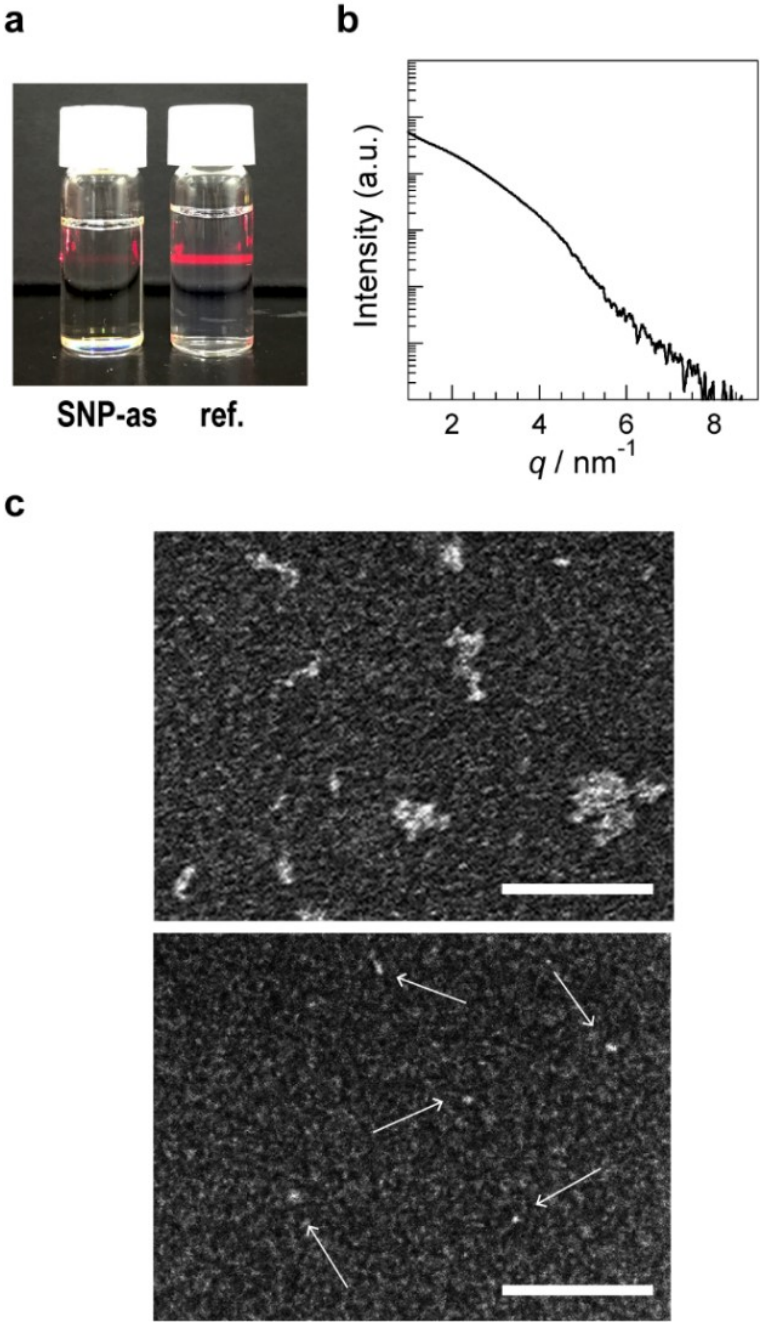

Figure 4.5. (a) Appearances of a 5 wt % solution of **SNP-as** in toluene and a water dispersion of silica nanoparticle (average diameter of 9 nm, see Figure 4.6) prepared by the method in ref 12. Note that the Rayleigh cross section is proportional to d^6, where d is the diameter of nanoparticles.[26] (b) SAXS pattern of **SNP-as** dissolved in toluene. (c) SEM images of dispersed nanoparticles on carbon grids by tuning the dilution ratios to lower (top) and higher (bottom) degrees. The scale bars show 50 nm.

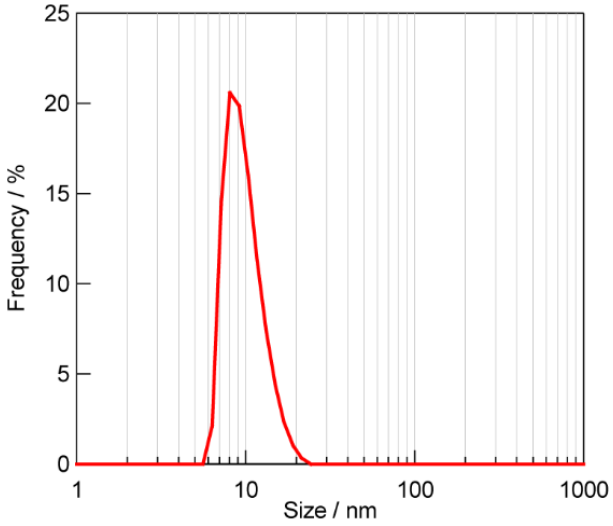

Figure 4.6. Dynamic light scattering (DLS) profile of silica nanoparticles prepared by the method reported in ref.12. The profile was measured by a HORIBA nano Partica SZ-100S instrument.

4.4.3 Surface modification of silica nanoparticles

Supposing that silica nanoparticles are applied to a nanofiller to produce polymer nanocomposites or a nanosized building block to construct higher-order architectures, chemical modification of the surface silanol groups is important. Silica nanoparticles in **SNP-as** are covered with cationic surfactants through noncovalent, electrostatic interactions, which should permit the silylation of the surface silanol groups with organosilicon compounds bearing Si−Cl or Si−OR (R: alkyl groups) groups. Surface modification was conducted by stirring a THF solution of **SNP-as** with chlorotrimethylsilane. The silylated nanoparticles (**SNP-TMS**) were easily separated from the surfactant by extraction with hexane, as confirmed by solidstate ^{13}C CP/MAS NMR analysis after solvent evaporation (Figure 4.7). A strong signal assigned to the ≡Si−CH_3 of trimethylsilyl groups was observed in the spectrum, whereas there were very weak signals arising from the surfactants. In the solid-state ^{29}Si MAS NMR spectrum of **SNP-TMS**, the signal of the trimethylsilyl groups (M^1) was observed at 12.2 ppm

(Figure 3a). In addition, the condensation degree of the silica nanoparticles increased from 79% to 96%. The average number of the Si−OH groups per Si ($(Q^2 \times 2 + Q^3)/(Q^2 + Q^3 + Q^4)$) decreased from 0.82 (**SNP-as**) to 0.16 (**SNP-TMS**). This decrease in the number of Si−OH groups by 0.66 is larger than the number of the introduced TMS groups ($M^1/(Q^3 + Q^4) = 0.48$), which means that dehydration condensation of a part of the Si−OH groups also occurred during silylation. The **SNP-TMS** could be dispersed in THF and hexane even after drying, which indicates that the TMS groups strongly suppress the formation of siloxane bonds between the particles.

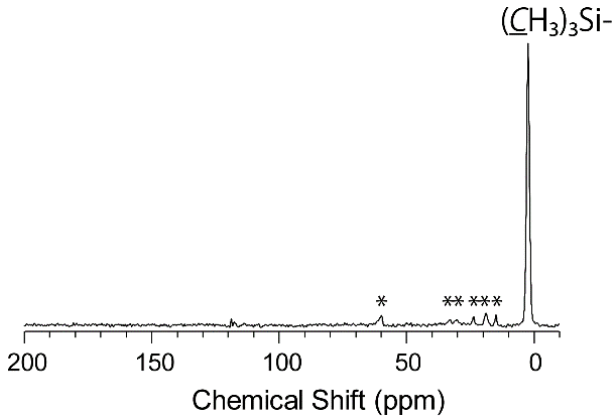

Figure 4.7. Solid-state ^{13}C CP/MAS NMR spectrum of **SNP-TMS** which was prepared by the ratio of 3C8MAC/Si = 0.39. The asterisks indicate the presence of a small amount of residual 3C8MAC.

On average, about half of the Si atoms in **SNP-as** were trimethylsilylated ($M^1/(Q^3 + Q^4) = 0.48$), which can be attributed to the high surface area of the ultrasmall silica nanoparticles. Assuming that the silica nanoparticles 2−3 nm in size in **SNP-as** have a similar density to the conventional silica nanoparticles,[12] the surface area was calculated to be ca. 1000 $m^2\ g^{-1}$. Notably, the number of attached TMS groups on **SNP-as** is apparently larger than those reported for mesoporous silica MCM-41 (M/Q

ratio < 0.16) having cylindrical mesopores, despite the similar surface areas (ca. 1000 $m^2\ g^{-1}$).[27] Such a difference can be attributed to the convex curvature of the small silica nanoparticles as well as to the higher density of the silanol groups (Q^2 and Q^3 sites) on their surfaces. Actually, we previously reported that the siloxane oligomers with a small size (ca. 1.6 nm) and a high density of outer silanol groups were successfully trimethylsilylated without steric hindrance, forming ca. 2 nm nanoparticles with an M/Q ratio of 1.5.[28]

4.4.4 Influence of surfactant concentration on nanoparticles

To study the effect of the surfactant/Si ratio on the formation of silica nanoparticles, samples prepared under different 3C8MAC/Si ratios of 0.26, 0.64, and 1.29, in addition to 0.39, were examined. When the 3C8MAC/Si ratio was 0.26, phase separation of the water and oil phases occurred during solvent evaporation. The resulting opaque film could not be dissolved in solvents. When samples were prepared with 3C8MAC/Si = 0.64 and 1.29, the products were clear viscous fluids, accompanied by the shift of XRD peaks from the original 2.5 nm to 2.3 and 2.1 nm, respectively (Figure 4.3b). Both the products obtained with the higher 3C8MAC/Si ratios were soluble in organic solvent, which suggests that they consisted of silica nanoparticles covered with the surfactant molecules.

The liquidlike behavior of the nanoparticles could be due to the high organic content of counterions and the small particle size.[29] Such nanoparticles are convenient for the formation of various morphologies, such as films, and could be useful as a solvent for their intrinsic physicochemical properties. Even in the absence of silica species, 3C8MAC forms a liquid phase with a small amount of water. This phase is immiscible with water and shows an XRD peak with a d-spacing of ca. 1.8 nm (Figure

4.8), which indicates that a mesophase consisting of reverse micelles is formed. The liquid state was preserved when relatively small amounts of silicate species were incorporated (3C8MAC/Si = 0.64 and 1.29). As the silica content increased (3C8MAC/Si = 0.39), the resulting silica−surfactant mesophase became solid, probably because of the lower mobility of the larger nanoparticles.

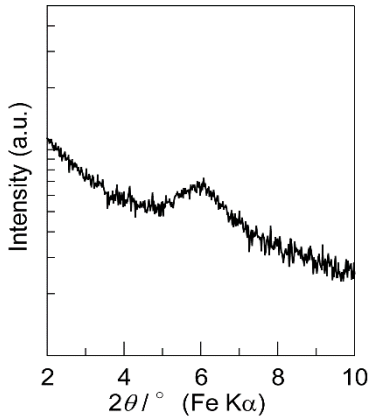

Figure 4.8. Theta–two theta XRD pattern of liquid-state 3C8MAC on a parallel sample holder.

Further analysis of the silica nanoparticles prepared with 3C8MAC/Si ratios of 0.64 and 1.29 was performed after trimethylsilylation. The solid-state ^{29}Si MAS NMR spectra (Figure 4.9a) showed that the relative intensity of the M^1 signal increased with increasing 3C8MAC/Si ratio. The M/Q ratio increased from 0.48 to 0.63 and 0.83 with the increase of the 3C8MAC/Si ratio from 0.39 to 0.64 and 1.29, respectively. This is suggestive of the larger specific surface area of smaller nanoparticles. The formation of smaller nanoparticles with higher 3C8MAC/Si ratios was also confirmed by SEM observation (Figure 4.9b). Unfortunately, the images were not clear because the samples were easily aggregated or decomposed under the electron beam irradiation, but there was at least a definite size difference between the samples prepared with 3C8MAC/Si =

0.39 and 0.64. Assuming that the surfactant density on the spherical surface is constant regardless of the 3C8MAC/Si ratio, the diameter of the nanoparticles should be in inverse proportion to the ratio because the number of surfactant molecules and the number of Si are proportional to the surface area and the volume of each nanoparticle, respectively. Therefore, if the particles were 3.0 nm when 3C8MAC/Si = 0.39, the sizes were theoretically calculated to be 1.8 and 0.9 nm when 3C8MAC/Si = 0.64 and 1.29, respectively. The particle size was thus controllable by adjusting the 3C8MAC/Si ratio in the precursor solution.

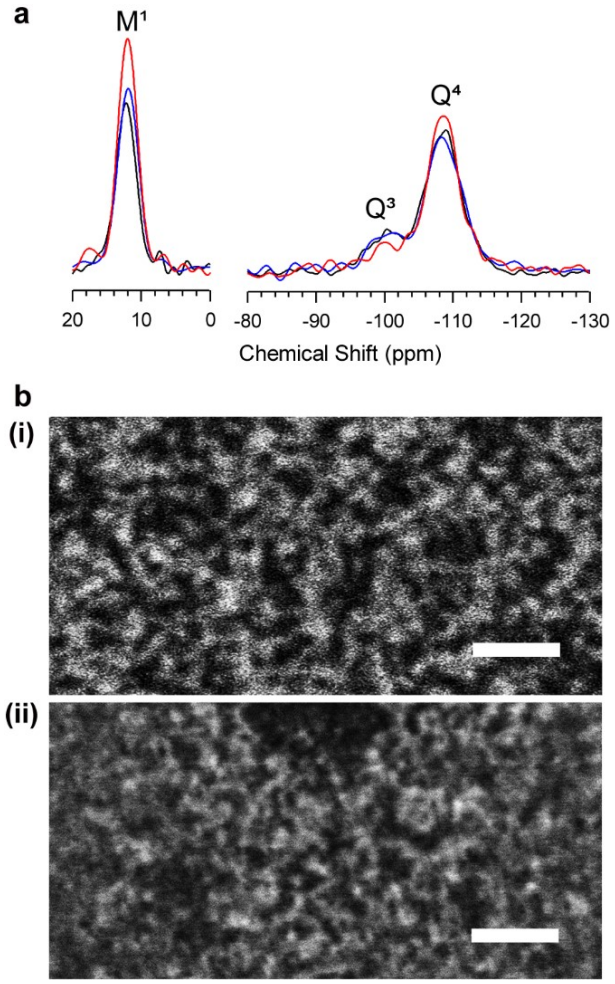

Figure 4.9. (a) Solid-state ^{29}Si MAS NMR spectra of **SNP-TMS** prepared with the 3C8MAC/TEOS molar ratios of (black) 0.39 (**SNP-as**), (blue) 0.64, and (red) 1.29. (b)

SEM images of **SNP-TMS** in which (i) and (ii) correspond to black and blue lines in a, respectively. Scale bars: 20 nm.

4.4.5 Advantages of new synthetic method of silica nanoparticles

In the conventional reverse micelle method, 3C8MAC is used to form silica nanoparticles with an average diameter of 20 nm by the reaction of sodium silicate in a water/butanol (1:1) mixture.[30] It has been concluded that the surface coating of 3C8MAC formed by the conventional process is not uniform, as judged from the interconnected state of the resulting nanoparticles. The nanoparticles obtained by the present EISA method were apparently smaller and more dispersed than those obtained by the conventional microemulsion method. The size distribution of these EISA-mediated nanoparticles should depend on the degree of ordering of the mesostructure, while the average diameter can be tuned by their periodicities. The periodicities of general silica−surfactant mesostructures consisting of spherical, cylindrical, and lamellar assemblies are in the range of 2−8 nm.[31] It is, therefore, reasonable that the single-digit nanoscale particles can be obtained via the formation of a reverse-type mesostructure. Moreover, the particle size reported in this study, using small surfactants, is smaller than the previously reported particle sizes of particles prepared using block copolymers as structure-directing agents.[18,19] There is still room to explore surfactants bearing various alkyl chain lengths and head groups to prepare wellordered mesostructures with various periodicities.

4.4.6 Synthesis of titanium oxide nanoparticles

The present method is also expected to be useful for the preparation of nonsiliceous oxide nanoparticles. The fabrication of titanium oxide is used here as an example. TTIP was hydrolyzed under strongly acidic conditions in THF and was

self-assembled with 3C8MAC under otherwise identical conditions to those for preparing **SNP-as**. The resulting film, denoted **TNP-as**, showed a structural periodicity of d = 3.0 nm in the XRD pattern (Figure 4.10a). Judging from the lack of diffraction peaks at a higher angle region (2θ > 10°, data not shown), the titania framework was amorphous. **TNP-as** can be dissolved in organic solvents such as THF, and discrete nanoparticles ca. 3 nm in size were observed by SEM (Figure 4.10b). Thus, the versatility of our EISA method for preparing oxide nanoparticles with different compositions was successfully proved.

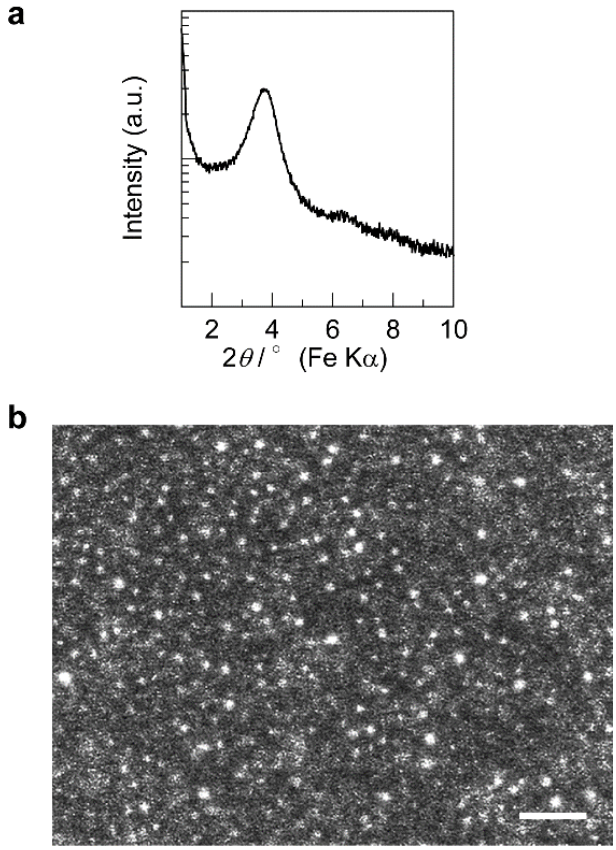

Figure 4.10. (a) XRD pattern of **TNP-as** and (b) SEM image of titanium oxide nanoparticle by dispersing **TNP-as** in THF. Scale bar: 20 nm.

4.5 Conclusion

A novel synthetic route to silica nanoparticles smaller than 5 nm in diameter was established through the evaporationinduced self-assembly of reverse-type silica−surfactant mesostructures. In addition to the small size, these particles can be functionalized by organosilylation, which is promising for their use as nanofillers and nanosized building blocks. Furthermore, the versatility of this methodology was demonstrated by fabricating titanium oxide nanoparticles. Judging from the smallness of the resulting nanoparticles, we concluded that the reverse-type mesostructure formed by the EISA process is more resistant as a template than the reverse micelles in a solution. The high productivity and the long-term stability of the nanoparticles should be advantageous for their industrial use in many fields.

4.6 References

1 Su, N. C.; Smith, Z. P.; Freeman, B. D.; Urban, J. J. Size-Dependent Permeability Deviations from Maxwell's Model in Hybrid Cross-Linked Poly(ethylene glycol)/Silica Nanoparticle Membranes. *Chem. Mater*. **2015**, *27*, 2421−2429.

2 Besinis, A.; De Peralta, T.; Tredwin, C. J.; Handy, R. D. Review of Nanomaterials in Dentistry: Interactions with the Oral Microenvironment, Clinical Applications, Hazards and Benefits. *ACS Nano* **2015**, *9*, 2255−2289.

3 Zidki, T.; Zhang, L.; Shafirovich, V.; Lymar, S. V. Water Oxidation Catalyzed by Cobalt(II) Adsorbed on Silica Nanoparticles. *J. Am. Chem. Soc*. **2012**, *134*, 14275−14278.

4 Tang, F.; Li, L.; Chen, D. Mesoporous Silica Nanoparticles: Synthesis, Biocompatibility and Drug Delivery. *Adv. Mater*. **2012**, *24*, 1504−1534.

5 Shrivastava, S.; Nuffer, J. H.; Siegel, R. W.; Dordick, J. S. Position- Specific Chemical Modification and Quantitative Proteomics Disclose Protein Orientation Adsorbed on Silica Nanoparticles. *Nano Lett*. **2012**, *12*, 1583−1587.

6 Shang, W.; Nuffer, J. H.; Dordick, J. S.; Siegel, R. W. Unfolding of Ribonuclease A on Silica Nanoparticle Surfaces. *Nano Lett.* **2007**, *7*, 1991−1995.

7 Heni, W.; Vonna, L.; Haidara, H. Experimental Characterization of the Nanoparticle Size Effect on the Mechanical Stability of Nanoparticle-Based Coatings. *Nano Lett.* **2015**, *15*, 442−449.

8 Kelly, K. L.; Coronado, E.; Zhao, L. L.; Schatz, G. C. The Optical Properties of Metal Nanoparticles: The Influence of Size, Shape, and Dielectric Environment. *J. Phys. Chem.* B **2003**, *107*, 668−677.

9 Choi, H. S.; Liu, W.; Misra, P.; Tanaka, E.; Zimmer, J. P.; Ipe, B. I.; Bawendi, M. G.; Frangioni, J. V. Renal Clearance of Quantum Dots. *Nat. Biotechnol.* **2007**, *25*, 1165−1170.

10 Kim, S. E.; Zhang, L.; Ma, K.; Riegman, M.; Chen, F.; Ingold, I.; Conrad, M.; Turker, M. Z.; Gao, M.; Jiang, X.; Monette, S.; Pauliah, M.; Gonen, M.; Zanzonico, P.; Quinn, T.; Wiesner, U.; Bradbury, M. S.; Overholtzer, M. Ultrasmall Nanoparticles Induce Ferroptosis in Nutrient-Deprived Cancer Cells and Suppress Tumour Growth. *Nat. Nanotechnol.* **2016**, *11*, 977−985.

11 Stöber, W.; Fink, A.; Bohn, E. Controlled Growth of Monodisperse Silica Spheres in the Micron Size Range. *J. Colloid Interface Sci.* **1968**, *26*, 62−69.

12 Yokoi, T.; Sakamoto, Y.; Terasaki, O.; Kubota, Y.; Okubo, T.; Tatsumi, T. Periodic Arrangement of Silica Nanospheres Assisted by Amino Acids. *J. Am.*

Chem. Soc. **2006**, *128*, 13664−13665.

13 Yokoi, T.; Wakabayashi, J.; Otsuka, Y.; Fan, W.; Iwama, M.; Watanabe, R.; Aramaki, K.; Shimojima, A.; Tatsumi, T.; Okubo, T. Mechanism of Formation of Uniform-Sized Silica Nanospheres Catalyzed by Basic Amino Acids. *Chem. Mater.* **2009**, *21*, 3719−3729.

14 Han, Y.; Lu, Z.; Teng, Z.; Liang, J.; Guo, Z.; Wang, D.; Han, M. − Y.; Yang, W. Unraveling the Growth Mechanism of Silica Particles in the Stöber Method: In Situ Seeded Growth Model. *Langmuir* **2017**, *33*, 5879−5890.

15 Carcouët, C. C. M. C.; van de Put, M. W. P.; Mezari, B.; Magusin, P. C. M. M.; Laven, J.; Bomans, P. H. H.; Friedrich, H.; Esteves, A. C. C.; Sommerdijk, N. A. J. M.; van Benthem, R. A. T. M.; de With, G. Nucleation and Growth of Monodisperse Silica Nanoparticles. *Nano Lett.* **2014**, *14*, 1433−1438.

16 Ma, K.; Mendoza, C.; Hanson, S.; Werner-Zwanziger, U.; Zwanziger, J.; Wiesner, U. Control of Ultrasmall Sub-10 nm Ligand- Functionalized Fluorescent Core−Shell Silica Nanoparticle Growth in Water. *Chem. Mater.* **2015**, *27*, 4119−4133.

17 Finnie, K. S.; Bartlett, J. R.; Barbé, C. J. A.; Kong, L. Formation of Silica Nanoparticles in Microemulsions. *Langmuir* **2007**, *23*, 3017−3024.

18 Ulrich, R.; Du Chesne, A.; Templin, M.; Wiesner, U. Nanoobjects with Controlled Shape, Size, and Composition from Block Copolymer Mesophases. *Adv. Mater.* **1999**, *11*, 141−146.

19 Yu, K.; Hurd, A. J.; Eisenberg, A.; Brinker, C. J. Syntheses of Silica/Polystyrene-block-Poly(ethylene oxide) Films with Regular and Reverse Mesostructures of Large Characteristic Length Scales by Solvent Evaporation-Induced Self-Assembly. *Langmuir* **2001**, *17*, 7961−7965.

20 Sakamoto, S.; Tamura, Y.; Hata, H.; Sakamoto, Y.; Shimojima, A.; Kuroda, K. Molecularly Designed Nanoparticles by Dispersion of Self-Assembled Organosiloxane-Based Mesophases. *Angew. Chem. Int. Ed.* **2014**, *53*, 9173−9177.

21 Mitchell, D. J.; Ninham, B. W. Micelles, Vesicles and Microemulsions. *J. Chem. Soc., Faraday Trans. 2* **1981**, *77*, 601−629.

22 Eltohamy, M.; Shin, U. S.; Kim, H.-W. Silica Nanoparticles with Enlarged Nanopore Size for the Loading and Release of Biological Proteins. *Mater. Lett*. **2011**, *65*, 3570−3573.

23 Lee, J. H.; Park, J.-H.; Eltohamy, M.; Perez, R.; Lee, E. − J.; Kim, H. − W. Collagen Gel Combined with Mesoporous Nanoparticles Loading Nerve Growth Factor as a Feasible Therapeutic Three-Dimensional Depot for Neural Tissue Engineering. *RSC Adv*. **2013**, *3*, 24202−24214.

24 Oaki, Y.; Anzai, T.; Imai, H. Homogeneous and Disordered Assembly of Densely Packed Nanocrystals. *Adv. Funct. Mater.* **2010**, *20*, 4127−4132.

25 Williams, C. E.; May, R. P.; Guinier, A. Small-Angle Scattering of X-Rays and Neutrons. In X-ray Characterization of Materials; Lifshin, E., Ed.; Wiley-VCH: New York, **2008**; pp 212−254.

26 Cox, A. J.; DeWeerd, A. J.; Linden, J. An Experiment to Measure Mie and Rayleigh Total Scattering Cross Sections. *Am. J. Phys.* **2002**, *70*, 620−625.

27 Hara, K.; Akahane, S.; Wiench, J. W.; Burgin, B. R.; Ishito, N.; Lin, V. S.-Y.; Fukuoka, A.; Pruski, M. Selective and Efficient Silylation of Mesoporous Silica: A Quantitative Assessment of Synthetic Strategies by Solid-State NMR. *J. Phys. Chem. C* **2012**, *116*, 7083−7090.

28 Kawahara, K.; Hagiwara, Y.; Shimojima, A.; Kuroda, K. Stepwise silylation of

double-four-ring (D4R) silicate into a novel spherical siloxane with a defined architecture. *J. Mater. Chem.* **2008**, *18*, 3193−3195.

29 Bourlinos, A. B.; Herrera, R.; Chalkias, N.; Jiang, D. D.; Zhang, Q.; Archer, L. A.; Giannelis, E. P. Surface-Functionalized Nanoparticles with Liquid-Like Behavior. *Adv. Mater.* **2005**, *17*, 234−237.

30 Le, V. H.; Thuc, C. N. H.; Thuc, H. H. Synthesis of Silica Nanoparticles from Vietnamese Rice Husk by Sol−Gel Method. *Nanoscale Res. Lett.* **2013**, *8*, 58−67.

31 Wan, Y.; Zhao, D. On the Controllable Soft-Templating Approach to Mesoporous Silicates. *Chem. Rev*. **2007**, *107*, 2821−2860.

32 Izutani, C.; Fukagawa, D.; Miyasita, M.; Ito, M.; Sugimura, N.; Aoyama, R.; Gotoh, T.; Shibue, T.; Igarashi, Y.; Oshio, H. The Materials Characterization Central Laboratory: An Open-Ended Laboratory Program for Fourth-Year Undergraduate and Graduate Students. *J. Chem. Educ*. **2016**, *93*, 1667−1670.

Chapter 5

Formation of Silica−Organic Hybrid Nanoparticles by Cross-Linking of Ultra-Small Silica Nanoparticles

Adapted with permission from S. Sakamoto, K.Fujino, A. Shimojima, and K. Kuroda, "Formation of Silica−Organic Hybrid Nanoparticles by Cross-Linking of Ultra-Small Silica Nanoparticles", *Chem. Lett.* **2018***, just accepted,* DOI: 10.1246/cl.180374. Copyright 2018 The Chemical Society of Japan.

5.1 Abstract

A new type of silica−organic hybrid nanoparticles (**HNPs**) ~33 nm in size, consisting of vinylsilylated silica nanoparticles (**SNPs**) of size ~2 nm and 1,6-hexanedithiol as the organic linker, were prepared by their interconnection via the thiol−ene reaction. The particle size of the **HNPs** varied depending on the concentration of the linker. Additionally, they could be dispersed in organic solvents and further successful chemical modification of the internal surfaces of **HNPs** indicated the accessibility of guest species into the internal nanospaces.

5.2 Introduction

Silica nanoparticles are of great importance in materials science as a nanoplatform for the design of functional materials.[1-4] Silica−organic hybrid nanoparticles have been utilized for a wide range of applications including catalysis,[5] optics,[6,7] and medicine.[8,9] To date, a variety of organic molecules and polymers have been used for the modification of silica nanoparticles in order to tune their surface properties and to integrate various functions. Porous silica−organic hybrid nanoparticles have attracted particular attention, owing to the high loading of organic groups on accessible internal surfaces and the ability to accommodate guest species into their pores.[10] These features are especially useful for catalysis and drug delivery applications.[11,12]

In recent years, organically bridged polyhedral oligomeric silsesquioxanes (POSSs) have emerged as a new type of silica−organic hybrid porous materials.[13,14] These hybrids are characterized by large internal surfaces and can be designed by tuning the rigidity and/or size of organic bridges. In this respect, various organic reactions can be utilized for the formation of cross-linked networks with desired structures and

functions.[15] The use of silica nanoparticles instead of POSSs can lead to enhanced accessibility because of the larger interparticle spaces than those generated by the small oligomers. Additionally, surface silanol groups on silica nanoparticles can be modified with diverse organic functional groups for not only interparticle cross-linking but also specific applications. Compared to commonly used colloidal silica nanoparticles larger than 10 nm in diameter, smaller-sized silica nanoparticles are more advantageous because of their higher surface area.

Recently, we reported a new synthetic method for ultra-small (2−3 nm in diameter) silica nanoparticles, which involved the dispersion of silica−surfactant mesostructures that were formed by evaporation-induced self-assembly processes.[16] These silica nanoparticles permitted the organic post−modification by silylation. Herein, we report a new class of silica−organic hybrid nanoparticles (**HNPs**) that were prepared by surface modification of silica nanoparticles with dimethylvinylsilyl groups and subsequent interconnection via the thiol−ene reaction using 1,6−hexanedithiol as the linker (Figure 5.1). These hybrid nanoparticles were well−dispersed in organic solvents, and the particle size of **HNPs** could be adjusted by using an appropriate amount of the organic linker. Furthermore, the residual vinyl groups inside these **HNPs** were accessible for post chemical modification. Although organically-linked nanoparticle networks using various nanoparticles and organic linkers are known,[17-19] neither the accessibility of guest molecules onto individual primary nanoparticles constituting the networks nor the morphological control to nano-sized networks have been reported to the best of our knowledge.

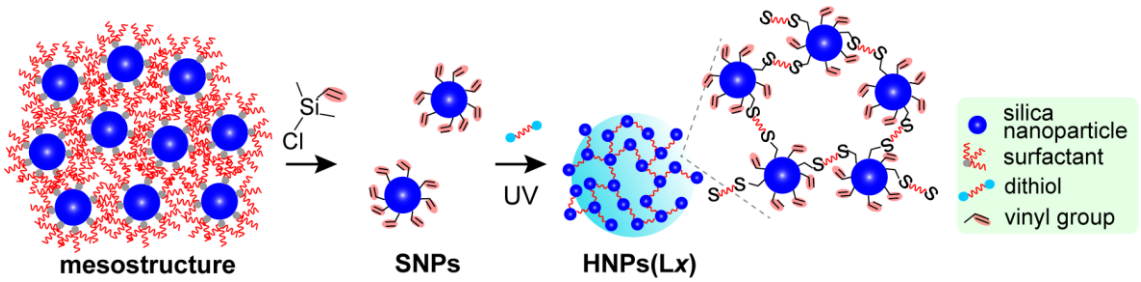

Figure 5.1. Synthetic route to silica−organic hybrid nanoparticles **HNPs(L*x*)** via the preparation of dimethylvinylsilylated silica nanoparticles (**SNPs**) and the subsequent interconnection with dithiol linkers.

5.3 Experimental

5.3.1 Materials

Tetrahydrofuran (THF, super dehydrated, stabilizer free), ethanol (super dehydrated), hexane, 0.01 mol/L hydrochloric acid, 1,6−hexanedithiol, and 2−propanol (super dehydrated) were purchased from Wako Pure Chemical Industries, Ltd. Tetraethoxysilane (Si(OCH2CH3)4; TEOS, > 99.0%) was purchased from Kishida Chemical Co., Ltd. Chlorodimethylvinylsilane (> 98.0%) and methyltri−n−octylammonium chloride (3C8MAC, > 95.0%) were purchased from Tokyo Chemical Industry Co., Ltd. These chemicals were used as received. Glass substrates (48 × 24 mm, Matsunami Glass Ind., Ltd.) were washed by ultra-sonication in deionized water for 10 min and air-dried before use.

5.3.2 Synthesis of Silica Nanoparticles Modified with Dimethylvinylsilanes (SNPs)

In a typical synthesis, 167 μL of TEOS was hydrolyzed in a mixture of 0.01 mol/L hydrochloric acid (54 μL) and THF (208 μL) by stirring at room temperature for 2 h, followed by the addition of 3C8MAC (0.15 g). The molar composition of TEOS/THF/H_2O/HCl/3C8MAC was 1.0:3.5:4.1:7.5 × 10^{-4}:0.50. The hydrolyzed

solution was cast on a glass substrate and air-dried at room temperature for 1 d. Then, 2 g of the resulting viscous solid, which is the silica−surfactant mesostructured material consisting of silica nanoparticles, was dispersed in 8 mL of THF, followed by the addition of chlorodimethylvinylsilane (8 mL) with vigorous stirring at room temperature for 5 min. After adding 8 mL of ethanol to lower the reactivity of the unreacted silylating agent, the volatile components were removed by a rotary evaporator. The silylated nanoparticles were extracted with hexane. The hexane dispersion was air−dried in a petri dish, dried further at 100 °C, and pulverized into a white powder, which was denoted as **SNPs**.

5.3.3 Synthesis of Organically-Linked Hybrid Nanoparticles (HNPs(L*x*)).

In a typical synthesis, a mixture of **SNPs** (100 mg), 1,6−hexanedithiol (3, 4, 5, or 10 mg), and 2-propanol (1.0 mL) was exposed to a UV light (20 W low−pressure Hg lamp from a distance of ca. 5 cm) for 3 h in air. Then the solvent was evaporated at 70 °C. The resulting solid was pulverized into a white powder, and further dried at 150 °C in vacuo to remove residual dithiols, which was denoted as **HNPs(L*x*)**. Here, *x* represents the weight percentage of dithiols to **SNPs**.

5.3.4 Characterization

Solid-state ^{29}Si magic-angle spinning (MAS) NMR spectra were recorded on a JEOL JNM−CMX−400 spectrometer at a resonance frequency of 79.43 MHz with a 45° pulse and a recycle delay of 200 or 300 s. The samples were put in a 5 mmϕ zirconia rotor and spun at a spinning frequency of 8 kHz. The chemical shifts were externally referenced to the silicon atoms of poly(dimethylsilane) at −33.8 ppm. Solid-state ^{13}C CP/MAS NMR spectra were also recorded on a JEOL JNM−CMX−400 spectrometer at

a resonance frequency of 100.53 MHz with a recycle delay of 10 s and a contact time of 5 ms. The samples were put in a 5 mm silicon nitride tube and spun at 8 kHz. The chemical shifts were externally referenced to the methyl groups of hexamethylbenzene at 17.4 ppm. High-resolution scanning electron microscopy (SEM) observation was carried out on a HITACHI S-5500 microscope operated at 30 kV. For SEM observation, samples were arbitrarily diluted in ethanol, followed by dropping on carbon supported Cu grids and air-drying. The nitrogen gas adsorption–desorption isotherms were recorded on a Quantachrome Instruments Autosorb-iQ instrument at −196 °C. Samples were preheated at 150 °C for 4 h in vacuo. Dynamic light scattering (DLS) profiles were measured on a Horiba nanopartica SZ-100-S instrument at 25 °C. For spectroscopic data, transparent solutions were measured after filtration of the solution with a 0.45 μm filter. Fourier−transform infrared spectroscopy (FT−IR) spectra were obtained using JASCO FT/IR−6100 by the KBr disk method. Gel permeation chromatography (GPC) were recorded on JASCO LC-NET 2 with a column of K-804 (Shodex). Chloroform was used as an eluent with a flow rate of 1.5 mL min-1. The molecular weights were calculated as polystyrene equivalents by the software of ChromNAV.

5.4 Results and discussion

5.4.1 Characterization of Silica Nanoparticles Modified with Dimethylvinylsilanes (SNPs)

The solid-state ^{29}Si magic angle spinning (MAS) nuclear magnetic resonance (NMR) spectrum of **SNPs** showed three signals at around 0.4 ppm, −100.0 ppm, and −108.6 ppm that were assigned to M^1 ($Me_2ViSi(OSiO_3)$), Q^3, and Q^4 units (Q^x: $Si(OSi)_x(OH)_{4-x}$), respectively (Figure 5.2).[20] There was no signal corresponding to tetramethyldivinyldisiloxane (10 ppm),[14] which is formed upon self-condensation of the

silylating agent. The solid-state ^{13}C cross polarization (CP)/MAS NMR spectrum (Figure 5.3(i)) showed three signals at 134.7 ppm, 128.9 ppm, and −3.3 ppm attributable to the vinyl and methyl groups (CH_2=CHSi−, CH_2=CHSi−, and $(CH_3)_2$Si−, respectively). The signals corresponding to the surfactants were not observed, confirming their complete removal. These results indicated that the silica nanoparticles were successfully modified with dimethylvinylsilyl groups.

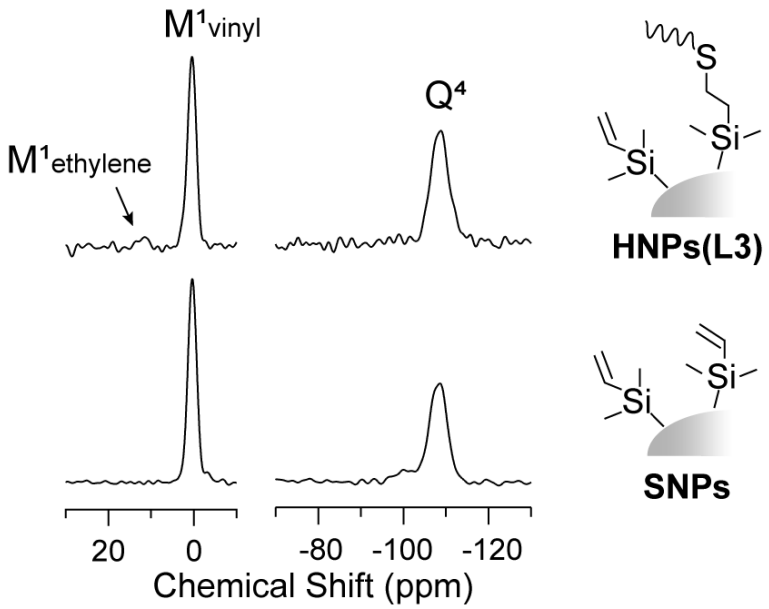

Figure 5.2. Solid-state ^{29}Si MAS NMR spectra of **SNPs** and **HNPs(L3)**.

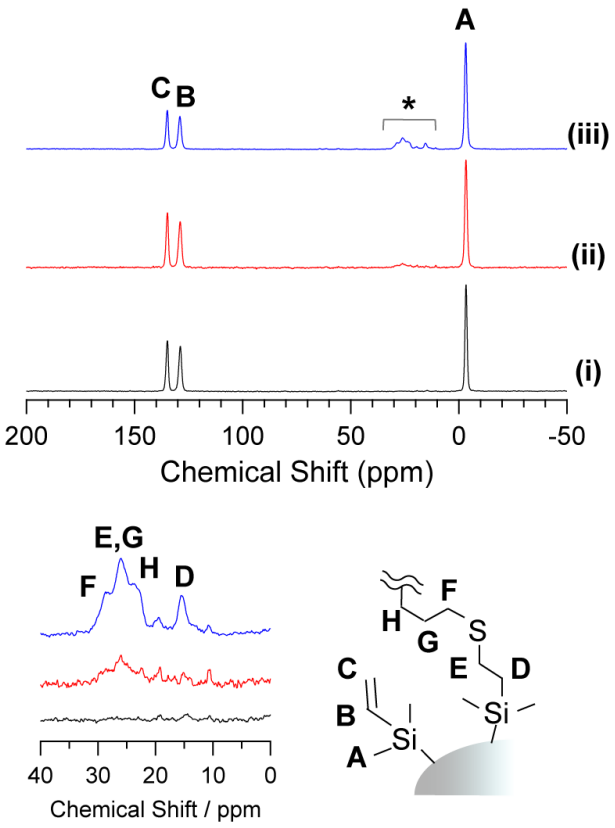

Figure 5.3. Solid-state ^{13}C CP/MAS NMR spectra of (i) **SNPs**, (ii) **HNPs(L3)**, and (iii) **HNPs(L10)**. The spectral region indicated by an asterisk (*) is expanded at the bottom.

The integral intensity ratio of the ^{29}Si signals (M^1:Q^3:Q^4 = 1.0:0.16:0.99) indicated that the number of Si atoms in each nanoparticle increased by 87% on average after silylation. This high ratio of silylation can be attributed to the high surface to volume ratio of the ultra-small silica nanoparticles before silylation. This value was comparable to the case of trimethylsilylation (91%). As discussed in our previous paper, the surfaces of such small silica nanoparticles were modified with more silylating agents as compared to conventional mesoporous silica powders with a similar surface area.[21] Therefore, the higher M/Q ratio represents a higher surface density of the organic groups.[16] This is likely due to the convex nature and high curvature of these small nanoparticles.

SNPs were dispersed in organic solvents, such as 2-propanol and THF. Their solutions were transparent even at the concentration of 10 wt% (Figure 5.4(i)). Furthermore, dispersion and solvent−evaporation were repeated, and the interparticle aggregation was avoided by the presence of densely modified organic groups on the surface. Indeed, the monodispersity of the silylated nanoparticles was confirmed by gel permeation chromatography (GPC) as the chloroform dispersion of **SNPs** showed a single peak in the chromatogram.

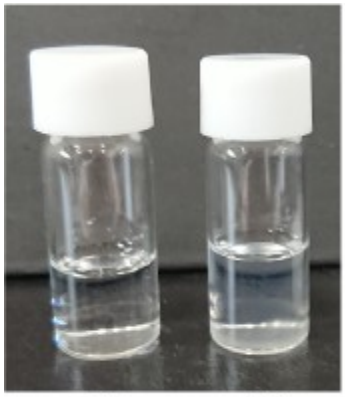

Figure 5.4. Appearances of (i) **SNPs** (10 wt% 2-propanol solution) and (ii) precursor solution of **HNPs(L3)** after UV irradiation.

5.4.2 Characterization of Organically-Linked Hybrid Nanoparticles (HNPs(L*x*))

In the thiol-ene reaction, the thiol (–SH) groups form thiyl radicals (–S·) under UV irradiation and then react with the vinyl groups, resulting in the formation of sulfide covalent bridges.[22,23] When 1,6-hexanedithiol was reacted with **SNPs** for the formation of **HNPs(L3)**, the clear precursor solution became slightly cloudy after UV irradiation and formed a colloidal solution (Figure 5.4(ii)). After solvent evaporation, the resulting solids were redispersed in organic solvents, indicating the stability of **HNPs(L3)** against aggregation.

The Fourier transform-infrared (FT-IR) spectrum of **HNPs(L3)** (Figure 5.5)

showed that the absorption bands of vinyl groups at 3054 cm^{-1}, 1598 cm^{-1}, and 1410 cm^{-1} decreased, while the CH_2 stretching vibrations at 2933 cm^{-1} (ν_{as}) and 2859 cm^{-1} (ν_s) increased.[24] This change was more clearly observed for **HNPs(L10)**, which were prepared with 10 wt% of the dithiol linker. The peak corresponding to S–H vibrations was not observed. These results indicated the progress of the thiol-ene reaction. The formation of the sulfide bond by the thiol-ene reaction was proved by the ^{13}C CP/MAS NMR spectrum showing five signals in the range from 15.5 ppm to 28.7 ppm (Figure 5.3).[25,26] In particular, the signal at 15.5 ppm was assigned to the methylene carbon adjacent to the Si atom (Si–CH_2CH_2–S–) formed by the thiol-ene reaction, because this signal cannot be observed for the polymerized species of vinylsilanes.[27] A slight decrease in the intensity of the signals due to vinyl groups was also observed. In the ^{29}Si MAS NMR spectrum of **HNPs(L3)**, a new M^1 signal emerged at 11.6 ppm (Figure 5.2a), which was ascribed to the formation of ethylene (Si–$(CH_2)_2$–S–) bridges. The integral intensity ratio of the – $(CH_2)_2SiMe_2(OSi)$ unit to the CH_2=$CHSiMe_2(OSi)$ unit (1:16) was comparable with the theoretical ratio of 1:14 when both terminal thiol groups in the dithiol molecules were completely reacted. This theoretical ratio was calculated by the number of thiol groups added for the reaction and the number of vinyl groups in an arbitrary weight of **SNPs**, which was estimated on the basis of the ^{29}Si MAS NMR data. Accordingly, the reaction ratio of the thiol groups was calculated to be 91%.

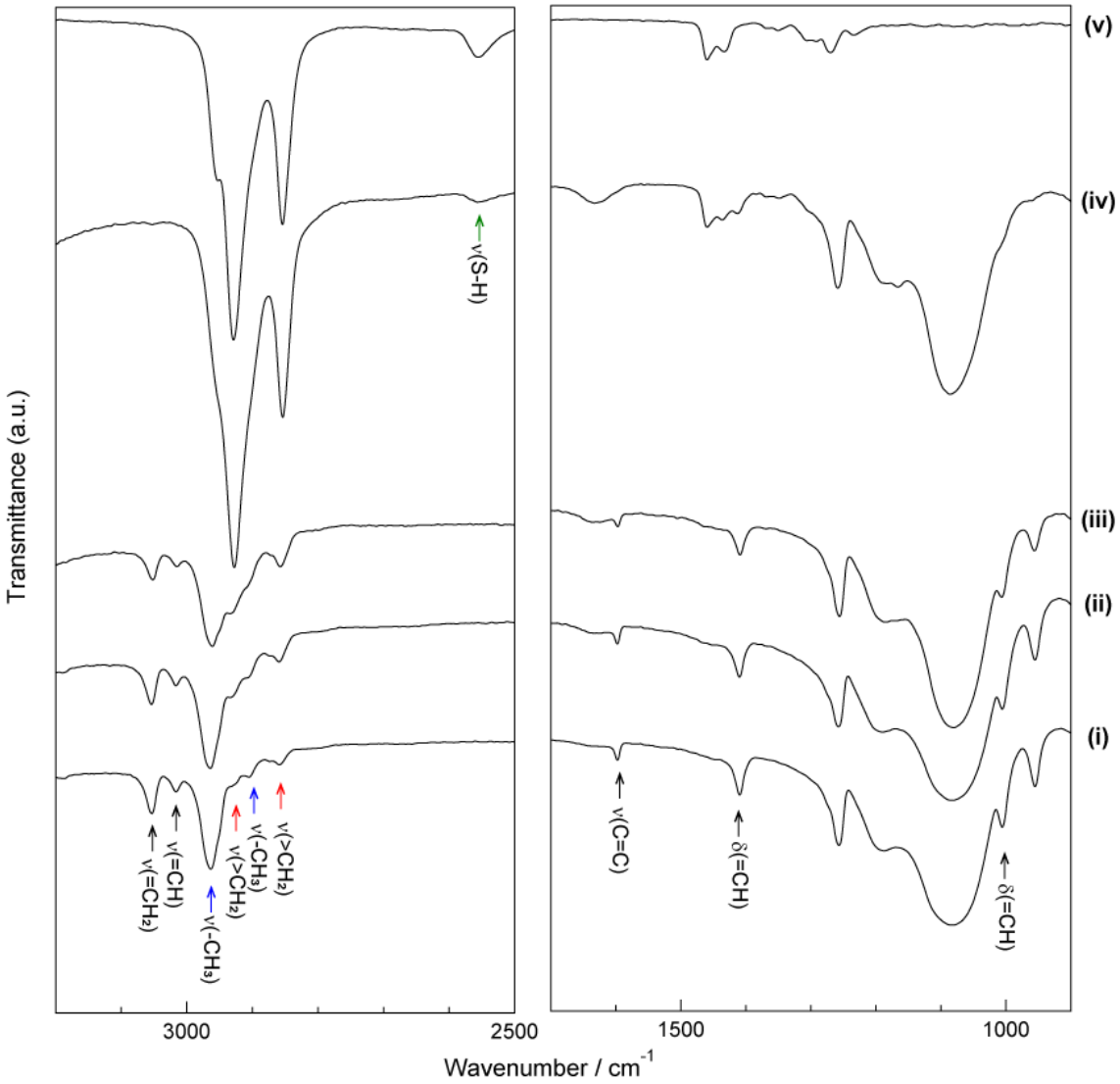

Figure 5.5. FT-IR spectra of (i) **SNPs**, (ii) **HNPs(L3)**, (iii) **HNPs(L10)**, (iv) **HNPs(L3)** after the additional thiol-ene reaction with an excess amount of dithiols, and (v) 1,6-hexanedithiol. The difference in the absorbance arising from ν(=CH_2) between (i) and (iv) was divided by the difference in the absorbance arising from ν(=CH_2) between (i) and (ii). The absorbance was normalized using the peak arising from ν(-CH_3) as a reference.

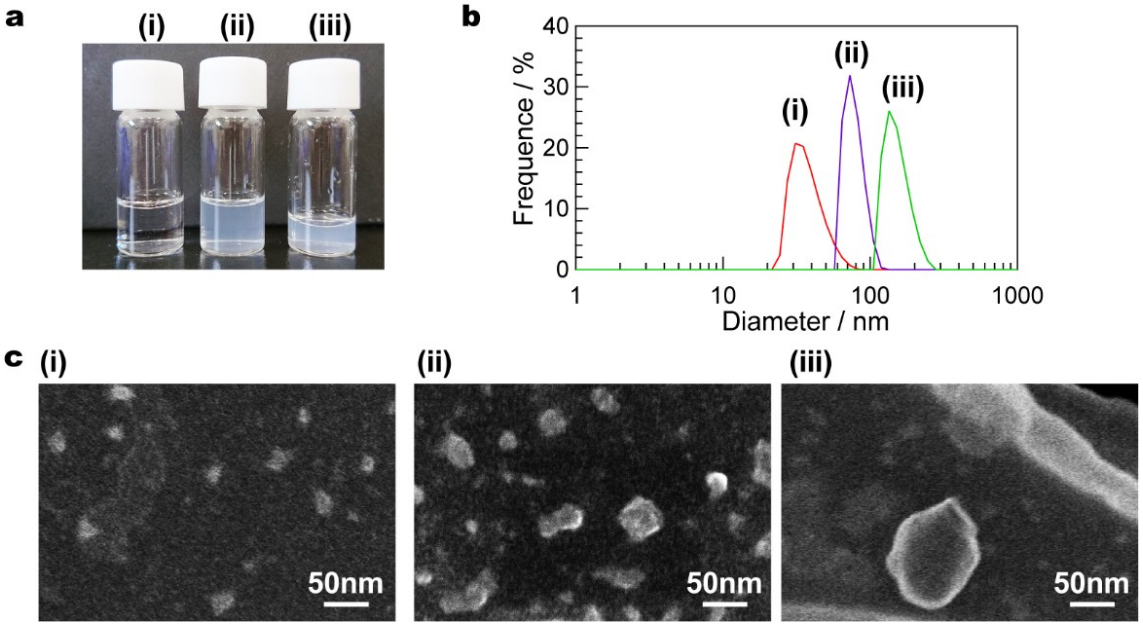

Figure 5.6. (a) Photograph and (b) DLS profiles of the precursor solutions of (i) **HNPs(L3)**, (ii) **HNPs(L4)**, and (iii) **HNPs(L5)** after UV irradiation. (c) HR−SEM images of (i) **HNPs(L3)**, (ii) **HNPs(L4)**, and (iii) **HNPs(L5)**. The samples for SEM observation were prepared by dilution of the precursor solutions in ethanol and subsequent dropping on a carbon supported Cu grid and air-drying.

Interestingly, dynamic light scattering (DLS) measurements showed that nanoparticles with a median diameter of 33 nm were present in the precursor solution of **HNPs(L3)** after UV irradiation (Figure 5.6a). On the other hand, the scanning electron microscopy (SEM) image of **HNPs(L3)** showed particles of smaller sizes (mainly 10–20 nm), as shown in Figure 5.6c(i). The N_2 adsorption–desorption measurements of **HNPs(L3)** (Figure 5.7) revealed the small BET area of 13 $m^2\ g^{-1}$. This value is much smaller than the theoretical surface area of the primary silica nanoparticles (~1300 $m^2\ g^{-1}$) calculated on the assumption of their density as 2.2 g cm^{-1} and particle size of 2.0 nm. The N_2 molecules seemed to be inaccessible to the high surface area of the primary nanoparticles because of their dense packing. It is also likely that the hybrid nanoparticles of **HNPs(L3)** were densely packed as a result of partial deformation,

because the BET area was still smaller than that for silica particles 20 nm in diameter (calculated as ~140 m^2 g^{-1}). It is likely that the lower surface area of **HNPs(L3)** is partly due to the flexibility of the linkers. Our preliminary result on the use of a more rigid linker (4,4'-thiobisbenzenethiol) showed that the surface area can be increased, although further studies need to be conducted.

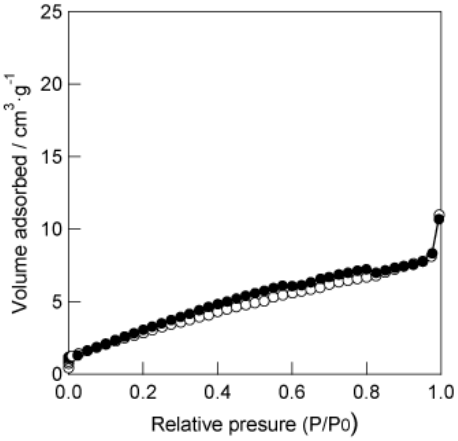

Figure 5.7. Nitrogen adsorption−desorption isotherms of **HNPs(L3)**. The open symbols and the filled symbols denote adsorption and desorption, respectively.

Nevertheless, in the 2-propanol dispersion of **HNPs(L3)**, successful post–modification of vinyl groups was almost complete by the additional thiol–ene reaction in the presence of an excess of 1,6–hexanedithiol (300 wt% of dithiols to **SNPs**). Full consumption of the vinyl groups was confirmed in the IR spectrum (Figure 5.5(iv)). Interestingly, ca. 12 times of the amount of 1,6–hexanedithiol were additionally reacted with vinyl groups on the internal surfaces of **HNPs(L3)**, as calculated by the IR data. This result was in good accordance with the ^{29}Si MAS NMR result of **HNPs(L3)**. This fact indicated the good accessibility of dithiol molecules into the surface of the primary nanoparticles and the existence of nanospaces inside the hybrid nanoparticles of

HNPs(L3) in the liquid phase. In addition, the high reactivity of both of the functional groups for the thiol-ene reaction was also confirmed even in the presence of densely reacted dithiol molecules. It is reasonable to conclude from these results that the nanoparticles were in a swollen state in the solution.

The particle growth of **HNPs(L*x*)** was further examined by changing dithiol concentration. Upon UV irradiation of the precursor solutions with larger *x*, the formation of white, gel-like aggregates was observed at the bottom of the vessels while the upper layer solutions turned cloudy. The upper layers of the precursor solutions of **HNPs(L4)** and **HNPs(L5)** after UV irradiation were more opaque than that of **HNPs(L3)** (Figure 5.6a), and the DLS measurements confirmed that the median diameter of the particles increased from 33 nm to 71 nm and 131 nm with the increase in the dithiol contents from $x = 3$ to $x = 4$ and 5, respectively (Figure 5.6b). The increase in the particle size was also confirmed by the SEM images of the particles after drying, as shown in Figure 5.6c. With further increase in *x*, for example, **HNPs(L10)**, a gel was formed exclusively after UV irradiation (Figure 5.8 inset). The SEM image of **HNPs(L10)** showed the fusion and deposition of submicrometer sized particles (Figure 5.8). It is likely that the particle growth resulted in interparticle aggregation. Thus, it was demonstrated that the particle size was adjustable to some extent by the dithiol concentration. Under the higher dithiol concentrations, larger amounts of dithiol molecules were grafted on the surface of the **SNPs** by the thiol-ene reaction. Therefore, the nanoparticles were more likely to connect with each other and grow via interparticle reactions involving the remaining vinyl groups and terminal thiol groups.

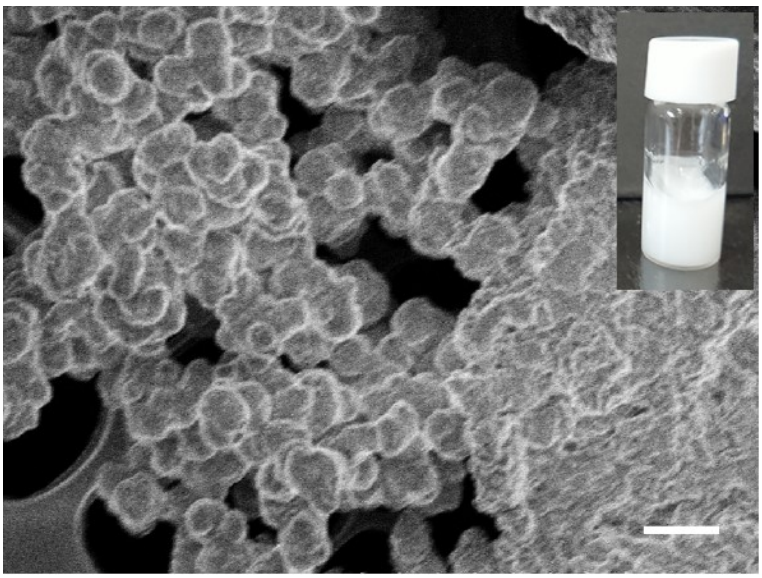

Figure 5.8. HR−SEM image of **HNPs(L10)** (Scale bar: 1 μm). The inset shows the appearance of the precursor gel of **HNPs(L10)** after UV irradiation.

5.5 Conclusion

A new class of silica–organic hybrid nanoparticles (**HNPs**) was synthesized by the interconnection of ultra–small silica nanoparticles (**SNPs**) with organic linkers. The particle size was adjustable simply by changing the amount of the organic linker. **HNPs** were well dispersed in organic solvents and the high accessibility to the internal functional groups was demonstrated. This study proposes a new design concept of hybrid nanoparticles that contain adaptive nanospaces in the liquid phase because of flexible organic linkers. This attribute is advantageous for medical applications such as in a drug delivery system.

5.6 References

1 M. E. Mackay, T. T. Dao, A. Tuteja, D. L. Ho, B. V. Horn, H. –C. Kim, C. J. Hawker, *Nat. Mater.* **2003**, *2*. 762–766.

2 S. Rose, A. Prevoteau, P. Elzière, D. Hourdet, A. Marcellan, L. Leibler, *Nature*

2014, *505*. 382–385.

3 M. Naqshbandi, J. Canning, B. C. Gibson, M. M. Nash, M. J. Crossley, *Nat. Commun.* **2012**, *3*, 1188.

4 L. Malassis, P. Massé, M. Tréguer–Delapierre, S. Mornet, P. Weisbecker, P. Barois, C. R. Simovski, V. G. Kravets, A. N. Grigorenko, *Adv. Mater.* **2014**, *26*, 324–330.

5 W. J. Zhou, L. Fang, Z. Fan, B. Albela, L. Bonneviot, F. De Campo, M. Pera–Titus, J. –M. Clacens, *J. Am. Chem. Soc.* **2014**, *136*, 4869–4872.

6 N. Atchison, W. Fan, D. D. Brewer, M. A. Arunagirinathan, B. J. Hering, S. Kumar, K. K. Papas, E. Kokkoli, M. Tsapatsis, *Angew. Chem. Int. Ed.* **2011**, *123*, 1655–1659.

7 J. Li, T. Shiraki, B. Hu, R. A. E. Wright, B. Zhao, J. S. Moore, *J. Am. Chem. Soc.* **2014**, *136*, 15925–15928.

8 S. Kim, T. Y. Ohulchanskyy, H. E. Pudavar, R. K. Pandey, P. N. Prasad, *J. Am. Chem. Soc.* **2007**, *129*, 2669–2675.

9 M. Montalti, L. Prodi, E. Rampazzo, N. Zaccheroni, *Chem. Soc. Rev.* **2014**, *43*, 4243–4268.

10 F. Tang, L. Li, D. Chen, *Adv. Mater.* **2012**. *24*, 1504–1534.

11 S. H. Joo, J. Y. Park, C. –K. Tsung, Y. Yamada, P. Yang, G. A. Somorjai, *Nat. Mater.* **2009**, *8*, 126–131.

12 C. Park, K. Oh, S. C. Lee, C. Kim, *Angew. Chem. Int. Ed.* **2007**, *46*, 1455–1457.

13 W. Chaikittisilp, M. Kubo, T. Moteki, A. Sugawara–Narutaki, A. Shimojima, T. Okubo, *J. Am. Chem. Soc.* **2011**, *133*, 13832–13835.

14 Y. Hagiwara, A. Shimojima, K. Kuroda, *Bull. Chem. Soc. Jpn*. **2010**, *83*, 424–

430.

15 F. Alves, I. Nischang, *Chem. Eur. J.* **2013**, *19*, 17310–17313.

16 S. Sakamoto, M. Yoshikawa, K. Ozawa, Y. Kuroda, A. Shimojima, K. Kuroda, *Langmuir*, **2018**, *34*, 1711–1717.

17 R. Elghanian, J. J. Storhoff, R. C. Mucic, R. L. Letsinger, and C. A. Mirkin, *Science*, **1997**, *277*, 1078-1081.

18 R. Shenhar, E. Jeoung, S. Srivastava, T. B. Norsten, and V. M. Rotello, *Adv. Mater.* **2005**, *17*, 2206-2210.

19 M. Litschauer, and M. –A. Neouze, *J. Mater. Chem.* **2008**, *18*, 640-646.

20 J. Mijatovic, W. H. Binder, H. Gruber, *Microchim. Acta,* **2000**, *133*, 175–181

21 T. Kimura, S. Saeki, Y. Sugahara, K. Kuroda, *Langmuir,* **1999**, *15*, 2794–2798.

22 C. Rissing, D. Y. Son, *Organometallics*, **2008**, *27*, 5394–5397.

23 N. B. Cramer, J. P. Scott, C. N. Bowman, *Macromolecules*, **2002**, *35*, 5361–5365.

24 H. –B. He, B. Li, J. –P. Dong, Y. –Y. Lei, T. –L. Wang, Q. –W. Yu, Y. –Q. Feng, Y. –B. Sun, *ACS Appl. Mater. Interfaces,* **2013**, *5*, 8058–8066.

25 L. Chabanne, S. P. firrmann, D. J. Lunn, I. Manners, *Polym. Chem.* **2013**, *4*, 2353−2360.

26 Y. Zheng, S. Cai, L. Peng, Y. Jin, H. Xu, Z. Weng, Z. Gao, B. Zhao, C. Gao, *Polym. Chem*. **2016**, *7*, 6202−6210.

27 T. Ganicz, W. A. Stańczyk, N. K. Gladkova, I. Śledzińska, *Macromolecules,* **2000**, *33*, 289–293.

Chapter 6

Conclusion

Chapter 6

In this chapter, all the results and findings of this thesis are shortly summarized, and general conclusions are presented. Future prospects of the studies on the synthesis of silica nanoparticles by controlling mesosturcture this thesis are also mentioned with possible applications of newly obtained nanomaterials.

Ultra-small silica nanoparticles around 2-3 nm in diameter have been successfully prepared using reverse-type mesostructures as the intermediates. First of all, the self-organization behaviors of organoalkoxysilanes are reported in Chapters 2 and 3. Three dimensional hybrid mesostructure with a tetragonally packed arrangement of spherical micelles was newly synthesized (Chapter 2). A bulky siloxane head of the precursor, composed of three disiloxane branches, exclusively resulted in the formation of the mesostructure with high curvature. Moreover, H_2O molecules have played as a hydrophilic expander to form the high curvature of sphere-type mesostructure. As described in Chapter 3, silica-organic hybrid of reverse-type mesostructure, where organically modified silica nanoparticles are hexagonally packed, was newly synthesized. Both of reverse micelle formation and polysiloxane formation are realized by the designed organoalkoxysilane consisting of three hexyl branches and a tetrasiloxane chain. These self-organization behaviors of amphiphilic organoalkoxysilanes well accorded with the theory of packing parameter. In contrast to the previous accomplishments on the formation of various silica-organic hybrid mesostructures possessing lamellar, 2D monoclinic, 2D hexagonal mesostructures using molecularly designed organoalkoxysilanes, 3D tetragonal and reverse-type mesostructures were synthesized in this study. This was realized for the first time because of the new molecular design of alkoxysilanes containing larger siloxane head or triple organic chains. The findings obtained in this thesis have expanded the possibility of controlling the periodic arragement in silica-organic hybrid mesostructures, which

should be of great importantce to develop the applications of such hybrid materials.

Next, the possibility of reverse-type mesostructure to form silica nanoparticles was investigated. The reverse-type mesostructure described in Chapter 3 was successfully dissociated in a solvent to form monodisperse silica-organic hybrid nanoparticles ~3 nm in size. The core size of resulting SiO_2 nanoparticles was smaller when organoalkoxysilanes of shorter siloxane chains were used. A hydrophilic dye in the precursor solution was preferentially incorporated into the resulting silica nanoparticles according to hydrophilicity of the dye during the EISA process. Thus, the synthetic procedure to small silica nanoparticles was newly established.

For deeper understanding of this new synthetic method, the possibility to form reverse-type mesostructures using concerted self-organization of a surfactant and a silica precursor was investigated in Chapters 4 and 5. In Chapter 4, the concerted self-organization resulted in the formation of a reverse-type mesostructure using commercial chemicals, and the mesostructure was dissociated to form individual silica nanoparticles in solution. The isolated silica nanoparticles are covered with surfactants through non-covalent electrostatic interaction, which accordingly permitted the post-modification of their surfaces. The nanoparticle size was tunable by the surfactant/Si ratio in the precursor solution, and this procedure was also applied to synthesize titanium oxide nanoparticles. Thus, silica nanoparticles that feature the high surface per volume ratio and the small particle size (<3 nm) was prepared using the concerted self-organization of surfactants and TEOS. As an application example of such extremely small silica nanoparticle, Chapter 5 describes the synthesis of a silica-organic nanohybrid by the interconnection of primary silica nanoparticles with flexible organic linkers. The high ratio of surface per volume of silica nanoparticles was confirmed by the amount of modified organic groups on the nanoparticle surface. In the solid-state of

the nanohybrid, N_2 gas cannot be introduced into the nanohybrid due to the densely packed primary nanoparticles. On the ther hand, a guest molecule can be incorporated into the emerging internal nanospaces of the nanohybrid after the swelling with a solvent. The resulting nanostructure of this nanohybrid is a sort of inverse of conventional mesoporous silica nanoparticles, and the porosity and the functionality can be molecularly designed with organic linkers. As a possible application of such a nanohybrid with adaptive nanospaces, medical applications of drug delivery systems or fluorescent probes should emerge.

In the studies described in Chapters 3 and 4, two different nanoparticles, denoted as **NPs_3** and **NPs_4** respectively, were prepared using self-organization of organoalkoxysilane (**NPs_3**) and concerted self-organization of surfactant and silica precursor (**NPs_4**). The nanoparticle sizes are similar (~3 nm), and the size was tunable in both of the cases. Considering the compositions of these nanoparticles, **NPs_3** are free from the aggregation because of the presence of the protective organic shell; on the other hand, the surface of **NPs_4** can be freely modified by organic silylation. Interestingly, the ^{29}Si MAS NMR spectra of these nanoparticles are similar in the Q units region. As the polysiloxane networks in **NPs_4** are changed to be well-condensed after surface trimethylsilylation, silanol groups are mainly located at nanoparticle surfaces in the case of **NPs_4**. In contrast, uncondensed silanol grous are dominantly located in the silica core because of the existing outer alkyl chains in the case of **NPs_3**. We can freely choose these different types of silica nanoparticles in order to achieve a specific purpose.

Monodisperse silica nanoparticles of unprecedentedly small sizes (~ 3 nm) are newly synthesized in this study by utilizing the EISA process. The emerging silica nanoparticles will expand the possibility of new applications including catalytic, optical,

mechanical, and medical ones. I do believe this new synthetic method to form ultra-small nanoparticles will be an opportunity to discover new applications which has not been accessible by conventional synthetic routes.

Structural control of silica-organic hybrid mesostructures has been realized through chemical design of precursor molecules. The synthesis of silica-organic hybrid nanoparticles was demonstrated as an application of the controlled mesostructures. Furthermore, silica nanoparticles were prepared through the same procedure using surfactant templates. Interestingly, the chemical design of precursor molecules governs the composition and structure of resulting products, including nanoparticles and mesostructures in this study. These ultra-small silica nanoparticles are simply the first example of the synthetic procedure, and it will be extended to prepare other nanomaterials through the chemical design of precursor molecules.

List of Acheivements

Original articles related to this thesis

(1) S. Sakamoto, K. Fujino, A. Shimojima, K. Kuroda

"Formation of Silica−Organic Hybrid Nanoparticles by Cross-Linking of Ultra-Small Silica Nanoparticles"

Chem. Lett. **2018**, *just accepted*, DOI: 10.1246/cl.180374.

(2) S. Sakamoto, M. Yoshikawa, K. Ozawa, Y. Kuroda, A. Shimojima, K. Kuroda

"Formation of Single-Digit Nanometer Scale Silica Nanoparticles by Evaporation-Induced Self-Assembly"

Langmuir, **2018**, *34*, 1711-1717.

(3) S. Sakamoto, Y. Tamura, H. Hata, Y. Sakamoto, A. Shimojima, K. Kuroda

"Molecularly Designed Nanoparticles by Dispersion of Self-Assembled Organosiloxane-Based Mesophases"

Angew. Chem. Int. Ed. **2014**, *53*, 9173-9177.

(4) S. Sakamoto, A. Shimojima, K. Miyasaka, J. Ruan, O. Terasaki, K. Kuroda

"Formation of Two- and Three-Dimensional Hybrid Mesostructures from Branched Siloxane Molecules"

J. Am. Chem. Soc. **2009**, *131*, 9634-9635.

Other articles (not related to this thesis)

(1) J. Du, M. Fukushima, S. Sakamoto, M. Sakurai, T. Suzuki, A. Shimojima, H. Miyata, C. M. Crudden, K. Kuroda

"Alignment Control of Self-Assembled Organosiloxane Films Derived from Alkyloligosiloxane Amphiphiles"

Langmuir, **2009**, *25*, 13614-13618.

Oral and poster presentations

(1) S. Sakamoto, A. Shimojima, K. Miyasaka, J. Ruan, O. Terasaki, K. Kuroda, "Formation of 2D and 3D Silica-Based Hybrid Mesostructures from a Designed Single Oligosiloxane Precursor", JSPS A3 Foresight Program Seminar, Fudan University, Shanghai, November 2009

(2) 阪本樹, 下嶋敦, 黒田一幸

"分岐した３つのジシロキサン鎖をもつアルキルシロキサン系分子からのメソ構造体の合成"

日本セラミックス協会第 21 回秋季シンポジウム, 1D08, 北九州国際会議場, 福岡, 2008 年 9 月

(3) 阪本樹, 下嶋敦, 黒田一幸

"新規シロキサン系分子からの３次元メソ構造を有するハイブリッドの合成"

日本ゾルゲル学会第 6 回検討会, 56, 名古屋市中小企業振興会館, 愛知, 2008 年 7 月

(4) 阪本樹, 櫻井美香子, 下嶋敦, 黒田一幸

"分岐したジシロキサンユニットをもつアルキルシロキサン系分子の合成とその自己組織化"

日本化学会第 88 回春季年会, 2L5-50, 立教大学, 東京, 2008 年 3 月

Acknowledgement

I express my deep gratitude for Professor Kazuyuki Kuroda for his kind and enthusiastic supervision. Logical thinking and scientific viewpoints have been steadily grown up through the series of activities in the labolatory. Also, I greatly appreciate the leadership by Professor Atsushi Shimojima. All of my researches are based on his polite guidance and technical support. It has always been my pleasure to have a hot discussion with the professors.

I am much greatful to Professor Yoshiyuki Sugahara for the kind comments and fruitful suggestions over the years from the bachelor course. The communication between two laboratories of inorganic chemistry had been important to know the diversity of each laboratory at that time. Also, I express my special thanks to Professor Toshiyuki Momma and Professor Hiroaki Wada because this thesis has been much improved by the valuable advices. Comments from the various fields of specialities are always stimulus and sometimes critical.

Colaboration with the group of Professor Osamu Terasaki is the grateful experience for me to learn how to communicate in English and collaborate with the experts in different fields. The opportunities to communicate with foreign students in the A3 Foresight Program had been also grateful for me in that the global viewpoints were cultivated through the cross-cultural communication.

I greatly appreciate all the members in Kuroda laboratory and Kuroda-Shimojima-Wada laboratory. The days had/has been always supported by everyone around me, through sometimes discussion and sometimes analytical help. My steady grow-up as a researcher is thanks to such a kind support of labolatory members. All the experiences in the laboratory are now much meaningful for the job life.

At last, I’d like to give special thanks to my important family for the comfortable encouragement in daily life. Moreover, the finantial support and the approval for the scholarship are both essential for the accomplishment of this thesis. Thanks a lot for giving me such a valuable and exciting chance.

July, 2018

Shigeru Sakamoto